



**NAM**

# **Development of v2 Partial Collapse Fragility and Consequence Functions for the Groningen Field**

---

**Helen Crowley, Rui Pinho, Barbara Polidoro and Peter Stafford**

Datum November 2015

Editors Jan van Elk & Dirk Doornhof



## **General Introduction**

The response of buildings to the ground accelerations caused by induced earthquakes is important for assessing the risk posed by these earthquakes. This report describes the studies into the fragility of buildings in the Groningen area. Emphasis is on severe damage and building collapse in support of risk assessment.

The report describes the building fragility assessment as used in the “Hazard and Risk Assessment – Interim Update 2015)” issued in November 2015. It incorporates the early results from the first shake-table test on a terraced house performed at EUCentre in Pavia.

NAM has assembled a team of experts in the field of building response to earthquakes to prepare a methodology for assessing the response of buildings in the Groningen area to the induced earthquakes in the Groningen area. This team is led by Helen Crowley and Rui Pinho and consists of academics from various universities and knowledge institutes.

Main members of this team are:

<b>External Expert</b>	<b>Affiliation</b>	<b>Main Expertise Area</b>
Rui Pinho	EUCentre	Fragility of buildings
Helen Crowley	EUCentre	Fragility of buildings
Peter Stafford	EUCentre / Imperial College London	Ground Motion Prediction
Barbara Polidoro	EUCentre	Fragility of buildings

The studies into the fragility of buildings are reviewed by a panel of independent experts from universities and knowledge institutes. The following experts have been invited.

<b>External Expert</b>	<b>Affiliation</b>	<b>Main Expertise Area</b>
Jack Baker	Stanford University, USA	Building Response to Earthquakes
Paolo Franchin	University of Rome 'La Sapienza', Italy	Building Response to Earthquakes
Michael Griffith	University of Adelaide, Australia	Building Response to Earthquakes
Curt Haselton	California State University, USA	Building Response to Earthquakes
Jason Ingham	University of Auckland, New Zealand	Building Response to Earthquakes
Nico Luco	U.S. Geological Survey, USA	Building Response to Earthquakes
Dimitrios Vamvatsikos	NTU Athens, Greece	Building Response to Earthquakes

The team met in October 2015 in London to discuss progress and further development of the building fragility model.



**NAM**

<b>Title</b>	<b>Development of v2 Partial Collapse Fragility and Consequence Functions for the Groningen Field</b>	<b>Date</b>	November 2015
		<b>Initiator</b>	NAM
<b>Author(s)</b>	Helen Crowley, Rui Pinho, Barbara Polidoro and Peter Stafford	<b>Editors</b>	Jan van Elk Dirk Doornhof
<b>Organisation</b>	Various universities and knowledge institutes	<b>Organisation</b>	NAM
<b>Place in the Study and Data Acquisition Plan</b>	<u>Study Theme:</u> Building Fragility <u>Comment:</u> The prediction of response of buildings to earthquakes is central to the risk assessment. This report describes the methodology for assessing (partial) collapse risk of buildings in the Groningen area.		
<b>Directly linked research</b>	(1) Ground Motion Prediction (incl. duration and spectral acceleration)m, (2) Structural upgrading of buildings, (3) Definition of Risk Metrics.		
<b>Used data</b>	Measurements of properties of building materials, experiments on building elements and push-over and shake-table tests.		
<b>Associated organisation</b>	EUcentre, University of Pavia, Mosayk, University of Delft and ARUP.		
<b>Assurance</b>	Assurance team has met in London in October 2015. Recommendations of the assurance team have been included in the report.		

**Groningen Field Seismic Hazard and Risk Assessment**

**Development of v2 Partial Collapse Fragility  
and Consequence Functions for the Groningen  
Field**

*13<sup>th</sup> November 2015*

*by*

*Helen Crowley, Rui Pinho, Barbara Polidoro and Peter Stafford*

## Table of Contents

Table of Contents .....	2
Executive Summary .....	4
Acknowledgments .....	13
1 Introduction .....	15
1.1 Development Phases .....	15
1.2 Building Typologies .....	16
1.3 Risk Metrics.....	19
1.3.1 Inside Local Personal Risk (ILPR).....	20
1.3.2 Community Risk.....	20
1.4 Adopted Methodology for Fragility and Consequence Functions.....	21
1.4.1 Analytical Approach.....	21
1.4.2 SDOF models .....	24
1.4.3 Key assumptions and areas of conservatism .....	25
1.5 Outline of Report .....	26
2 Partial Collapse Mechanisms .....	28
3 In-plane Backbone Curves .....	31
3.1 Introduction .....	31
3.2 URM Wall Buildings.....	31
3.2.1 Residential detached buildings .....	31
3.2.2 Residential terraced buildings .....	34
3.2.3 Residential apartment buildings .....	37
3.2.4 Industrial/commercial buildings .....	39
3.3 Timber Buildings .....	40
3.4 Steel Moment Frame Buildings .....	43
3.5 Steel Braced Frame Buildings.....	45
3.6 Reinforced Concrete Buildings.....	45
3.6.1 Residential buildings.....	46
3.6.2 Commercial and industrial buildings.....	47
3.7 Summary of Backbone Curves .....	49
3.8 Variability in Backbone Curves .....	55
4 Development of In-plane Hysteresis Models .....	56
4.1 Introduction .....	56
4.2 Calibration of Hysteresis Models.....	58
4.2.1 URM Walls.....	58
4.2.2 Timber Frames .....	59
4.2.3 Steel Moment Frames .....	60
4.2.4 Steel Braced Frames .....	61
4.2.5 Reinforced Concrete Beam-Column Frames .....	61
4.2.6 Reinforced Concrete dual wall-frames .....	62
4.2.7 Precast Reinforced Concrete Walls.....	62
4.3 Summary of all hysteresis models .....	63
5 Development and Calibration of Out-of-Plane Models .....	65

5.1	Background to Out-of-Plane Model .....	65
5.2	Comparison with Experimental Test Data .....	67
5.3	Out-of-Plane Backbone Curves .....	74
5.4	Variability in Out-of-Plane Backbone Curves .....	80
6	Nonlinear Response of SDOF systems .....	82
6.1	Introduction .....	82
6.2	Selection of Records .....	83
6.3	Linear Regression of Cloud Data .....	84
6.4	Influence of Building-to-Building Variability on Nonlinear Response .....	89
7	Fragility Functions.....	91
7.1	Introduction .....	91
7.2	Confidence Levels and Epistemic Uncertainties .....	96
7.3	History and Consistency Checks .....	98
7.3.1	History check .....	98
7.3.2	Consistency checks .....	99
7.4	Truncation of Lognormal Distribution .....	102
8	Consequence and Fatality Modelling.....	104
8.1	Introduction .....	104
8.2	Volume Loss .....	104
8.3	Inside Local Personal Risk Fatality Model .....	108
8.4	Consistency Checks.....	109
9	Future Developments .....	111
9.1	Structural Modelling (in-plane and out-of-plane) .....	111
9.2	Fragility Modelling .....	111
9.3	Consequence Modelling.....	112
10	References .....	114
Appendix A	Influence of SSI .....	119
Appendix B	Plots of Fragility Functions .....	121

## Executive Summary

This report summarises the partial collapse fragility and consequence (fatality) models that have been developed for 56 building typologies for NAM's v2 hazard and risk assessment of the Groningen field.

Equivalent SDOF models (Figure ES.1) are used to represent the structural systems of each building typology in the development of the v2 fragility functions. Such approach requires the definition of the effective mass ( $m$ ) and a hysteretic force-displacement ( $F$ - $D$ ) model to describe the dynamic response of the structural system, together with a lateral spring with stiffness  $K_x$  and a dashpot damper with viscous damping coefficient  $C_x$  that represent the foundation flexibility and damping (so-called soil-structure interaction, SSI), respectively.

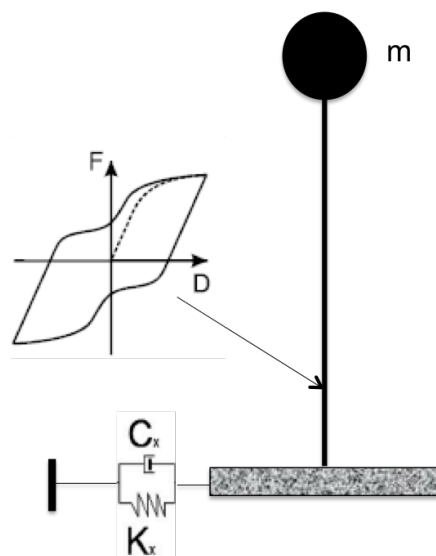


Figure ES.1. SDOF system used for development of v2 fragility functions

The hysteretic force-displacement models for each building typology have been calibrated using an extensive numerical modelling and experimental testing campaign, as described herein and in a number of other reports available on the NAM platform. Partial collapse mechanisms have been defined per building typology, as described in Table ES.1 - the key assumption that has been made in the v2 risk model is that partial collapse mechanisms (as opposed to global collapse/instability mechanisms) contribute predominantly to the inside local personal risk in Groningen, given the range of earthquake magnitudes and levels of ground motion expected in the Groningen field.

Table ES.1. Collapse mechanisms considered for each building typology

Building Typology	Partial Collapse of Structural System		
	1 (longitudinal direction)	2 (transverse direction)	3 (either direction)
RESD_W_A	Unseating due to sliding at base	Unseating due to sliding at base	-
RESS_W_A	Unseating due to sliding at base	Unseating due to sliding at base	-
A/I/C_W_B1	Connection failure of at least one base connection	Connection failure of at least one base connection	-
A/I/C_W_B2	In-plane failure of at least one URM wall	Connection failure of at least one base connection	-
A/I/C_W_A	In-plane failure of at least one URM wall	In-plane failure of at least one URM wall	OOP rocking of at least one bearing wall
COMO_S_B_L4S	Rotation capacity of at least one column	Rotation capacity of at least one column	-
COMO_S_B_G4S	Rotation capacity of at least one column	Rotation capacity of at least one column	-
A/I/C_S_A	Rotation capacity of at least one column	Rotation capacity of at least one column	-
A/I/C_S_B	Rotation capacity of at least one column	Rotation capacity of at least one column	-
A/I/C_S_C	Rotation capacity of at least one column	Rotation capacity of at least one column	-
COMO_S_A_L4S	Rotation capacity of at least one column	Rotation capacity of at least one column	-
COMO_S_A_G4S	Rotation capacity of at least one column	Rotation capacity of at least one column	-
REST_RC_A	Out of plane shear failure of at least one RC wall	Shear failure of at least one RC wall	-
RESA_RC_A_L4S	Shear or punching failure of at least one wall/slab	Shear failure of at least one RC wall	-
RESA_RC_A_G4S	Shear or punching failure of at least one wall/slab	Shear failure of at least one RC wall	-
RECA_RC_A_L4S	Shear or punching failure of at least one wall/slab	Shear failure of at least one RC wall	-
RECA_RC_A_G4S	Shear or punching failure of at least one wall/slab	Shear failure of at least one RC wall	-
COMO_RC_A1_L4S	Shear or punching failure of at least one wall/slab	Shear failure of at least one RC wall	-
COMO_RC_A1_G4S	Shear or punching failure of at least one wall/slab	Shear failure of at least one RC wall	-
COMO_RC_A2_L4S	Shear or punching failure of at least one wall/slab	Shear failure of at least one RC wall	-
COMO_RC_A2_G4S	Shear or punching failure of at least one wall/slab	Shear failure of at least one RC wall	-
A/I/C_RC_A	Rotation capacity of at least one column	Rotation capacity of at least one column	-
A/I/C_RC_B1	Rotation capacity of at least one column	Rotation capacity of at least one column	-
REST_RC_B	Connection failure of at least one panel	Connection failure of at least one panel	-
RESA_RC_B_L4S	Connection failure of at least one panel	Connection failure of at least one panel	-
RESA_RC_B_G4S	Connection failure of at least one panel	Connection failure of at least one panel	-



REST-URM-A	In-plane failure of at least one wall	In-plane failure of at least one wall	OOP rocking of at least one bearing wall
REST-URM-B	In-plane failure of at least one wall	In-plane failure of at least one wall	OOP rocking of at least one bearing wall
REST-URM-C	In-plane failure of at least one wall	In-plane failure of at least one wall	OOP rocking of at least one bearing wall
REST-URM-D	In-plane failure of at least one wall	In-plane failure of at least one wall	OOP rocking of at least one bearing wall
REST-URM-E	In-plane failure of at least one wall	In-plane failure of at least one wall	OOP rocking of at least one bearing wall
REST-URM-F	In-plane failure of at least one wall	In-plane failure of at least one wall	OOP rocking of at least one bearing wall

Best estimate fragility functions have been developed for each collapse mechanism through nonlinear dynamic analysis, using thousands of accelerograms to model the record-to-record variability. The functional form of the fragility functions is given as follows:

$$P_c = 1 - \Phi \left( \frac{\ln(D_u) - b_0 - b_1 \ln Sa(T) - b_2 \ln D_{S5-75}}{\beta_T} \right) \quad (\text{ES.1})$$

where  $\Phi$  is the cumulative distribution function of the standard normal distribution,  $D_u$  is ultimate displacement capacity (in metres),  $Sa(T)$  is spectral acceleration (in terms of g) for a given period of vibration  $T$ ,  $D_{S5.75}$  is 5-75% significant duration (in seconds) and  $\beta_T$  is the total dispersion. The parameters of Equation ES.1 for each building typology and collapse mechanism are provided in Tables ES.2, ES.3 and ES.4.

Table ES.2. Parameters of the best estimate transverse direction fragility functions

Typology	Transverse direction					
	$b_1$	$b_2$	$b_0$	$\beta_T$	$D_u$	$T$ (s)
AGRI_INDU_COML_RC_A	0.998	-0.041	-2.001	0.384	0.218	0.85
AGRI_INDU_COML_RC_B1	0.829	-0.070	-1.224	0.424	0.218	1.5
AGRI_INDU_COML_RC_B2	3.483	0.000	-2.782	0.719	0.110	0.01
AGRI_INDU_COML_S_A	0.826	0.039	-2.315	0.349	0.420	0.6
AGRI_INDU_COML_S_B	0.621	0.000	-2.803	0.324	0.330	0.4
AGRI_INDU_COML_S_C	0.933	-0.119	-3.275	0.316	0.350	0.5
AGRI_INDU_COML_URM_A	4.900	0.000	-1.612	0.783	0.045	0.01
AGRI_INDU_COML_W_A	2.290	0.000	-7.792	0.758	0.021	0.2
AGRI_INDU_COML_W_B1	0.706	0.000	-2.360	0.306	0.290	0.5
AGRI_INDU_COML_W_B2	0.706	0.000	-2.360	0.306	0.290	0.5
CHURCH	2.290	0.000	-7.792	0.758	0.021	0.2

Typology	Transverse direction					
	$b_1$	$b_2$	$b_0$	$\beta_T$	$D_u$	T (s)
COMO_RC_A1_G4S	1.482	0.000	-1.238	0.391	0.200	1
COMO_RC_A1_L4S	1.516	-0.272	-3.391	0.445	0.100	0.6
COMO_RC_A2_G4S	1.482	0.000	-1.238	0.391	0.200	1
COMO_RC_A2_L4S	1.516	-0.272	-3.391	0.445	0.100	0.6
COMO_RC_B_G4S	3.483	0.000	-2.782	0.719	0.110	0.01
COMO_RC_B_L4S	3.483	0.000	-2.782	0.719	0.110	0.01
COMO_S_A_G4S	1.034	0.053	-1.460	0.359	0.350	1
COMO_S_A_L4S	0.933	-0.119	-3.275	0.316	0.350	0.5
COMO_S_B_G4S	0.559	-0.088	-1.636	0.376	0.350	1.5
COMO_S_B_L4S	0.982	-0.093	-3.188	0.325	0.350	0.5
COMO_URM_A	4.900	0.000	-1.612	0.783	0.045	0.01
COMO_URM_B	4.900	0.000	-1.612	0.783	0.045	0.01
HOSPITAL	1.516	-0.272	-3.391	0.445	0.100	0.6
RECA_RC_A_G4S	1.222	0.000	-3.777	0.517	0.060	0.4
RECA_RC_A_L4S	0.839	0.000	-4.830	0.498	0.060	0.3
RECA_RC_B_G4S	2.727	0.000	-2.963	0.626	0.110	0.01
RECA_RC_B_L4S	2.727	0.000	-2.963	0.626	0.110	0.01
RECA_URM_A	3.867	0.000	-4.772	0.614	0.042	0.01
RECA_URM_B	1.404	0.000	-3.789	0.450	0.044	0.01
RESA_RC_A_G4S	1.222	0.000	-3.777	0.517	0.060	0.4
RESA_RC_A_L4S	0.839	0.000	-4.830	0.498	0.060	0.3
RESA_RC_B_G4S	2.098	0.000	-3.528	0.639	0.110	0.01
RESA_RC_B_L4S	2.098	0.000	-3.528	0.639	0.110	0.01
RESA_URM_A	3.867	0.000	-4.772	0.614	0.042	0.01
RESA_URM_B	1.404	0.000	-3.789	0.450	0.044	0.01
RESD_URM_A	2.290	0.000	-7.792	0.758	0.021	0.2
RESD_URM_B	5.167	0.000	-3.832	0.757	0.014	0.01
RESD_URM_C	2.398	-0.078	-3.919	0.530	0.011	0.01
RESD_URM_D	2.290	0.000	-7.792	0.758	0.021	0.2
RESD_URM_E	4.717	0.000	-5.093	0.845	0.021	0.01
RESD_URM_F	3.049	0.000	-2.487	0.704	0.042	0.01
RESD_W_A	1.075	0.000	-4.586	0.393	0.120	0.2
RESS_URM_A	2.290	0.000	-7.792	0.758	0.021	0.2
RESS_URM_B	5.293	0.000	-3.713	0.771	0.045	0.01
RESS_URM_C	2.368	0.000	-4.593	0.601	0.047	0.01
RESS_W_A	1.075	0.000	-4.586	0.393	0.120	0.2
REST_RC_A	2.309	0.000	-7.402	0.543	0.080	0.01
REST_RC_B	2.727	0.000	-2.963	0.626	0.110	0.01
REST_URM_A	4.510	0.000	-4.195	0.674	0.045	0.01
REST_URM_B	4.055	0.000	-4.121	0.764	0.045	0.01
REST_URM_C	2.368	0.000	-4.593	0.601	0.047	0.01
REST_URM_D	2.368	0.000	-4.593	0.601	0.047	0.01

Typology	Transverse direction					
	$b_1$	$b_2$	$b_0$	$\beta_T$	$D_u$	T (s)
REST_URM_E	2.706	0.000	-4.619	0.656	0.027	0.01
REST_URM_F	2.706	0.000	-4.619	0.656	0.027	0.01
SCHOOL	4.900	0.000	-1.612	0.783	0.045	0.01

Table ES.3. Parameters of the best estimate longitudinal direction fragility functions

Typology	Longitudinal direction					
	$b_1$	$b_2$	$b_0$	$\beta_T$	$D_u$	T (s)
AGRI_INDU_COML_RC_A	0.824	-0.033	-1.198	0.398	0.218	1.5
AGRI_INDU_COML_RC_B1	0.829	-0.070	-1.224	0.424	0.218	1.5
AGRI_INDU_COML_RC_B2	0.875	-0.255	-3.432	0.521	0.110	0.5
AGRI_INDU_COML_S_A	0.826	0.039	-2.315	0.349	0.420	0.6
AGRI_INDU_COML_S_B	0.826	0.039	-2.315	0.349	0.420	0.6
AGRI_INDU_COML_S_C	0.678	0.000	-1.791	0.334	0.480	1
AGRI_INDU_COML_URM_A	7.614	0.000	-7.723	0.815	0.032	0.01
AGRI_INDU_COML_W_A	2.290	0.000	-7.792	0.758	0.021	0.2
AGRI_INDU_COML_W_B1	0.987	0.058	-2.745	0.432	0.640	0.5
AGRI_INDU_COML_W_B2	0.728	0.000	-3.429	0.527	0.045	0.3
CHURCH	2.290	0.000	-7.792	0.758	0.021	0.2
COMO_RC_A1_G4S	1.482	0.000	-1.238	0.391	0.200	1
COMO_RC_A1_L4S	1.516	-0.272	-3.391	0.445	0.100	0.6
COMO_RC_A2_G4S	1.482	0.000	-1.238	0.391	0.200	1
COMO_RC_A2_L4S	1.516	-0.272	-3.391	0.445	0.100	0.6
COMO_RC_B_G4S	0.875	-0.255	-3.432	0.521	0.110	0.5
COMO_RC_B_L4S	0.875	-0.255	-3.432	0.521	0.110	0.5
COMO_S_A_G4S	0.705	0.000	-0.371	0.342	0.480	2.5
COMO_S_A_L4S	0.678	0.000	-1.791	0.334	0.480	1
COMO_S_B_G4S	0.671	0.000	-0.534	0.327	0.480	2.5
COMO_S_B_L4S	0.726	0.000	-1.739	0.313	0.480	1
COMO_URM_A	7.614	0.000	-7.723	0.815	0.032	0.01
COMO_URM_B	7.614	0.000	-7.723	0.815	0.032	0.01
HOSPITAL	1.516	-0.272	-3.391	0.445	0.100	0.6
RECA_RC_A_G4S	1.090	0.052	-1.313	0.378	0.133	1
RECA_RC_A_L4S	1.325	0.000	-2.656	0.414	0.067	0.5
RECA_RC_B_G4S	0.772	-0.224	-3.446	0.532	0.110	0.5
RECA_RC_B_L4S	0.772	-0.224	-3.446	0.532	0.110	0.5
RECA_URM_A	1.625	0.000	-3.253	0.485	0.026	0.01
RECA_URM_B	1.365	0.000	-3.609	0.442	0.016	0.4
RESA_RC_A_G4S	1.214	0.057	-1.536	0.368	0.200	0.85
RESA_RC_A_L4S	1.369	0.000	-3.294	0.412	0.100	0.4
RESA_RC_B_G4S	1.100	0.000	-3.876	0.529	0.110	0.3
RESA_RC_B_L4S	1.100	0.000	-3.876	0.529	0.110	0.3

Typology	Longitudinal direction					
	$b_1$	$b_2$	$b_0$	$\beta_T$	$D_u$	T (s)
RESA_URM_A	1.625	0.000	-3.253	0.485	0.026	0.01
RESA_URM_B	0.992	0.000	-3.783	0.342	0.019	0.3
RESD_URM_A	2.290	0.000	-7.792	0.758	0.021	0.2
RESD_URM_B	5.167	0.000	-3.832	0.757	0.014	0.01
RESD_URM_C	2.398	-0.078	-3.919	0.530	0.011	0.01
RESD_URM_D	4.717	0.000	-7.792	0.758	0.021	0.2
RESD_URM_E	3.049	0.000	-5.093	0.845	0.021	0.01
RESD_URM_F	3.049	0.000	-2.487	0.704	0.042	0.01
RESD_W_A	1.075	0.000	-4.586	0.393	0.120	0.2
RESS_URM_A	2.290	0.000	-7.792	0.758	0.021	0.2
RESS_URM_B	5.293	0.000	-3.713	0.771	0.045	0.01
RESS_URM_C	1.091	0.000	-3.668	0.417	0.053	0.3
RESS_W_A	1.075	0.000	-4.586	0.393	0.120	0.2
REST_RC_A	1.056	0.049	-1.664	0.349	0.400	0.85
REST_RC_B	0.772	-0.224	-3.446	0.532	0.110	0.5
REST_URM_A	1.294	0.128	-3.055	0.512	0.068	0.01
REST_URM_B	1.282	0.111	-3.031	0.510	0.068	0.01
REST_URM_C	1.091	0.000	-3.668	0.417	0.053	0.3
REST_URM_D	1.091	0.000	-3.668	0.417	0.053	0.3
REST_URM_E	1.010	-0.065	-3.917	0.496	0.064	0.3
REST_URM_F	1.010	-0.065	-3.917	0.496	0.064	0.3
SCHOOL	7.614	0.000	-7.723	0.815	0.032	0.01

Table ES.4. Parameters of the best estimate out-of-plane (OOP) fragility functions

Typology	Out-of-plane					
	$b_1$	$b_2$	$b_0$	$\beta_T$	$D_u$	T (s)
AGRI_INDU_COML_RC_A	-	-	-	-	-	-
AGRI_INDU_COML_RC_B1	-	-	-	-	-	-
AGRI_INDU_COML_RC_B2	-	-	-	-	-	-
AGRI_INDU_COML_S_A	-	-	-	-	-	-
AGRI_INDU_COML_S_B	-	-	-	-	-	-
AGRI_INDU_COML_S_C	-	-	-	-	-	-
AGRI_INDU_COML_URM_A	1.075	0.000	-2.521	0.405	0.100	0.5
AGRI_INDU_COML_W_A	1.149	0.000	-2.514	0.346	0.140	0.5
AGRI_INDU_COML_W_B1	-	-	-	-	-	-
AGRI_INDU_COML_W_B2	-	-	-	-	-	-
CHURCH	1.728	0.000	-5.271	0.721	0.083	0.1
COMO_RC_A1_G4S	-	-	-	-	-	-
COMO_RC_A1_L4S	-	-	-	-	-	-
COMO_RC_A2_G4S	-	-	-	-	-	-
COMO_RC_A2_L4S	-	-	-	-	-	-

Typology	Out-of-plane					
	$b_1$	$b_2$	$b_0$	$\beta_T$	$D_u$	T (s)
COMO_RC_B_G4S	-	-	-	-	-	-
COMO_RC_B_L4S	-	-	-	-	-	-
COMO_S_A_G4S	-	-	-	-	-	-
COMO_S_A_L4S	-	-	-	-	-	-
COMO_S_B_G4S	-	-	-	-	-	-
COMO_S_B_L4S	-	-	-	-	-	-
COMO_URM_A	1.075	0.000	-2.521	0.405	0.100	0.5
COMO_URM_B	1.075	0.000	-2.521	0.405	0.100	0.5
HOSPITAL	-	-	-	-	-	-
RECA_RC_A_G4S	-	-	-	-	-	-
RECA_RC_A_L4S	-	-	-	-	-	-
RECA_RC_B_G4S	-	-	-	-	-	-
RECA_RC_B_L4S	-	-	-	-	-	-
RECA_URM_A	0.996	0.000	-2.432	0.409	0.140	0.5
RECA_URM_B	1.857	0.000	-5.240	0.741	0.083	0.1
RESA_RC_A_G4S	-	-	-	-	-	-
RESA_RC_A_L4S	-	-	-	-	-	-
RESA_RC_B_G4S	-	-	-	-	-	-
RESA_RC_B_L4S	-	-	-	-	-	-
RESA_URM_A	0.996	0.000	-2.432	0.409	0.140	0.5
RESA_URM_B	1.728	0.000	-5.271	0.721	0.083	0.1
RESD_URM_A	1.149	0.000	-2.514	0.346	0.140	0.5
RESD_URM_B	1.261	0.000	-4.290	0.595	0.067	0.2
RESD_URM_C	0.777	-0.109	-3.372	0.524	0.067	0.4
RESD_URM_D	1.149	0.000	-2.514	0.346	0.140	0.5
RESD_URM_E	1.148	0.000	-2.511	0.347	0.140	0.5
RESD_URM_F	1.191	0.041	-2.288	0.347	0.140	0.5
RESD_W_A	-	-	-	-	-	-
RESS_URM_A	1.149	0.000	-2.514	0.346	0.140	0.5
RESS_URM_B	1.261	0.000	-4.290	0.595	0.067	0.2
RESS_URM_C	2.262	0.000	-4.236	0.767	0.067	0.1
RESS_W_A	-	-	-	-	-	-
REST_RC_A	-	-	-	-	-	-
REST_RC_B	-	-	-	-	-	-
REST_URM_A	1.290	0.041	-2.218	0.331	0.140	0.5
REST_URM_B	1.632	0.126	-1.818	0.645	0.067	0.01
REST_URM_C	2.262	0.000	-4.236	0.767	0.067	0.1
REST_URM_D	2.262	0.000	-4.236	0.767	0.067	0.1
REST_URM_E	1.945	0.000	-2.438	0.784	0.067	0.01
REST_URM_F	1.945	0.000	-2.438	0.784	0.067	0.01
SCHOOL	1.728	0.000	-5.271	0.721	0.083	0.1

Volume losses have been estimated for each collapse mechanism through both advanced numerical modelling and empirical evidence from past earthquakes. The volume losses have been related to fatality ratios using data from a number of fatal earthquakes, with different relationships obtained for buildings with different construction materials (Figure ES.2).

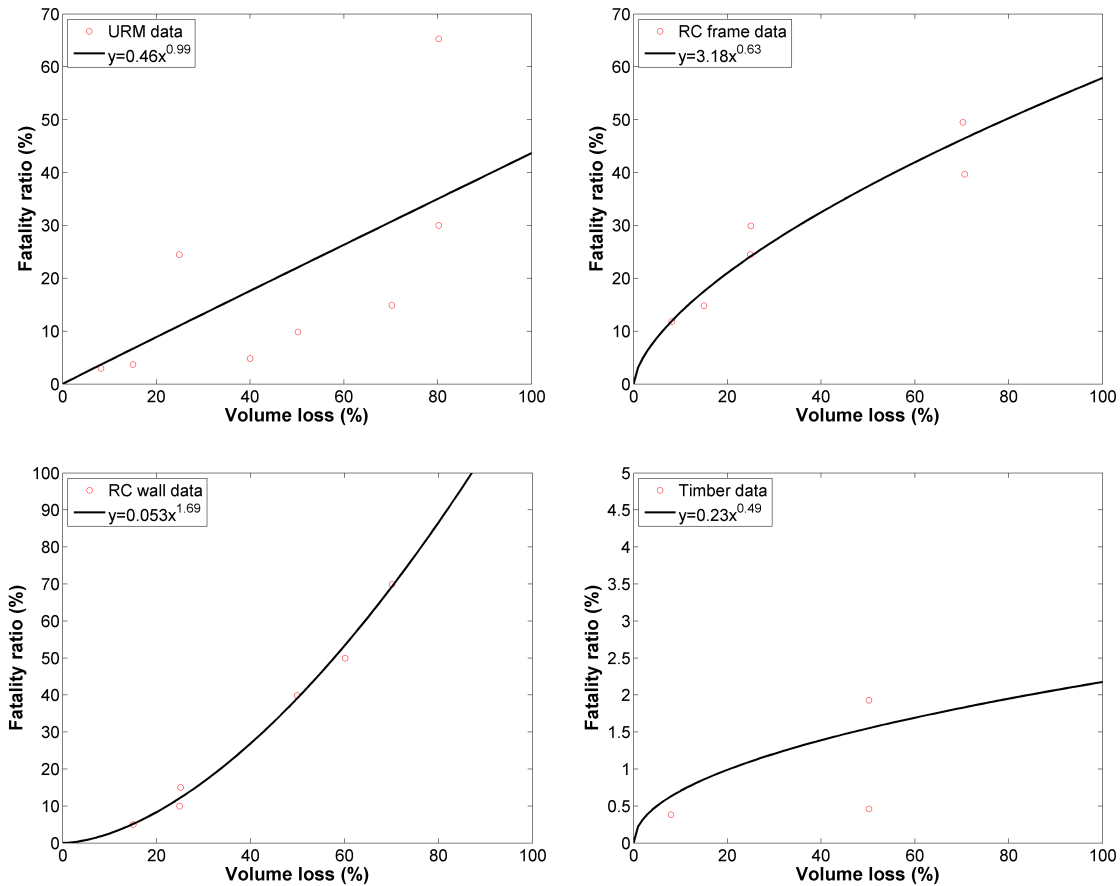


Figure ES.2. Best-fit relationships between volume loss (%) and indoor fatality ratios (%)

A logic tree has been developed to model the epistemic uncertainty of the fatality and consequence models. In both cases, three branches have been defined, with the central branch given by the results presented above, and upper and lower branches defined through expert judgment.

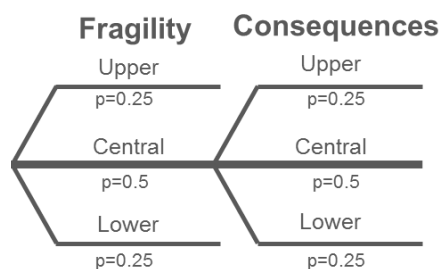


Figure ES.3. Logic tree for fragility and consequence models

## Acknowledgments

The authors would like to express their gratitude to Jan van Elk who, with the assistance of Dirk Doornhof, has provided the support, guidance and conditions that have allowed this study to be carried out and completed within the necessary timeframe. Additional support from Jeroen Uilenreef is also gratefully acknowledged, in particular for what concerns the management of the experimental testing campaign, given the large impact that these tests have had on the calibration of the fragility functions presented herein.

The work presented herein has benefitted greatly from discussions and feedback from Julian Bommer, who is responsible for the development of the ground-motion prediction equations for the region. The important interface between ground shaking and building damage has been ensured through this strong collaboration with Julian. Other members of NAM's Hazard and Risk Assessment Team, namely Stephen Bourne and Steve Oates, have also provided useful feedback and checks, in particular whilst implementing the fragility and consequence models in their risk calculation engines.

The technical contributions of Arup employees Damian Grant, Rein de Vries and Gerben de Vries, with managerial support from Rinke Kluwer, during the development of previous fragility models (v0 and v1), are most gratefully acknowledged. Many of the initial developments made in those previous models have contributed to allowing a high level of maturity of the work presented herein.

There is a large team working on modelling and testing of components and structures for calibration of the numerical models used herein, with the main contributions coming from collaborators at EUCENTRE, Arup, TU-Delft and Mosayk. Not all of those involved can be mentioned and acknowledged here, but particular thanks are given to Francesco Graziotti, Simone Peloso, Alberto Pavese, Guido Magenes and Roberto Nascimbene (from EUCENTRE) for all the dedication and hard work that went into ensuring the tests were completed to schedule, including that of the full-scale house tested on the shaking table, and all results were rendered available in a timely fashion, such that they could be used as input to the v2 fragility model.

The consequence model has been developed in collaboration with a team at Cambridge Architectural Research Ltd (Robin Spence, Emily So and Hannah Baker), with useful input and discussions with Tony Taig (TTAC Ltd), responsible for NAM's falling object risk model. Discussions with Stuart Hardy on risk metrics were also very informative for the development of the fatality model.

The models described herein were presented to an expert review panel during a two-day workshop in London on 29<sup>th</sup>-30<sup>th</sup> October 2015. The members of this panel were: Jack Baker (Stanford University), Paolo Franchin (University of Rome, La Sapienza), Mike Griffith (University of Adelaide), Curt Haselton (California State

University, Chico), Jason Ingham (University of Auckland), Nico Luco (U.S. Geological Survey), Dimitrios Vamvatsikos (University of Athens). A number of comments provided during this workshop were used to improve a first draft of this document, whilst additional feedback was used to draft the final chapter of this report, which outlines the priority areas that have been identified for further development. The authors of this report would like to sincerely thank the panel for travelling to London to participate in this workshop and for all the useful feedback and advice that they shared, which will undoubtedly lead to significant improvements in the v3 models.

The work presented herein has been presented at different stages in numerous meetings with Exxon Mobil, the Groningen Scientific Advisory Committee (SAC), chaired by Lucia van Geuns, and the Dutch State Supervision of Mines (SodM), as well as observers and advisors to these two bodies. Feedback and questions at these meetings have helped us to develop our justifications for the modelling choices made and to explain and justify our results. We note in particular the comments from Ron Hamburger, Iunio Iervolino, Ilse de Vent, Jan Gijbbers, Raphael Steenbergen.

A significant part of the strong-motion database used for the derivation of the v2 fragility functions was provided by Julian Bommer. The Groningen recordings were provided to Julian by Bernard Dost of KNMI. The European database was made available to Julian by Professor Sinan Akkar from Bogazici University, Istanbul. The masonry damage database from the Christchurch earthquakes was provided to the lead author of this report by Lisa Moon, former PhD student of the University of Adelaide. Feedback from Johan Pool on the characteristics of buildings from the Groningen region is also gratefully acknowledged.

# 1 Introduction

## 1.1 Development Phases

In preparation for the Winningsplan due for submission in July 2016, NAM is developing models to quantify the hazard and risk due to induced seismicity in the Groningen field.

As discussed further in the following sections, a key component of the risk assessment involves the definition of fragility functions (which give the probability of exceeding a given limit state, conditional on a level of input ground motion) for each building typology within the exposure model. Although many fragility functions have been developed over the years (see e.g. Calvi et al., 2006), the vast majority are not appropriate for use in Groningen, both due to the specific characteristics of the structures as well as the ground motions expected from induced seismicity events. A predominantly analytical approach, which also includes elements of expert judgment and empirical data calibration, is thus being followed for developing new Groningen-specific fragility and consequence functions.

Extensive work has been planned until spring 2016 in order to develop calibrated and tested fragility functions for the predominant building typologies in Groningen. In addition, it has also been decided that an iterative approach to the development of these new functions will be followed, with functions being updated every 6 months (from v0 in October 2014 to v3 in March 2016), to allow the lessons learned from these intermediate “beta” functions to be fed back into the methodology. Furthermore, setting these intermediate milestones helps to ensure that the work is kept on track. This report describes the development of the v2 fragility and consequence functions, which includes a number of improvements over the previous v0 and v1 versions, as summarised in the table below.

Table 1.1. Overview of development features in v0, v1 and v2 models

<b>Feature</b>	<b>v0</b>	<b>v1</b>	<b>v2</b>
Number of building typologies	94	65	56
Foundation types	-	-	✓
Soil-foundation-structure interaction	-	-	✓
Methodology	SDOF nonlinear static	SDOF nonlinear static	SDOF nonlinear dynamic
Intensity measure	PGA	Spectral acceleration (Sa) at 5 periods	Sa at 16 periods and 5-75% significant duration
Capacity of structures	Weakest direction for URM, no out-of-plane (OOP)	Weakest direction for URM, OOP model, not used in risk	Transverse and longitudinal directions and OOP

Feature	v0	v1	v2
Experimental calibration of analytical models	-	-	Based on URM component tests (in-plane and OOP), shaking table test, in-situ material tests and precast connection tests

## 1.2 Building Typologies

There are currently 56 building typologies in the v2 exposure model (Table 1.2). The identification of the building typologies and development of the exposure model for the Groningen field is further documented in the following reports:

- Exposure Model v1 – Updated Typologies and Inference Rules. 23<sup>rd</sup> March 2015.
- Arup (2015) 229746\_031.0\_REP1003\_Rev.0.02\_Issue Exposure Database V2. 11<sup>th</sup> September 2015.

Figure 1.1 shows the extent of the area for which the exposure model has been developed. There are over 150,000 populated buildings in the model, of which over 90% are unreinforced masonry (URM) buildings (Figure 1.2), and the remaining 10% are constructed with reinforced concrete (RC), steel (S) or wood (W).



Figure 1.1. Extent of the exposure model (Groningen field + 5km buffer)



Table 1.2. List and description of v2 exposure model typologies

No.	Use category	Material	Sub-typology	Description of lateral load resisting system	Modifier	
1	Residential Detached (RESD)	URM	A	Detached house - timber diaphragms, solid walls		
2			B	Detached house - timber diaphragms, cavity walls		
3			C	Detached house - RC diaphragms, cavity walls		
4			D	Labourer's cottage - timber diaphragms, solid walls, particular shape		
5			E	Mansion - timber diaphragms, solid walls - 1+attic storeys, mansard roof		
6			F	Large URM villa - timber diaphragms, solid walls - $\geq 2$ +attic storeys		
7		W	A	Timber or steel frame, timber shear panels		
8	Residential semi-detached (RESS)	URM	A	Semi-detached house - timber diaphragms, solid walls		
9			B	Semi-detached house - timber diaphragms, cavity walls		
10			C	Semi-detached house - RC diaphragms, cavity walls		
11		W	A	Timber or steel frame, timber shear panels		
12	Residential terraced (REST)	URM	A	Timber floors, solid party walls, solid gable/façade walls		
13			B	Timber floors, solid party walls, cavity gable/façade walls		
14			C	Concrete floors, solid party walls, cavity gable/façade walls		
15			D	Concrete floors, cavity party walls, cavity gable/façade walls		
16			E	Mixed floors (timber ground/concrete first/timber attic), solid party walls, cavity gable/façade walls		
17			F	Nehobo or Mixed floors (timber ground/concrete first/timber attic), cavity party walls, cavity gable/façade walls		
18		RC	A	Cast-in-place (CIP) tunnelgietsbouw or CIP gable/façade walls with hollow block slab (unreinforced walls may be present)		
19			B	Precast floors, Precast party/gable walls, precast walls long direction		
20		Residential apartment (RESA)	URM	A	Clay brick walls	
21				B	Calcium silicate walls	
22	RC		A	Cast-in-place (CIP) tunnelgietsbouw or CIP structural walls (predominantly in one direction) with hollow block slab (unreinforced walls may be present)	$\leq 4$ storeys	
23			A	Cast-in-place (CIP) tunnelgietsbouw or CIP structural walls (predominantly in one direction) with hollow block slab (unreinforced walls may be present)	$> 4$ storeys	
24			B	Precast structural walls	$\leq 4$ storeys	
25	B	Precast structural walls	$> 4$ storeys			
26	Mixed residential / commercial apartment (RECA)	URM	A	Solid walls, timber diaphragms, reduced walls at ground floor replaced with steel frame or precast columns		
27			B	Structural URM walls (predominantly calcium silicate), reduced walls at ground floor replaced with steel frame or precast columns		
28		RC	A	Cast-in-place (CIP) tunnelgietsbouw or CIP structural walls (predominantly in one direction) with hollow block slab (unreinforced walls may be present), reduced walls at ground floor, replaced by RC frame	$\leq 4$ storeys	
29			A	Cast-in-place (CIP) tunnelgietsbouw or CIP structural walls (predominantly in one direction) with hollow block slab (unreinforced walls may be present), reduced walls at ground floor, replaced by RC frame	$> 4$ storeys	
30			B	Precast structural walls with reduced walls at ground floor, replaced by precast columns	$\leq 4$ storeys	
31			B	Precast structural walls with reduced walls at ground floor, replaced by precast columns	$> 4$ storeys	
32	Agricultural, industrial and large commercial (AIC)	S	A	Steel braced frame (w/ and w/out basement)		
33			B	Steel portal frame one direction, braced frame in other (w/ and w/out basement)		
34			C	Steel or precast columns with concrete beams and hollowcore slab, w/ steel stability bracing		
35		W	A	Wooden trussed roof with URM façade walls (which may become bearing)		
36			B1	Glulam portal frame, steel braces in other direction		
37		B2	Glulam portal frame, URM wall in other direction			
38		URM	A	URM soild or cavity wall, steel or timber roof (may feature precast gravity system)		
39		RC	A	Cast-in-place (CIP) reinforced concrete (RC) portal frame		
40			B1	Precast RC portal frame (grouted dowels)		
41	B2		Precast RC structural walls			
42	Commercial (other) (COMO)	URM	A	Clay brick walls		
43			B	Calcium silicate walls		
44		RC	A1	Cast-in-place (CIP) reinforced concrete (RC) core walls	$\leq 4$ storeys	
45			A1	Cast-in-place (CIP) reinforced concrete (RC) core walls	$> 4$ storeys	
46			A2	Cast-in-place (CIP) RC moment frame	$\leq 4$ storeys	
47			A2	Cast-in-place (CIP) RC moment frame	$> 4$ storeys	
48			B	Precast RC walls	$\leq 4$ storeys	
49			B	Precast RC walls	$> 4$ storeys	
50		S	A	Steel braced frame	$\leq 4$ storeys	
51			A	Steel braced frame	$> 4$ storeys	
52			B	Steel moment frame	$\leq 4$ storeys	
53		B	Steel moment frame	$> 4$ storeys		
54		Schools				
55	Churches					
56	Hospitals					

Figure 1.4 shows the most predominant URM building typology (detached with solid walls and timber floors, RESD-URM-A) is well distributed across the region, with a higher density in many of the villages. Despite the abundance of masonry buildings, it is important to point out that close to 30% of the population live or work in non-URM buildings (Figure 1.3), though Figure 1.4 shows that high-rise reinforced concrete buildings are mainly concentrated in the city of Groningen (and so they may be subjected to very different levels of hazard).

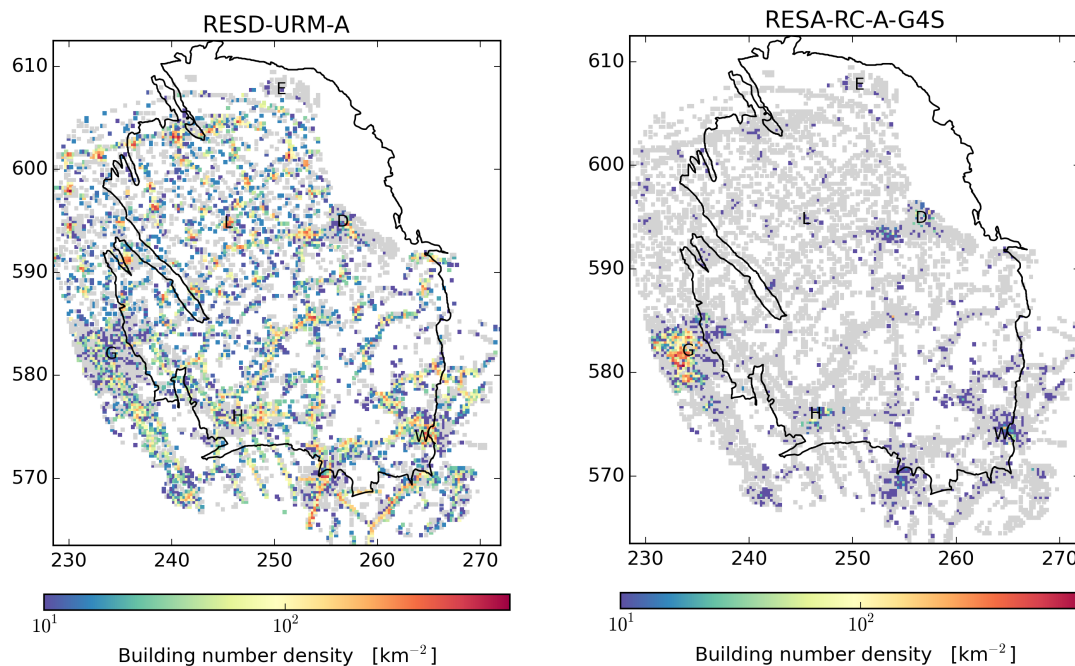


Figure 1.4. Maps showing the building number density of two building typologies (RESD-URM-A and RESA-RC-A-G4S) on a regular 250 x 250 m grid. The grey cells denote areas where buildings of other typologies are located. The letters 'D', 'E', 'H', 'L', 'W' denote the place names Delfzijl, Eemshaven, Hoogezand, Loppersum and Winschoten respectively, and the black line denotes the outline of the field.

Finally, it is also important to note that given the large regional scale characteristic of the risk assessment study, it is not feasible to identify buildings which feature design/construction flaws that render them of particularly high risk for their occupants. These are instead the focus of alternative efforts (e.g. Structural Upgrading work stream of NAM), which try to detect such critical structures and urgently deploy remedy measures.

### 1.3 Risk Metrics

When measuring risk, it is important to select a risk metric that is appropriate for the purpose of the study; however, in many cases, there is more than one option available as to which metric to use. An advisory committee, Commissie Meijdam, was established in early 2015 to advise on risk policy related to Groningen

earthquakes, including the selection of risk metrics. As of October 2015, discussion (led by Commissie Meijdam) amongst key stakeholders and risk experts on the choice of risk metrics is ongoing. The current selection of risk metrics is based upon a judgment on which metrics are most suitable for each purpose, and reflects the discussions hosted by Commissie Meijdam to date. However, it is recognized that alternative options are available, and the choice of metrics may change for future versions of the probabilistic hazard and risk analysis (PHRA) depending on the final advice from Commissie Meijdam.

Currently, the results from the PHRA are summarised via risk metrics which are related to the annualised probability of fatality for an individual person or for groups of people, taken as an average across the forecast period of the PHRA. The primary risk metrics used in the v2 PHRA are “Inside Local Personal Risk” and “Community Risk”, which are defined below.

### *1.3.1 Inside Local Personal Risk (ILPR)*

“Local Personal Risk” (LPR) is generally defined as the annual probability of fatality for a fictional person, who is continuously present without protection at a specific at-risk location. For Groningen earthquakes, LPR is defined as follows: *“the probability of death of a fictional person who is permanently in or near a building”* (Risk Analysis of Groningen Earthquakes by SoDM - P500 Engels ref-06-risico-analyse-aardgasbevingen-groningen.docx). “Inside LPR” (ILPR) focuses on the risk to people inside of buildings, and assumes that the fictional person is permanently present inside the building, and the location of the person is uniformly and randomly distributed inside the building. In probabilistic analysis, the expectation value of the ILPR is used to determine whether the level of risk for the people inside a specific building is acceptable, and can be compared to the Commissie Meijdam advice, which requires the fatality risk for a person inside a building to be less than  $10^{-5}$  per year. This report focuses on developing the input needed for calculating inside local personal risk.

### *1.3.2 Community Risk*

Community Risk (CR) is the annualised rate of fatalities for a specified risk, with units of fatalities per year. CR is calculated by multiplying the LPR for a specified risk by the average number of people present in the at-risk area. Inside a building, the at-risk area is defined as the entire area inside the building, and CR is calculated by multiplying LPR by average number of building occupants (taking into account the proportion of time that the building is occupied). Outside of buildings, the at-risk area is defined as the area up to 5m from the building façade (based on empirical evidence of masonry falling from buildings), and CR is calculated by multiplying the LPR for this at-risk area by the average number of people in the at-risk area.

CR is used for two main purposes:

- To measure the risk to people outside of buildings from falling objects (e.g. chimneys, parapets, gables) and façade walls. CR is considered a superior metric for this purpose rather than LPR because it considers the likelihood that people will be present, which is highly variable for the area outside of buildings. For example, the average number of people present on a busy shopping street will be many orders of magnitude higher than those present in a garden.
- To prioritise buildings/objects for upgrading within the structural upgrading program. CR (rather than LPR) is considered to be the most suitable metric for prioritisation because it allows a reasonable comparison to be made between collapse risks for different types of buildings and falling object risks, with different average occupancies inside buildings and beneath the potential falling objects.

The v2 risk assessment has only considered outside risk due to falling objects, as discussed elsewhere (NAM, 2015), whereas the outside risk due to the collapse of façade and veneer walls has not yet been considered and will be addressed in the v3 model. Hence, this report does not address the inputs necessary to calculate outside risk.

## **1.4 Adopted Methodology for Fragility and Consequence Functions**

### *1.4.1 Analytical Approach*

Given that all of the currently proposed risk metrics focus on loss of life, a model is needed to predict the probability of loss of life given different levels of ground shaking.

Methodologies for estimating fatalities from earthquakes range from those that directly attempt to predict the number of deaths from the magnitude of the earthquake (e.g. Samardjieva and Badal, 2002) or a level of ground shaking such as macroseismic intensity (e.g. Jaiswal et al., 2009), to those that propose ratios between the mean number of deaths (or injured persons) and the number of people exposed to a building with a given level of damage, so-called mean fatality ratios (e.g. Coburn and Spence 2002).

The latter approach has been selected for the Groningen risk model, given that it has been observed in past earthquakes that the number of earthquake shaking deaths is clearly related to the number of buildings that fully or partially collapse (e.g. Alexander, 1996). Furthermore, by estimating the fatality risk for different typologies of buildings, it will be possible to guide the strengthening efforts that are currently being applied to the buildings in the region.

The volume of a structure that collapses will influence the number of people within the building that are affected (Seligson, 2008; Spence and So, 2009; So and

Pomonis, 2012). So (2015) has shown (Figure 1.5) that mean fatality ratios are directly correlated with volume loss in collapsed buildings (defined by Okada (1996) as the “void index, or volume loss of survival space, given by volume of debris ( $V_d$ ) divided by the space capacity ( $V_c$ , which is the volume given by 2 metres height from floor level)” - see Figure 1.6.). Furthermore, for a given volume loss, the main construction material can further influence the fatality ratio.

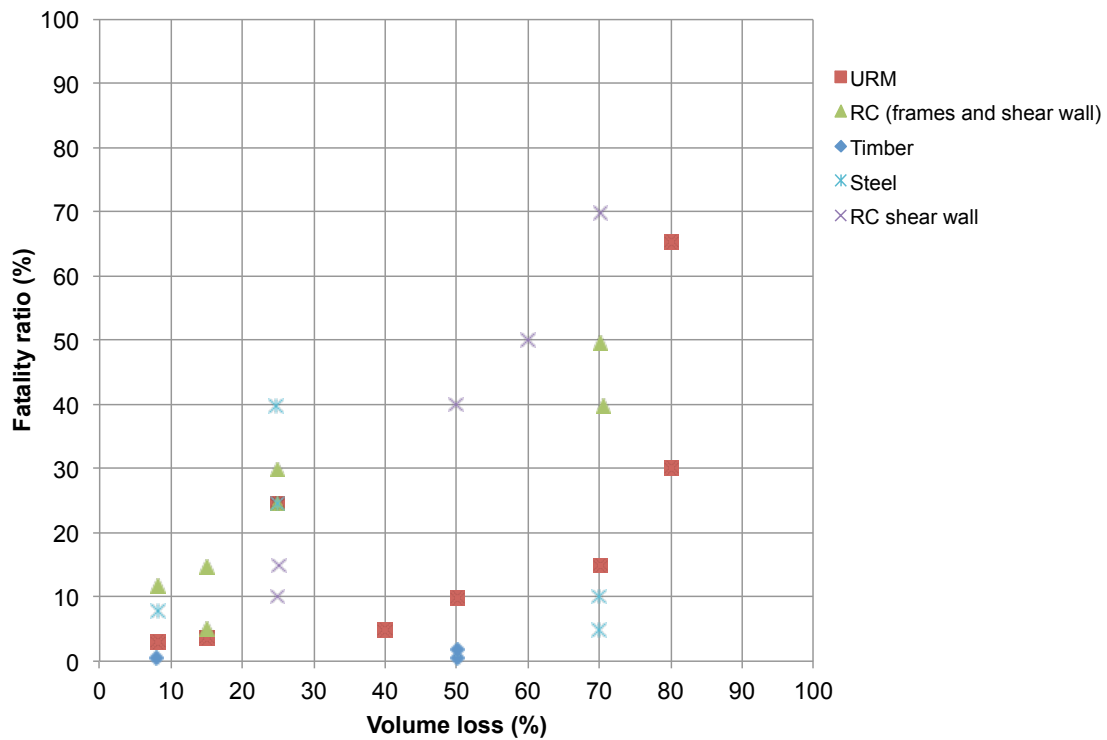


Figure 1.5. Relationship between fatality ratios and volume loss (So, 2015)

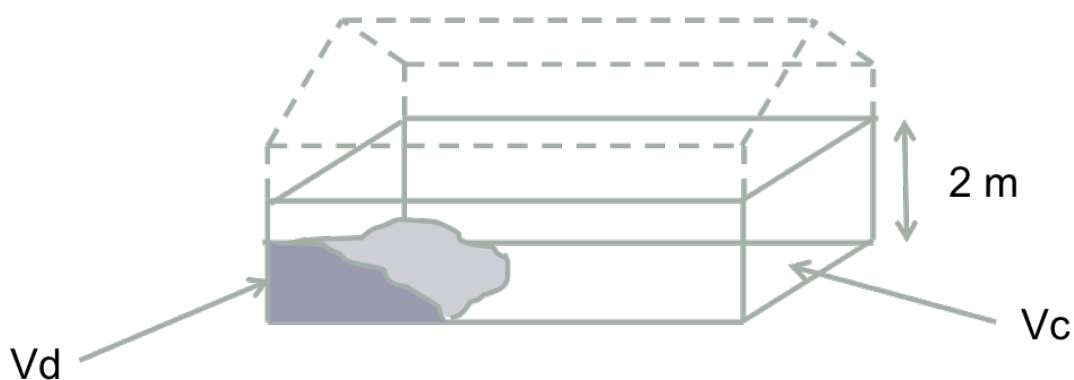


Figure 1.6. Illustration of volume loss (adapted from Okada, 1996)

Despite the observed differences in collapsed volumes in buildings that have collapsed in earthquakes, these buildings are generally defined as having the same “damage state” in post-earthquake reconnaissance missions (see Figure 1.7). This is one of the drawbacks in using empirical data to derive fragility functions, which are

then used to estimate fatalities, and this can be overcome by using analytical models that allow different collapse mechanisms and associated volumes to be estimated.

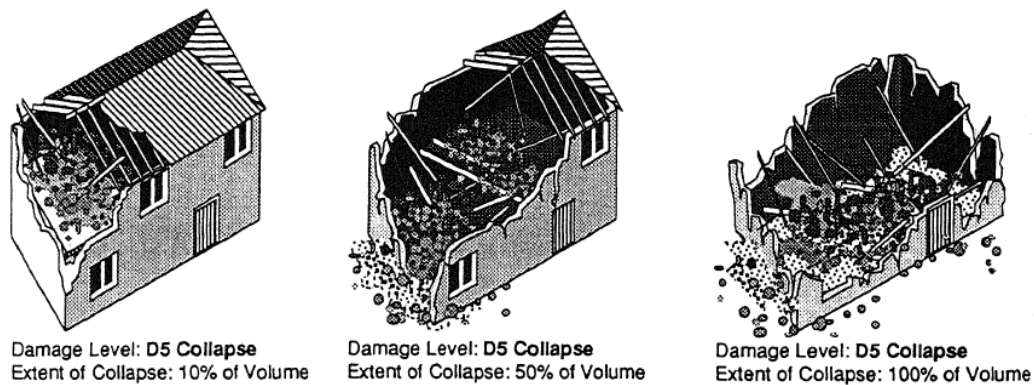


Figure 1.7. Varying volumetric reduction of a building defined as having a “collapse” or D5 EMS (Grunthal et al., 1998) damage level (from Coburn et al., 1992),

The collapse mechanism plays an important role in the estimation of casualties. A study by So et al. (2015) of 458 photos of partially collapsed (D4) and collapsed (D5) buildings in 47 different earthquake events (Figure 1.8) further enforces this message: different collapse mechanisms do indeed lead to different volume losses. A similar study was also carried out for the debris falling outside of the building, to understand the risk to people outside of buildings, and again collapse mechanisms and area of debris were seen to be correlated (Baker et al., 2015). There are a number of limitations to the direct use of the data given in Figure 1.8, which include the fact that only some sides of the building can be observed in photos, the volume loss inside the building can not always be seen, and the data is from buildings which can have very different construction practices to those in Groningen. An analytical approach to estimate the probability of collapse and associated volume loss for different collapse mechanisms, supported by the empirical evidence from the photos used to produce Figure 1.8, has thus been followed herein.

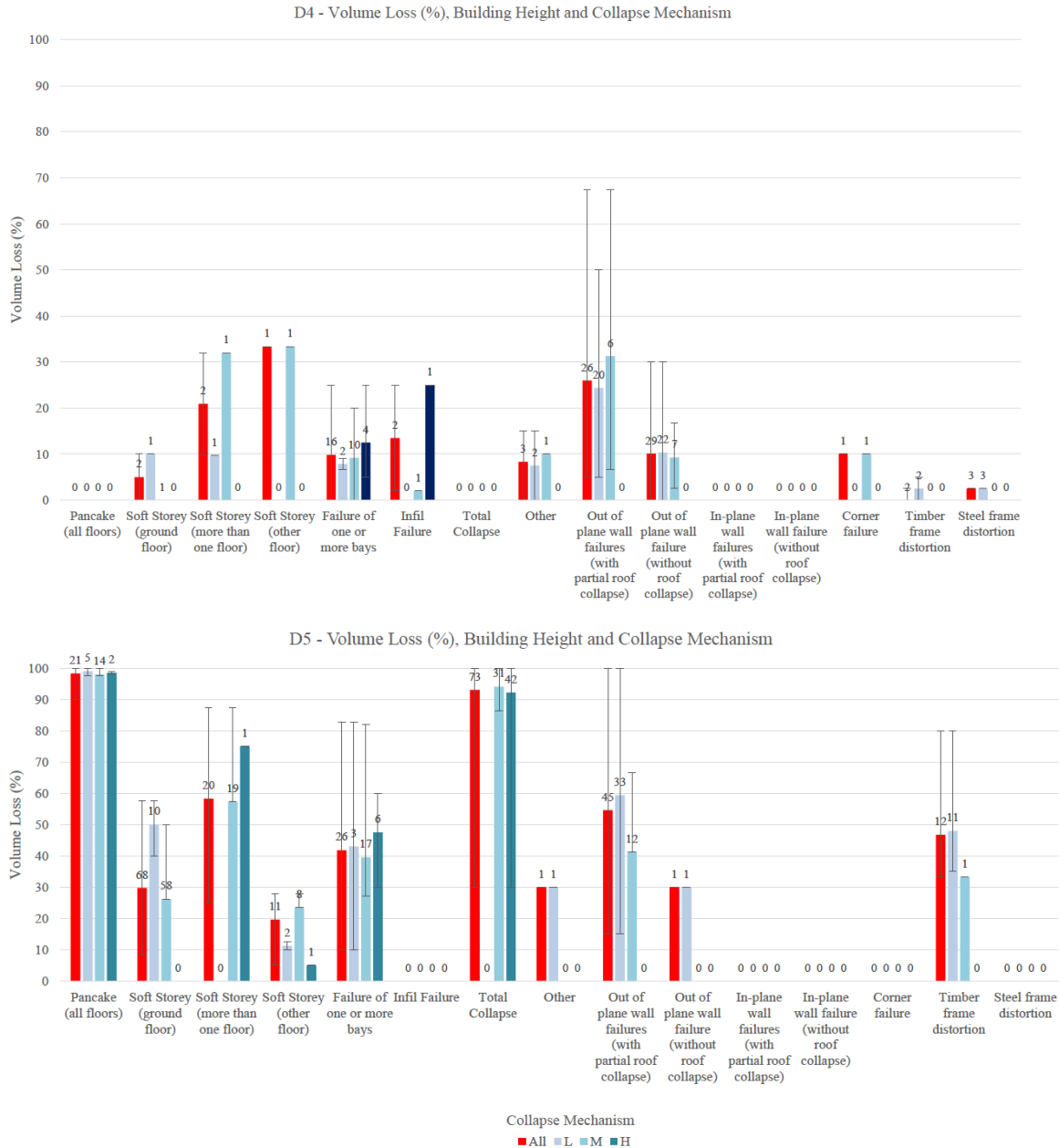


Figure 1.8. Distribution of volume loss by collapse mechanism and height for collapsed buildings based on damage observations assigned to EMS damage scale DS4 (top) and DS5 (bottom) (So et al., 2015)

#### 1.4.2 SDOF models

Although multi-degree-of-freedom (MDOF) models have been developed for a large number of the building typologies in Groningen (see Chapter 3), the computational effort associated to running nonlinear dynamic analysis of such structures subjected to tens of records effectively rendered such approach unfeasible at this stage. Therefore, a simplified single-degree-of-freedom (SDOF) equivalent system approach has been used instead to analytically represent each typology, and a large suite of records has been employed in the nonlinear dynamic analyses to model the record-to-record variability.

Figure 1.9 shows the equivalent SDOF model that is used to represent each structural system in the development of the v2 fragility functions. This model requires the definition of the effective mass ( $m$ ), a hysteretic force-displacement model to describe the dynamic response of the system, and a lateral spring with stiffness  $K_x$  and a dashpot damper with viscous damping coefficient  $C_x$  that represent the foundation flexibility and damping (so-called soil-structure interaction, SSI), respectively. A simplified approach to modelling SSI has been taken, with the ground motion introduced at the base of the SSI spring/damper.

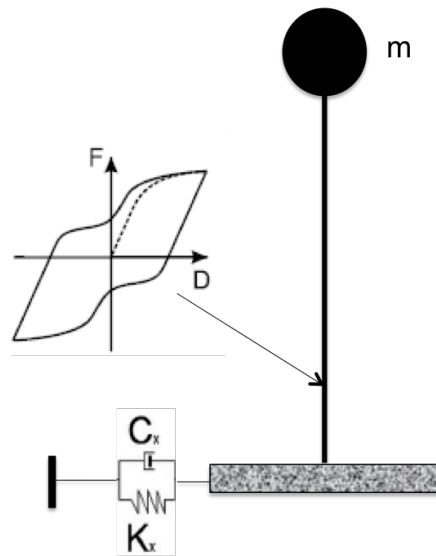


Figure 1.9. SDOF system used for development of v2 fragility functions

The possibility of structural collapse due to failure of part of the structural system in either direction of each building typology has been considered, as many structures have different lateral load resisting systems/strengths in their longitudinal and transverse directions. The additional possibility of structural collapse due to out-of-plane failure of URM walls has also been considered. The collapse mechanisms are further discussed in Chapter 2.

#### 1.4.3 Key assumptions and areas of conservatism

The approach that has been followed to develop fragility and consequence functions for the v2 risk model relies on the key assumption that partial collapse mechanisms (i.e. those which would most likely be identified as D4 according to the EMS damage scale) contribute more to the inside local personal risk in Groningen than global collapse/instability mechanisms (i.e. those that would be identified as D5), for the reasons outlined in what follows.

In order to produce the data shown in Figure 1.8 above, a survey of photographic evidence from past earthquakes from around the world that caused partial or full structural collapses was carried out (So et al., 2015), and only 3 of 47 identified events had magnitudes less than 6, none of which had buildings that experienced a D5 damage state. Given that the mean maximum magnitude of the v2 hazard model

is 5.75 and the v2 model for ground shaking has a central logic tree branch that estimates levels of ground shaking that are lower than tectonic earthquakes of the same magnitude (Bommer et al., 2015), a clear judgment can be made that the level of hazard in the v2 model is lower than that of areas where buildings have experienced global collapse in the past.

In the v2 hazard and risk assessment model, a number of potentially conservative assumptions were made regarding issues such as e.g. maximum magnitude distribution, minimum site amplification factor, use of point sources rather than finite faults etc. For what concerns the fragility and consequence functions presented herein, conservative estimates of risk might also arise for the following reasons:

- The URM models have been calibrated using the shaking-table response of a building that (i) did not have partition walls and door/window frames, (ii) was constructed with mortar weaker than commonly observed, and (iii) was subjected to repeated earthquakes.
- All out-of-plane failures have been assumed to occur in one-way bending (which is weaker than two-way bending, that is also commonly observed).
- The volume loss versus fatality model (Figure 1.5) has been developed by combining the volume losses from both partial and global collapse mechanisms.

In addition, the following issues have not been explicitly considered in the v2 fragility model (due to lack of time and/or sufficient information) and their potential impact on the risk analysis output is not known at this stage:

- Variations in the connections between URM walls, as well as between URM walls and slabs/roof.
- Foundation failure.
- Vertical motion effects (in particular for those typologies with inadequate anchorage and/or connections).
- Multiple partial collapse and global instability mechanisms.

During the v3 development phase, sensitivity studies on at least some of the aforementioned issues will be carried out in order to gain insight on their impact on the risk results (e.g. a global collapse mechanism will produce higher levels of consequences with respect to a partial collapse mechanism, but features much lower probability of occurrence).

## **1.5 Outline of Report**

Chapter 2 of this report describes the partial collapse mechanisms that have been considered per typology, and explains how they have been combined in the risk engine.

Chapters 3 and 4 of this report discuss how the SDOF systems have been calibrated for each in-plane direction of the building typologies, whilst Chapter 5 describes the out-of-plane SDOF models. The derivation of the impedance functions used to model the springs and dashpot dampers for soil-foundation-structure interaction is discussed in Mosayk (2015b). The horizontal stiffness and damping at the fundamental period of vibration of each SDOF has been obtained from the impedance functions using the mean soil profile and highest scaling factor (for nonlinearity). A short study on the sensitivity of the nonlinear response to the modelled soil-structure interaction is included in Appendix A.

Chapter 6 of this report describes the approach taken to probabilistically model the nonlinear response of the SDOF systems, and Chapter 7 presents the fragility functions for all considered collapse mechanisms. Chapter 8 discusses the modelling of consequences in terms of volume loss/debris area and fatality ratios. The final chapter summarises the future developments that are planned before the submission of the Winningsplan in July 2016.

## 2 Partial Collapse Mechanisms

As discussed in Section 1.4.3, collapse due to global instability has not been considered in the current modelling activities, as it is judged that the fatality risk will be dominated by partial collapse mechanisms under the levels of ground motions that are expected in the Groningen field. The risk of fatalities due to falling objects has been dealt with elsewhere (NAM, 2015).

Up to three partial collapse mechanisms have been considered per typology. These mechanisms have been judged to be the predominant mechanisms that would lead to partial collapse, based on the experience gained during the numerical modelling and testing activities (see Mosayk, 2015; Arup, 2015a, b and c; EUCENTRE 2015b and c).

Table 2.1. Collapse mechanisms considered for each building typology

Building Typology	Partial Collapse of Structural System		
	1 (longitudinal direction)	2 (transverse direction)	3 (either direction)
RESD_W_A	Unseating due to sliding at base	Unseating due to sliding at base	-
RESS_W_A	Unseating due to sliding at base	Unseating due to sliding at base	-
A/I/C_W_B1	Connection failure of at least one base connection	Connection failure of at least one base connection	-
A/I/C_W_B2	In-plane failure of at least one URM wall	Connection failure of at least one base connection	-
A/I/C_W_A	In-plane failure of at least one URM wall	In-plane failure of at least one URM wall	OOP rocking of at least one bearing wall
COMO_S_B_L4S	Rotation capacity of at least one column	Rotation capacity of at least one column	-
COMO_S_B_G4S	Rotation capacity of at least one column	Rotation capacity of at least one column	-
A/I/C_S_A	Rotation capacity of at least one column	Rotation capacity of at least one column	-
A/I/C_S_B	Rotation capacity of at least one column	Rotation capacity of at least one column	-
A/I/C_S_C	Rotation capacity of at least one column	Rotation capacity of at least one column	-
COMO_S_A_L4S	Rotation capacity of at least one column	Rotation capacity of at least one column	-
COMO_S_A_G4S	Rotation capacity of at least one column	Rotation capacity of at least one column	-
REST_RC_A	Out of plane shear failure of at least one RC wall	Shear failure of at least one RC wall	-
RESA_RC_A_L4S	Shear or punching failure of at least one wall/slab	Shear failure of at least one RC wall	-
RESA_RC_A_G4S	Shear or punching failure of at least one wall/slab	Shear failure of at least one RC wall	-
RECA_RC_A_L4S	Shear or punching failure of at least one wall/slab	Shear failure of at least one RC wall	-
RECA_RC_A_G4S	Shear or punching failure of at least one wall/slab	Shear failure of at least one RC wall	-

COMO_RC_A1_L4S	Shear or punching failure of at least one wall/slab	Shear failure of at least one RC wall	-
COMO_RC_A1_G4S	Shear or punching failure of at least one wall/slab	Shear failure of at least one RC wall	-
COMO_RC_A2_L4S	Shear or punching failure of at least one wall/slab	Shear failure of at least one RC wall	-
COMO_RC_A2_G4S	Shear or punching failure of at least one wall/slab	Shear failure of at least one RC wall	-
A/I/C_RC_A	Rotation capacity of at least one column	Rotation capacity of at least one column	-
A/I/C_RC_B1	Rotation capacity of at least one column	Rotation capacity of at least one column	-
REST_RC_B	Connection failure of at least one panel	Connection failure of at least one panel	-
RESA_RC_B_L4S	Connection failure of at least one panel	Connection failure of at least one panel	-
RESA_RC_B_G4S	Connection failure of at least one panel	Connection failure of at least one panel	-
RECA_RC_B_L4S	Connection failure of at least one panel	Connection failure of at least one panel	-
RECA_RC_B_G4S	Connection failure of at least one panel	Connection failure of at least one panel	-
A/I/C_RC_B2	Connection failure of at least one panel	Connection failure of at least one panel	-
COMO_RC_B_L4S	Connection failure of at least one panel	Connection failure of at least one panel	-
COMO_RC_B_G4S	Connection failure of at least one panel	Connection failure of at least one panel	-
A/I/C-URM-A	In-plane failure of at least one wall	In-plane failure of at least one wall	OOP rocking of at least one bearing wall
COMO-URM-A	In-plane failure of at least one wall	In-plane failure of at least one wall	OOP rocking of at least one bearing wall
COMO-URM-B	In-plane failure of at least one wall	In-plane failure of at least one wall	OOP rocking of at least one bearing wall
RECA-URM-A	In-plane failure of at least one wall	In-plane failure of at least one wall	OOP rocking of at least one bearing wall
RECA-URM-B	In-plane failure of at least one wall	In-plane failure of at least one wall	OOP rocking of at least one bearing wall
RESA-URM-A	In-plane failure of at least one wall	In-plane failure of at least one wall	OOP rocking of at least one bearing wall
RESA-URM-B	In-plane failure of at least one wall	In-plane failure of at least one wall	OOP rocking of at least one bearing wall
RESD-URM-A	In-plane failure of at least one wall	In-plane failure of at least one wall	OOP rocking of at least one bearing wall
RESD-URM-B	In-plane failure of at least one wall	In-plane failure of at least one wall	OOP rocking of at least one bearing wall
RESD-URM-C	In-plane failure of at least one wall	In-plane failure of at least one wall	OOP rocking of at least one bearing wall

RES-URM-D	In-plane failure of at least one wall	In-plane failure of at least one wall	OOP rocking of at least one bearing wall
RES-URM-E	In-plane failure of at least one wall	In-plane failure of at least one wall	OOP rocking of at least one bearing wall
RES-URM-F	In-plane failure of at least one wall	In-plane failure of at least one wall	OOP rocking of at least one bearing wall
RE-URM-A	In-plane failure of at least one wall	In-plane failure of at least one wall	OOP rocking of at least one bearing wall
RE-URM-B	In-plane failure of at least one wall	In-plane failure of at least one wall	OOP rocking of at least one bearing wall
RE-URM-C	In-plane failure of at least one wall	In-plane failure of at least one wall	OOP rocking of at least one bearing wall
RE-URM-A	In-plane failure of at least one wall	In-plane failure of at least one wall	OOP rocking of at least one bearing wall
RE-URM-B	In-plane failure of at least one wall	In-plane failure of at least one wall	OOP rocking of at least one bearing wall
RE-URM-C	In-plane failure of at least one wall	In-plane failure of at least one wall	OOP rocking of at least one bearing wall
RE-URM-D	In-plane failure of at least one wall	In-plane failure of at least one wall	OOP rocking of at least one bearing wall
RE-URM-E	In-plane failure of at least one wall	In-plane failure of at least one wall	OOP rocking of at least one bearing wall
RE-URM-F	In-plane failure of at least one wall	In-plane failure of at least one wall	OOP rocking of at least one bearing wall

## **3 In-plane Backbone Curves**

### **3.1 Introduction**

The hysteretic model shown previously in Figure 1.9 is divided into two components: a backbone model describing the envelope force-displacement response and a hysteretic model describing the stiffness and strength degradation as well as possible pinching that is observed under cyclic/dynamic loading.

The in-plane backbone curves (in terms of yield and ultimate lateral strength and displacement capacity) for each direction of the building typologies presented in Table 1.2 have been obtained from pushover analysis, as described further in this chapter.

It is noted that there are a number of drawbacks in using pushover analyses to define the backbone curves of SDOF systems. Although the majority of the buildings in the exposure database have one or two stories, they may still not respond predominantly in the first mode. This is particularly the case for irregular URM buildings and those with flexible diaphragms, and in this case the use of the envelope from nonlinear dynamic analyses might be more appropriate. This has not yet been feasible due to time constraints, but will be investigated in the future.

The ultimate displacement capacity has been taken as the point at which the collapse mechanisms described in Table 2.1 are reached, which is explicitly included in the numerical models for what concerns unseating, rotation capacity, and connection failure. For in-plane failure of walls, the ultimate displacement is taken as the minimum of either the last point at which the analysis converges or the displacement at which 60% of the ultimate base shear capacity is reached (based on the recommendations of CNR, 2013).

### **3.2 URM Wall Buildings**

There are 22 typologies in the v2 exposure model which have URM walls as the main lateral load resisting system. Some of these typologies are assumed to have similar lateral load capacity, but the typologies have been kept separate in the exposure model either because they have different population distributions or because the consequences of structural collapse are judged to be different (see Section 8).

#### *3.2.1 Residential detached buildings*

An actual residential detached building from Groningen that has concrete floors and calcium silicate / clay cavity walls has been modelled using the Applied Element Method software Extreme Loading for Structures, ELS (ASI, 2010) and a pushover

analysis has been undertaken in each direction to understand the lateral capacity of the structure (see Figure 3.2a). This model has been taken as representative of the typology RESD-URM-C.



Figure 3.1. URM detached building and associated Extreme Loading for Structures (ELS) model (where the concrete slab is not shown and the gable walls and roof are applied as line loads to the appropriate ground floor bearing walls)

These structures do not tend to have significant differences in the lateral capacity in each orthogonal direction, due to a similar distribution of walls, openings and slab/roof loading. Hence, it would seem to be reasonable to use a single backbone curve to represent detached URM buildings based on the average capacity in each direction.

The properties of the bricks and mortar used in the model were based on initial findings from laboratory and in-situ field material tests, as the final report of the latter (EUCENTRE et al., 2015) was not available at the time the model was developed. The properties described in the aforementioned report (and subsequent updates) will thus feed into the v3 fragility functions. Figure 3.2a shows the pushover curves in both directions for the RESD-URM-C typology.

The aforementioned model has been modified by replacing the concrete floor loads with those from timber floors, in order to represent the typology RESD-URM-B, and a pushover curve in each direction has been calculated (see Figure 3.2b). The whole of the diaphragm has been pushed, and thus it has been considered to be rigid. The use of pushover analysis for structures with flexible diaphragms is not ideal as they are more likely to respond as 2DOF systems (see e.g. Brignola et al., 2008). Future calibration of the capacity curves for structures with flexible diaphragms will instead need to make use of the envelope from incremental dynamic analyses.

The typology RESD-URM-C has been developed by using timber floor loads and replacing the internal calcium silicate cavity walls with 200 mm solid clay walls, and the results are shown in Figure 3.2c.

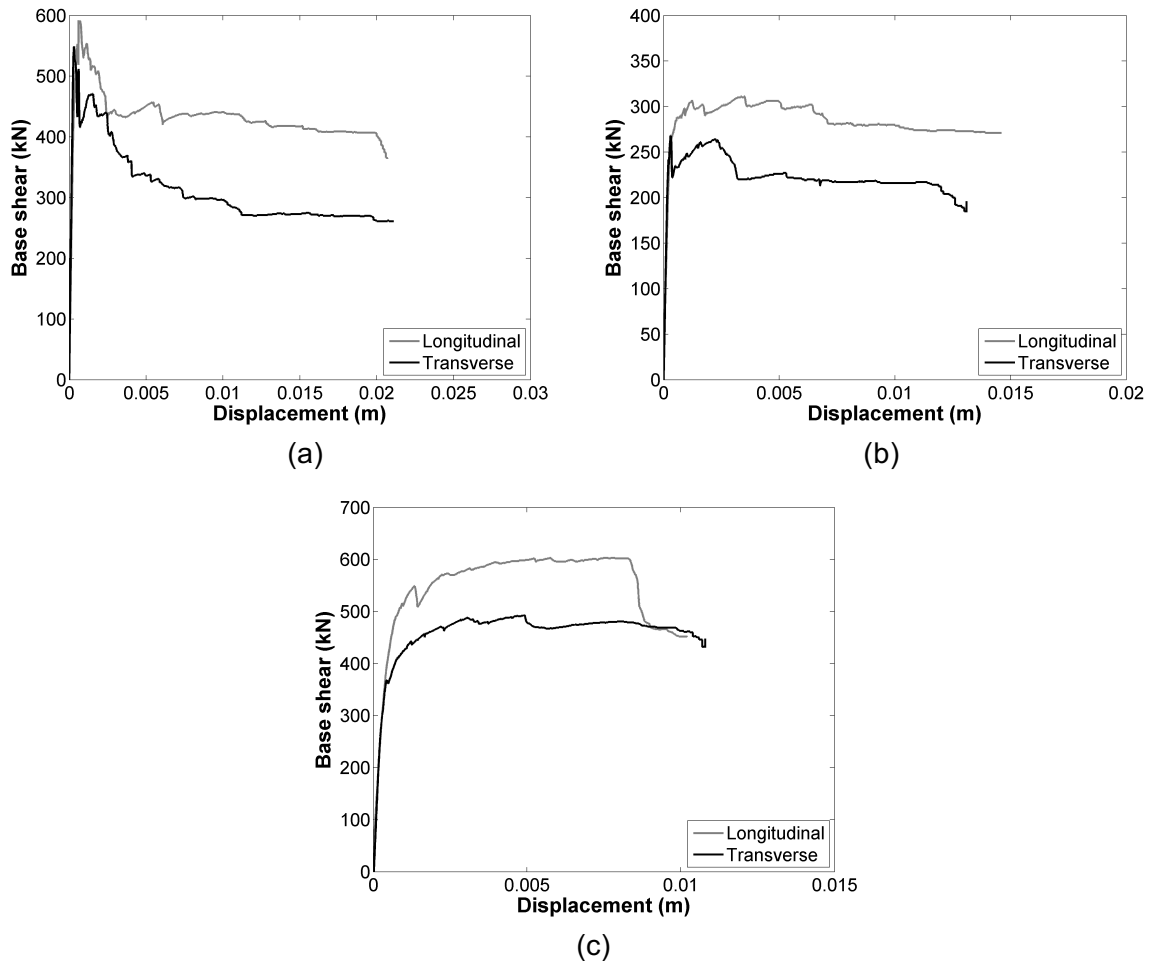


Figure 3.2. SDOF pushover curves for detached house with (a) solid clay walls with timber floor, (b) calcium silicate internal cavity walls with timber floor, (c) calcium silicate internal cavity walls with concrete floor

There are three more residential building typologies for which structural models are not currently available, and so engineering judgment has been applied to modify the existing pushover curves. The typology RESD-URM-D (Labourer's cottage, see Figure 3.3) and the typology RESD-URM-E (Mansion, see Figure 3.3) both have one storey with an attic, solid walls and timber floors, and so they have been assigned the same capacity as RESD-URM-A. The typology RESD-URM-F (Large Villa, see Figure 3.3), on the other hand, has two storeys with an attic, though it still has solid walls and timber floors. The same base shear capacity has been assumed (to account for the fact that the overburden load has increased, but so too has the effective height), and the displacement capacity has been doubled to account for the higher effective height.



Figure 3.3. Labourer's cottage (RESD-URM-D, left), Mansion (RESD-URM-E, middle) and Large Villa (RESD-URM-F, bottom) building typologies

### 3.2.2 Residential terraced buildings

There are a number of different types of terraced buildings in Groningen (see Table 1.2), and a replica of one of the most predominant typologies (REST-URM-D), for which initial studies have shown poses a high fatality risk, has been designed, constructed and tested on the shaking table at the EUCENTRE laboratory in Pavia (EUCENTRE, 2015a and 2015b). This structure has concrete floors and cavity walls with a load-bearing calcium silicate inner leaf and a non load-bearing clay outer leaf, with an 8cm gap and approximately 2 steels ties per  $m^2$  connecting the two leaves. The structure was subjected to incremental dynamic testing, and the envelope of all test results (in terms of base shear versus 2<sup>nd</sup> floor displacement) is shown in Figure 3.4.

Following the application of a number of accelerograms of increasing levels of ground shaking intensity, which caused stiffness reduction of the structure and an increase in the fundamental period of vibration from 0.16 to 0.26 s (as obtained by the dynamic identification tests carried out after each test run), under the maximum level of shaking the base shear reached 130 kN (about 25% of the weight) and the second floor displaced by 40 mm. The structure did not collapse but was near collapse, as verified by the significant drop in strength and stiffness that was observed when the damaged structure was subjected to a subsequent final test run.

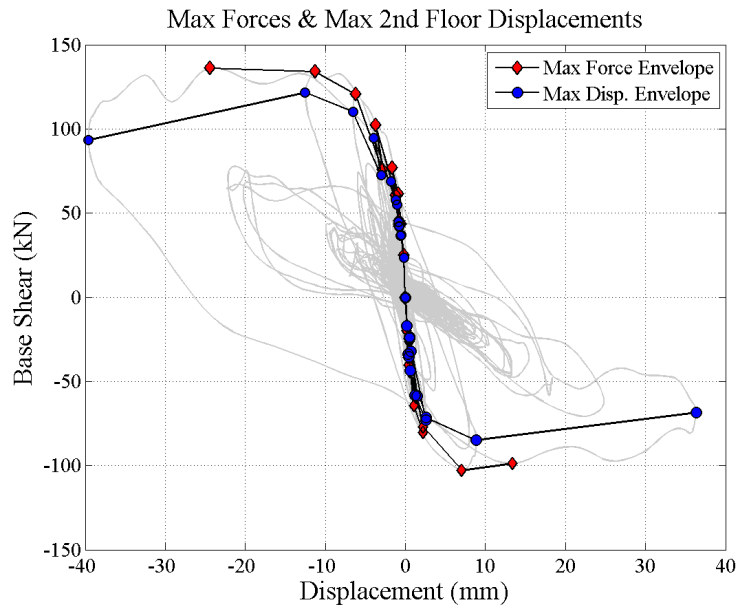


Figure 3.4. Envelope of the incremental dynamic testing results of the terraced building unit tested on the shaking table

The work of validating numerical models with the numerous sets of experimental test data is ongoing (Arup, 2015a, 2015b, 2015c) and will be fully integrated into the v3 fragility function derivation. For the purposes of the v2 model, the aforementioned terraced building has been modelled in the ELS software, and an initial calibration using the experimental results has been carried out, with particular focus given to the predicted values of base shear and ultimate displacement response (Figure 3.5). Both the experimental test results and the numerical models have confirmed that the lateral resistance of these terraced buildings in the longitudinal direction is mainly provided by the transverse walls, provided the “flange-effect” that is created by the connection of the transverse walls to the longitudinal piers is maintained. The transverse walls obviously also provide the majority of the lateral resistance in the transverse direction.

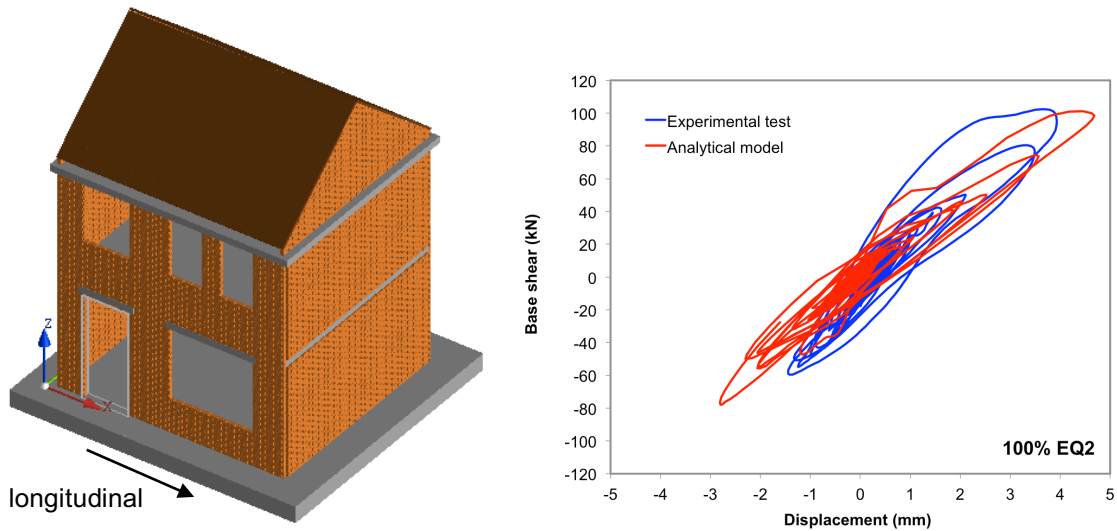


Figure 3.5. ELS model of URM terraced house (left) tested on the shake table and calibrated to the experimental results (right)

To represent an average REST-URM-D typology in the field, the preliminary in-situ masonry properties mentioned previously have been used in this model (replacing therefore the characteristics of the masonry for the structure tested on the shake table). A pushover analysis of the structure has been undertaken to understand the in-plane capacity and has been transformed to a SDOF curve, as presented in Figure 3.6. The same pushover curve has been adopted for typology REST-URM-C, as the influence of the party walls (solid versus cavity) is judged to have a limited impact on the capacity. This assumption will be tested in the future using structural models with more than one terraced building unit, with both cavity and solid party walls.

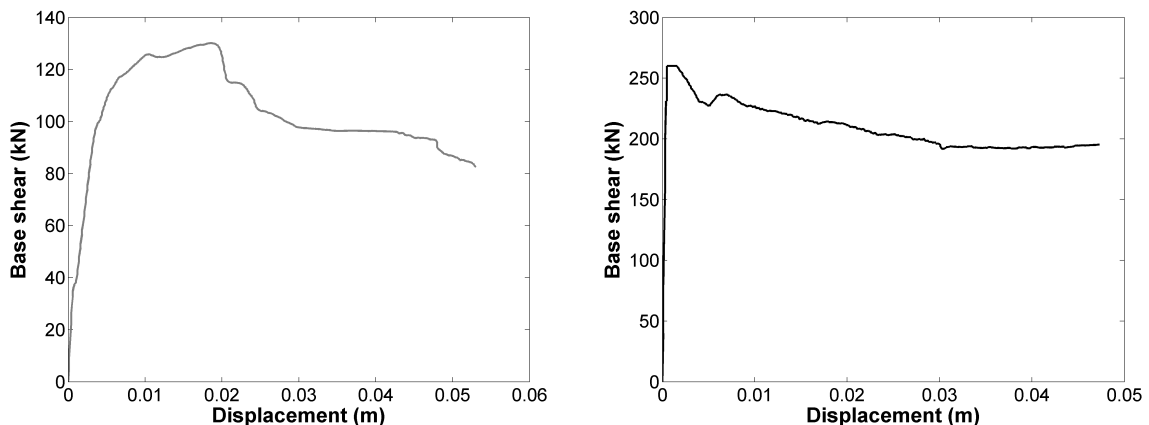


Figure 3.6. SDOF pushover curve for REST-URM-C/D in longitudinal direction (left) and transverse direction (right)

Modifications to this model have been made to represent the other terraced building typologies. The typology REST-URM-B has been developed by reducing the load on the floors considering that they are constructed with timber, whilst the REST-URM-A model has been produced by also changing the walls to solid clay bricks of 200 mm

width. The SDOF pushover curves of these two typologies were found to be very similar, and so the same average pushover curve has been assumed for both (see Figure 3.7). The typology REST-URM-E has been developed by changing the top floor to timber, and REST-URM-F has been assumed to have the same in-plane capacity (see Figure 3.8).

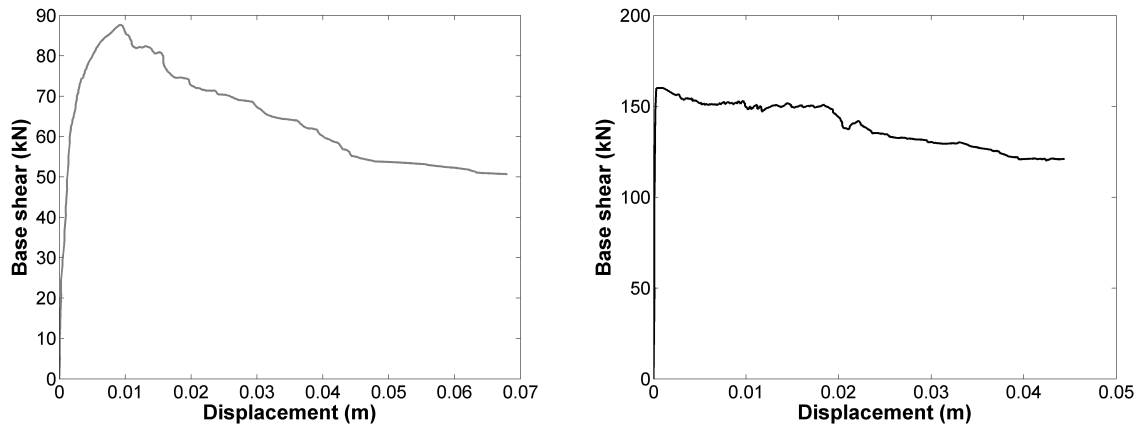


Figure 3.7. SDOF pushover curve for REST-URM-A/B in longitudinal direction (left) and transverse direction (right)

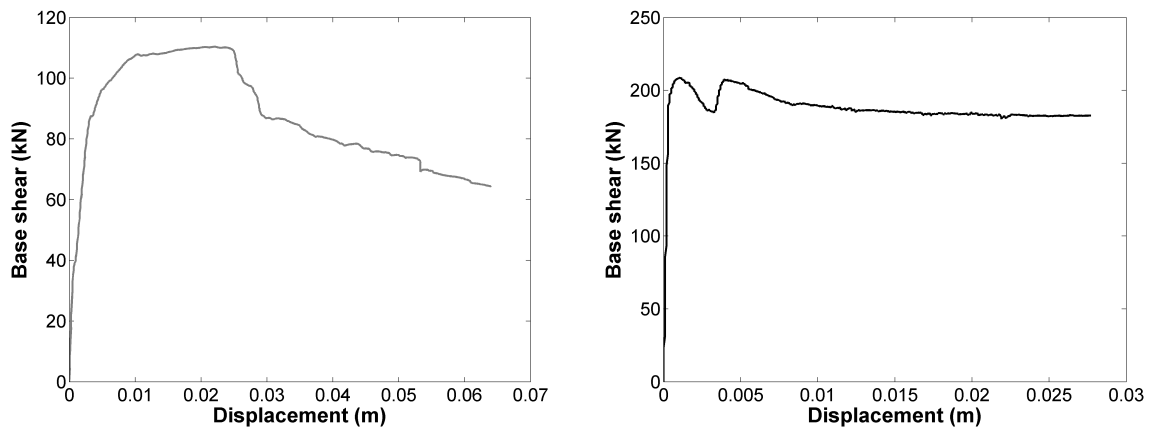


Figure 3.8. SDOF pushover curve for REST-URM-E/F in longitudinal direction (left) and transverse direction (right)

### 3.2.3 Residential apartment buildings

Residential apartment buildings in unreinforced masonry are typically three to four storeys and are constructed with either two-wythe solid clay brick walls and timber floors (so-called ‘herenhuis’, labelled RESA-URM-A in Table 1.2) or with calcium silicate inner leaf and clay outer leaf cavity walls with hollow core concrete floors (REST-URM-B), as illustrated in Figure 3.9.



Figure 3.9. Typical RESA-URM-A (left) and RESA-URM-B (right) buildings

Structural drawings of real buildings are not currently available for these typologies and so a prototype model for RESA-URM-A has been created in ELS using typical dimensions and the aforementioned calcium silicate properties. The SDOF pushover curve is shown in Figure 3.10. The façade, party and transverse walls of this model are similar to those of the terraced buildings, but additional longitudinal walls have been added to withstand the gravity loads from the long span floors (as shown in the model in Figure 3.10). This model has been modified to represent RESA-URM-B by reducing the 0.2m solid clay walls to 0.15m calcium silicate walls, and increasing the loads to those of a typical concrete floor. The SDOF pushover curve for this typology is shown in Figure 3.11.

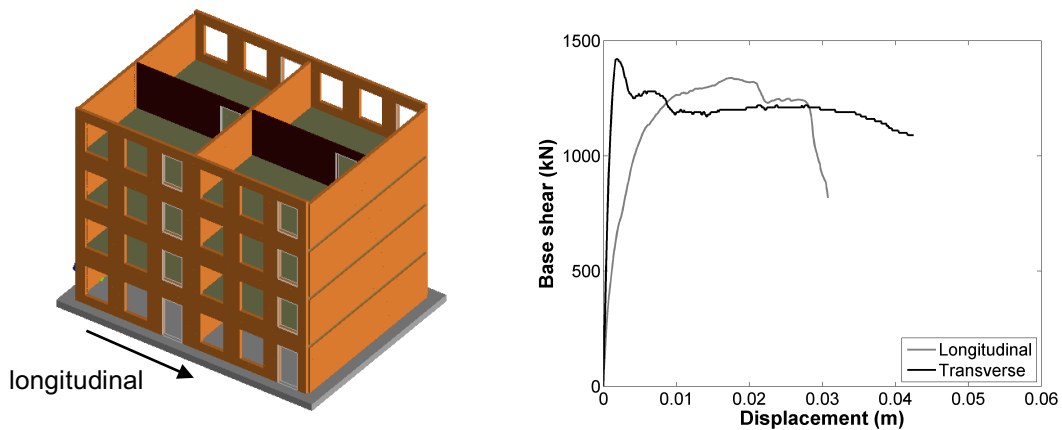


Figure 3.10. ELS model for RESA-URM-A without roof slab (left) and SDOF pushover curve (right)

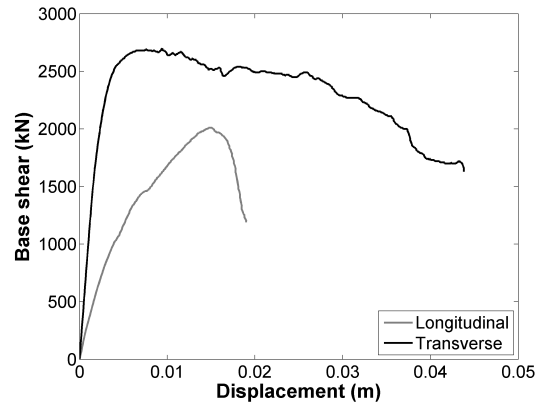


Figure 3.11. SDOF pushover curves for RESA-URM-B

When these building typologies have commercial activities at the ground floor, some of the ground floor walls are replaced with steel frames or precast columns (typologies RECA-URM-A and RECA-URM-B in Table 1.2). Although the latter structural elements will ensure that gravity loads are supported and transmitted to the foundation, they will typically lack the lateral stiffness/strength that characterised the removed walls. The aforementioned prototype model has been modified to represent RECA-URM-A/B by increasing the size of the openings in the front façade wall and the internal longitudinal walls. As expected, this typology features a soft storey response, and the SDOF pushover of this model is shown in Figure 3.12.

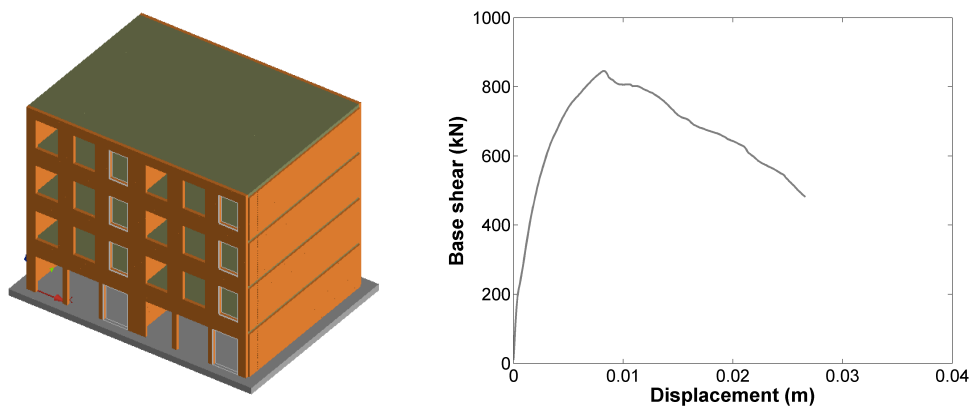


Figure 3.12. ELS model of RECA-URM-A (left) and SDOF pushover curve in longitudinal direction (right)

### 3.2.4 Industrial/commercial buildings

There are three URM industrial/commercial typologies in the exposure database (Table 1.2 – AGRI/INDU/COML-URM-A, COMO-URM-A and COMO-URM-B). There are currently no available structural drawings for buildings from these categories,

and so a prototype model of the structure shown in Figure 3.13 has been developed in ELS using typical dimensions. The SDOF pushover curves for this model are shown in Figure 3.14. The transverse direction pushover curve has been manually manipulated as the high stiffness of the structure in this direction led to a significant peak in the base shear which was found to be purely numerical when the loading step of the pushover was reduced. It was not possible to produce the full pushover curve using the smaller loading step due to the computational effort required.



Figure 3.13. A typical industrial/commercial URM building (left) and ELS prototype structure (right)

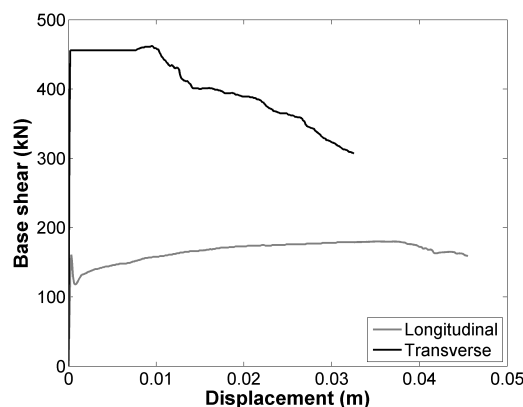


Figure 3.14. SDOF pushover curves from the ELS model of AGRI/INDU/COML-URM-A

### 3.3 Timber Buildings

There are five building typologies with timber structural members in the exposure model (see Table 1.2): detached and semi-detached timber frame/panel houses (RESD/RESS-W-A), barns with wooden trussed roofs (AGRI/INDU/COML-W-A) and glulam portal frames with either steel bracing or URM walls for lateral stability (AGRI/INDU/COML-W-B1 and B2). A model for each of these building types (based on the structural details of actual buildings from Groningen) has been produced using SeismoStruct (Seismosoft, 2015), as described in Mosayk (2015a), and

pushover curves have been developed and transformed to equivalent SDOF capacity curves in terms of base shear and displacement.

The same pushover curves have been assumed for detached and semi-detached timber frame/panel houses (RESD/RESS-W-A), as shown in Figure 3.15. The ultimate displacement capacity occurs following sliding and unseating of the frame from its foundation beam.

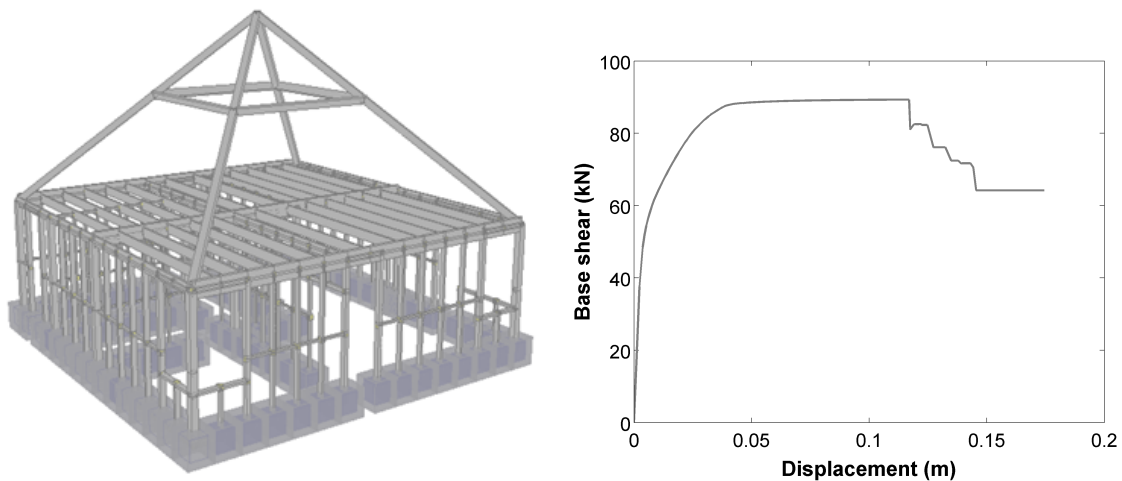


Figure 3.15. SeismoStruct model of RESD-W-A (left) and SDOF pushover curve (right)

The wooden trussed roofs of the old barns are highly ductile (see Figure 3.16), but they are assumed to rest on the non-bearing URM walls following settlement. As shown in Mosayk (2015a), including these URM walls (and modelling the friction between the roof and walls), significantly decrease the lateral displacement capacity of these structures due to convergence difficulties at drifts of around 0.5%. Given that the failure at these low levels of displacement would be at most a local collapse of the URM walls, and the integrity of the timber roof would still be maintained, the fatality risk would be very low. The main fatality risk of these buildings was instead judged to be from the internal URM structures shown in Figure 3.16 or the URM house, which is often attached to these old barns. These houses are not explicitly included in the exposure model (as they are grouped together with the barn) and so a decision has been taken to currently model AGRI/INDU/COML-W-A using the older detached URM building pushover curves (i.e. RESD-URM-A).

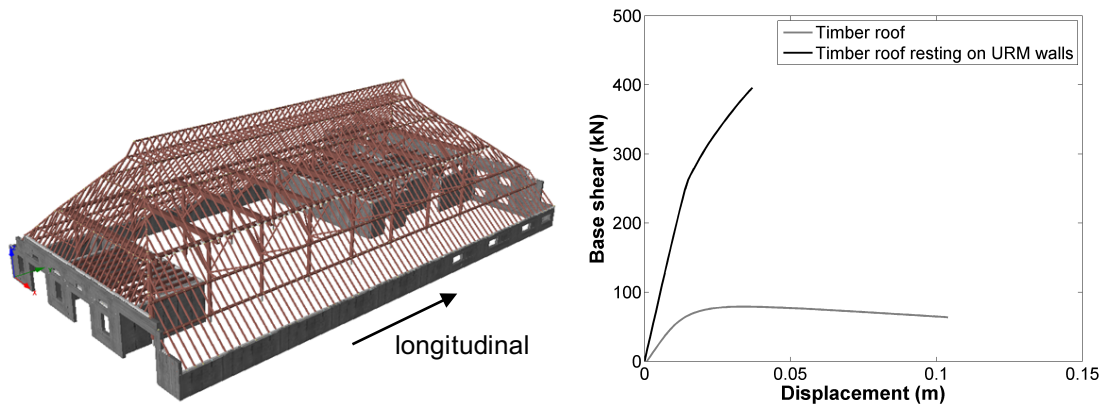


Figure 3.16. SeismoStruct model for AGRI/INDU/COML-W-A (left) and SDOF pushover curve both with and without URM walls (right)

Prototype models for the two glulam portal frames (AGRI/INDU/COML-W-B1 and B2) are assumed to have the same pushover curve in the transverse (shorter) direction, which is the direction in which the glulam portal acts (Mosayk, 2015a); this curve is shown in Figure 3.17. Semi-rigid connections have been included in this model, both at the base and the apex, and the ultimate displacement capacity is reached due to exceedance of their rotational capacity, after which the analyses are no longer able to converge.

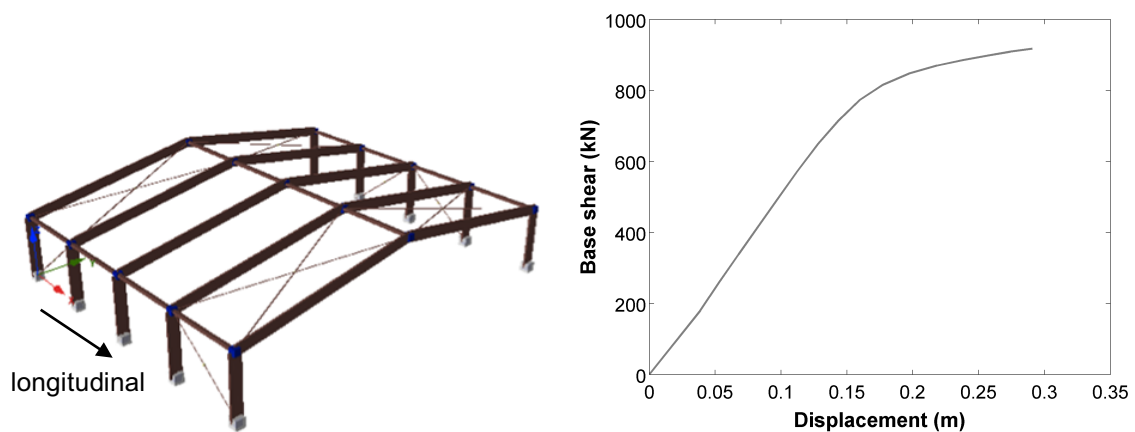


Figure 3.17. SeismoStruct model of AGRI/INDU/COML-W-B1 (left) and SDOF pushover curve (right) for the transverse direction of both AGRI/INDU/COML-W-B1 and B2

These glulam portal frames can have either steel bracing (B1) or URM infill panels (B2) in the longitudinal direction; the SDOF pushover curves are shown in Figure 3.18 and Figure 3.19, respectively. The ultimate displacement capacity in this direction occurs either due to excessive rotational capacity of the semi-rigid connections at the base (in the case of steel stability bracing), or in-plane collapse of the URM walls.

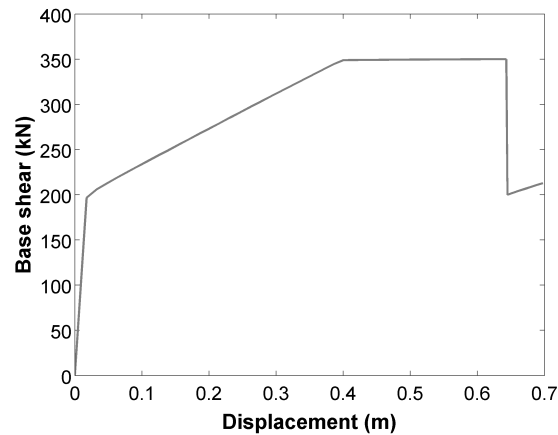


Figure 3.18. SDOF pushover curve for longitudinal direction of glulam portal frames with steel stability bracing (AGRI/INDU/COML-W-B1)

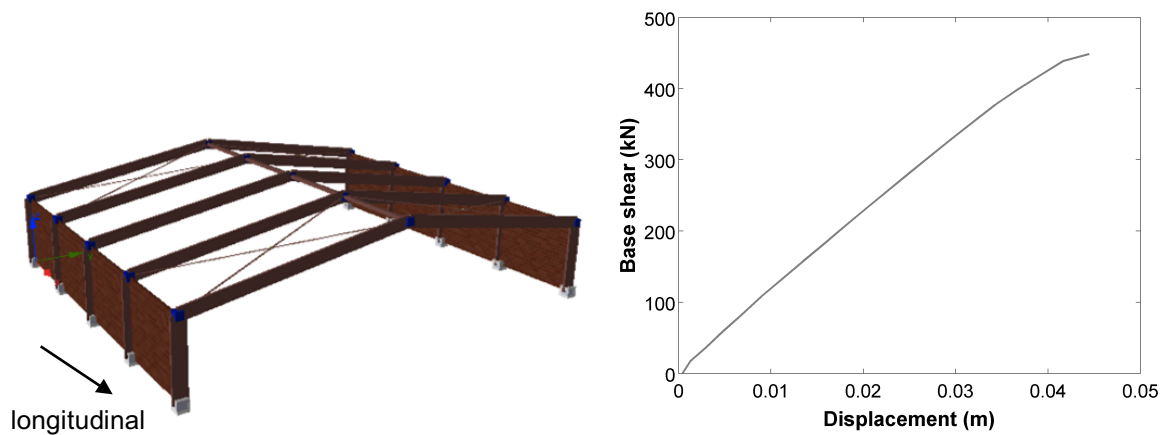


Figure 3.19. SeismoStruct model for glulam portal frames with URM infill walls (AGRI/INDU/COML-W-B2) and SDOF pushover curve for longitudinal direction

### 3.4 Steel Moment Frame Buildings

As shown in Table 1.2, there are three typologies with steel moment frames in the exposure model. It has been possible to produce models for only two of these typologies due to limited availability of time and data. The results of these two typologies have been used to inform the backbone curve for the remaining moment frame typologies.

A real steel portal frame building both with and without steel bracing has been modelled (Mosayk, 2015a) and the moment frame direction has been taken to represent AGRI/INDU/COML-S-B. The SDOF pushover curve is provided in Figure 3.20. The ultimate displacement has been taken at the point at which the base shear reduces to 60% of the ultimate base shear, which occurs following the exceedance

of the ultimate rotation capacity of the steel columns (where the latter has been defined following the recommendations of EC8; CEN, 2003).

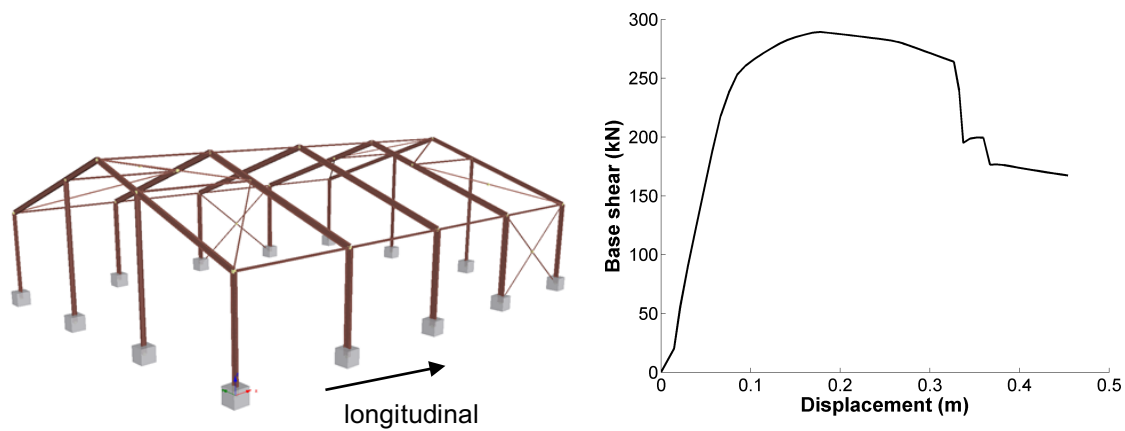


Figure 3.20. SeismoStruct model for AGRI/INDU/COML-S-A (left) and SDOF pushover curve in transverse direction (right), taken to represent AGRI/INDU/COML-S-B

Another real steel moment frame building has been modelled (Mosayk, 2015a) and has been used to present the less than 4 storeys steel moment frame typology (COMO-S-B-L4S). This building has very different base shear capacities in the two orthogonal directions, which is judged to be a common characteristic of such buildings.

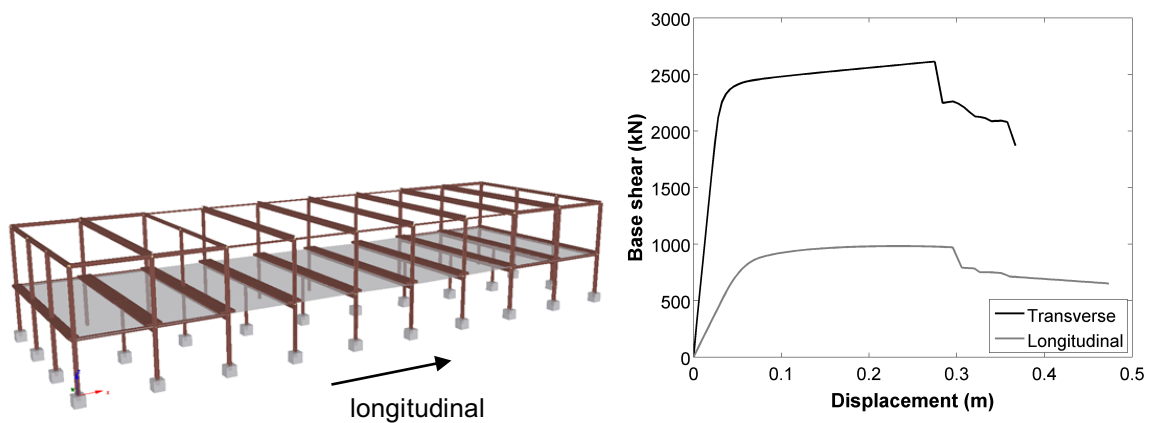


Figure 3.21. SeismoStruct model for COMO-S-B-L4S (left) and SDOF pushover curve (right)

In order to adapt these pushover curves for the greater than 4 storeys category, the effective mass of the structure has been increased proportionally, whilst the ultimate displacement capacity and moment capacity at the base have been kept the same (as they are dictated by the capacity of the ground floor, which is assumed to be unchanged), and the base shear has thus been recalculated assuming twice the effective height.

### 3.5 Steel Braced Frame Buildings

There are four typologies with steel braced frames in the exposure model (see Table 1.2). It has been possible to produce a model for only one of these typologies due to limited availability of time and data (this model has been shown previously in Figure 3.20). The SDOF pushover curve of this steel braced frame (AGRI/INDU/COML-S-A) is provided in Figure 3.20. Buckling of the bracing has been modelled (see Mosayk, 2015a) and the ultimate displacement capacity occurs due to excessive rotation of the columns.

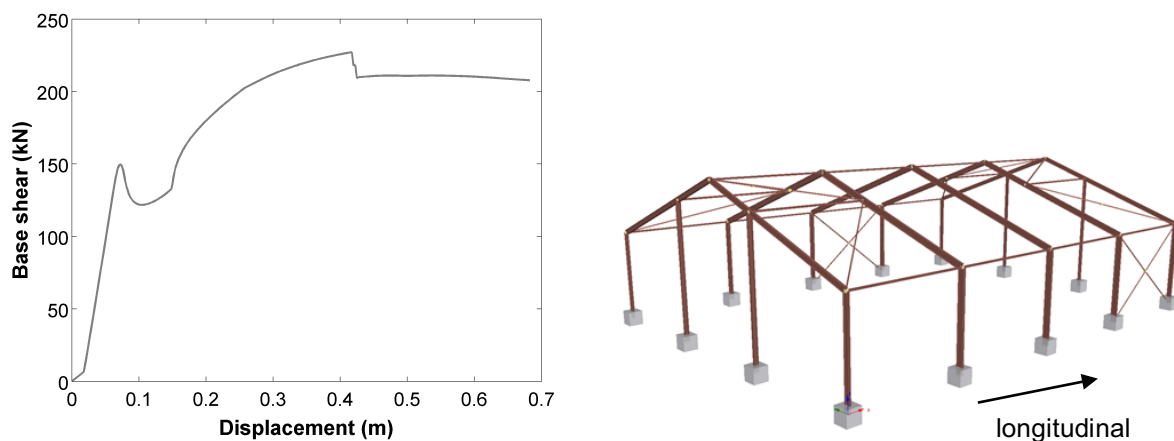


Figure 3.22. SDOF pushover curve (left) for AGRI/INDU/COML-S-A (longitudinal direction, right)

For the other three braced frame typologies, judgment-based adjustments to the capacity curves from the steel moment frame presented in Figure 3.21 have been made. The same mass has been assumed, whilst the structure has been assumed to be 20% stiffer/stronger with the same displacement capacities.

### 3.6 Reinforced Concrete Buildings

There are 19 reinforced concrete typologies in the exposure model, 10 of which are cast-in-place and 9 are pre-cast (see Table 1.2).

Five of these typologies relate to a cast-in-place tunnel form construction (so-called tunnelgietbouw) and two structural models have been used to develop the associated capacity curves. Given that the beam-column element formulation used in SeismoStruct may not represent well the response of these wall-dominated buildings, these structures have been modelled with the ELS software (also used previously for the URM buildings).

### 3.6.1 Residential buildings

The prototype model (described further in Mosayk, 2015a) for low-rise tunnelgietsbouw terraced houses (REST-RC-A) is presented in Figure 3.23, together with the SDOF pushover curve for the longitudinal direction, whilst the transverse direction is presented in Figure 3.24. This model has been developed based on advice from Groningen structural engineers, but it is felt that it may not feature a realistic reinforcement mesh (given the very high levels of ductility in the longitudinal direction) and this will need to be verified using structural drawings for this typology in the future. To account for this possible overestimation of the lateral displacement capacity in the model, the fragility functions have been developed using a reduced longitudinal ultimate capacity of 0.4m.

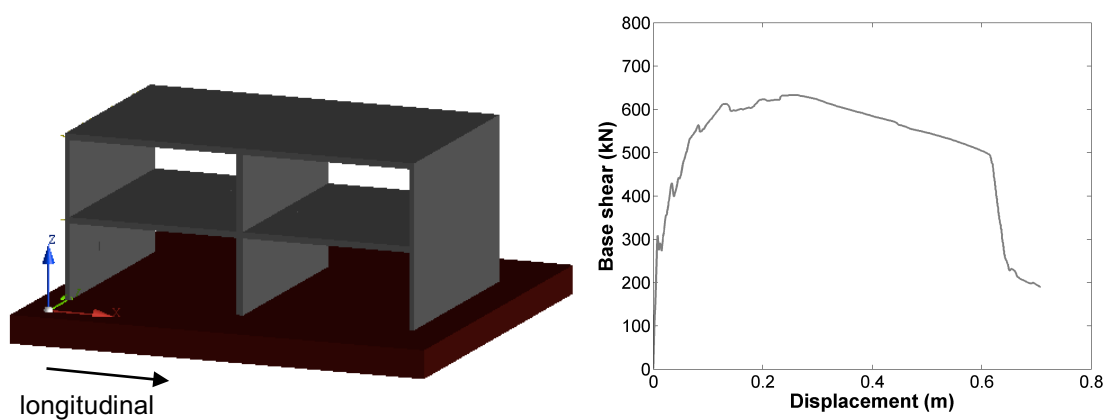


Figure 3.23. ELS model of an RC tunnel frame terraced building (left) and SDOF pushover curve for longitudinal direction (right)

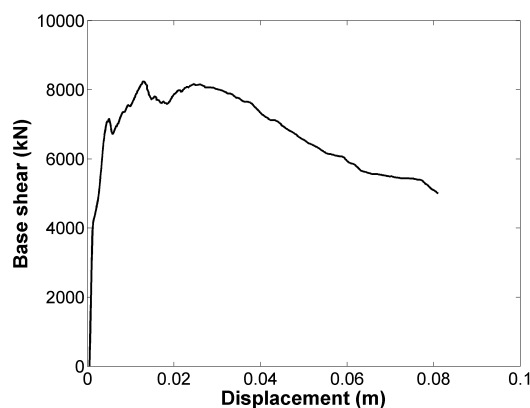


Figure 3.24. SDOF pushover curve transverse direction of RC tunnel frame terraced buildings

When this construction type is used for buildings of more than two storeys (i.e. for apartments, so-called RESA-RC-A-L4S and RESA-RC-A-G4S), additional walls are placed in the longitudinal direction and less transverse reinforcement (per area of wall) has been observed, as well as the possibility of no reinforcement in some of the

walls that were not expected, by the original designers, to be subjected to tensile forces (under gravity and wind loading).

A real building from Groningen has been modelled for this category using the ELS software, as further described in Mosayk (2015a). The SDOF pushover curves for both the longitudinal and transverse directions are presented in Figure 3.25.

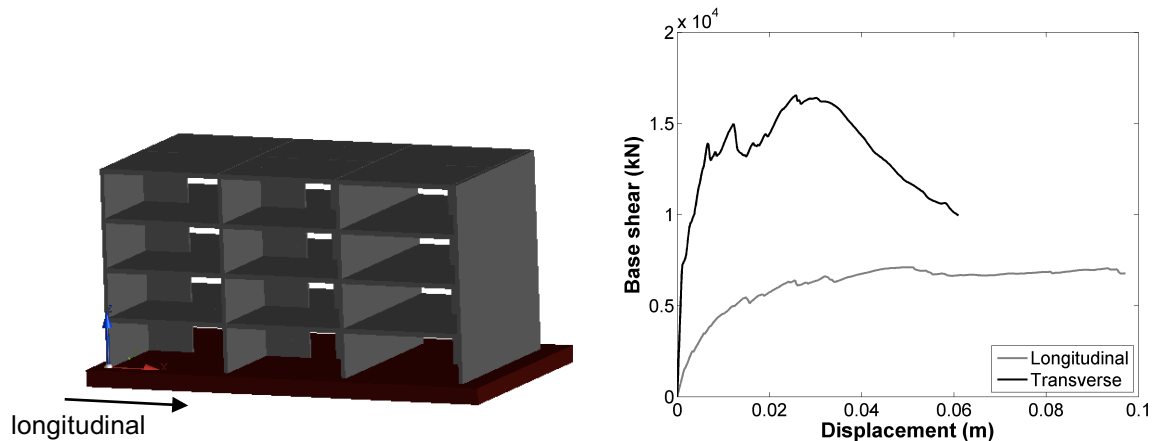


Figure 3.25. ELS model for RESA-RC-A-L4S and SDOF pushover curves (left)

The greater than 4-storey version of this typology has been developed through judgment. For an 8 storey structure it is assumed that a higher moment capacity would be reached at the base of the structure (due to more reinforcement being provided in the walls), and a base shear that is 75% of that of the low-rise structure has been assumed. The displacement capacity in the longitudinal direction has been assumed to be double, given that the response is dominated by a flexural mechanism in this direction, whilst in the transverse direction the displacement capacity has been kept the same.

For apartment buildings with commercial activities at the ground floor (RECA-URM-A-L4S and RECA-URM-A-G4S), it is assumed that the additional walls in the longitudinal direction would be replaced with columns, leading to a more flexible structure (with an assumed 20% increase in the period of vibration). In order to modify the ultimate base shear and displacement capacities, the relationship between the pushover curves for RESA-URM-A and RECA-URM-A has been used.

### 3.6.2 Commercial and industrial buildings

Although commercial RC moment frame buildings have been included in the exposure model (COMO-RC-A-L4S and COMO-RC-A-G4S), whilst searching the local municipalities for relevant drawings and details for this building typology, it was not possible to find a purely moment-frame building, and many also had structural walls. Hence, cast-in-place moment frame and core wall buildings (COMO-RC-B-L4S and COMO-RC-B-G4S) are currently assumed to have the same capacity

curves which, due to limitations of time, have currently been defined using the longitudinal direction of the apartment tunnel frame buildings (see Figure 3.25).

For the RC portal frames used in industrial buildings, it has been assumed that these are fairly standard buildings that follow typical construction practices elsewhere in Europe, and so models from Italian portal frame buildings have been used (see Mosayk, 2015a). Figure 3.26 presents the pushover curves of cast-in-place portal frames, whilst those with precast members (and steel dowel connections) are given in Figure 3.27. The latter are the same in both transverse and longitudinal directions as the capacity is conditioned by the beam-column connections. The ultimate displacement capacity in both cases is dictated by the rotational capacity of the reinforced concrete columns.

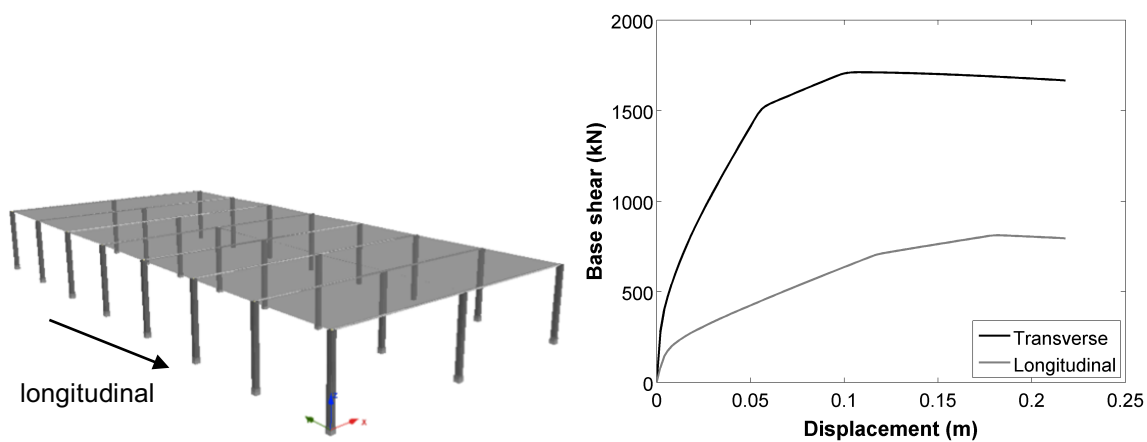


Figure 3.26. SeismoStruct model for RC cast-in-place beam-column frame buildings (left) and SDOF pushover curves (right)

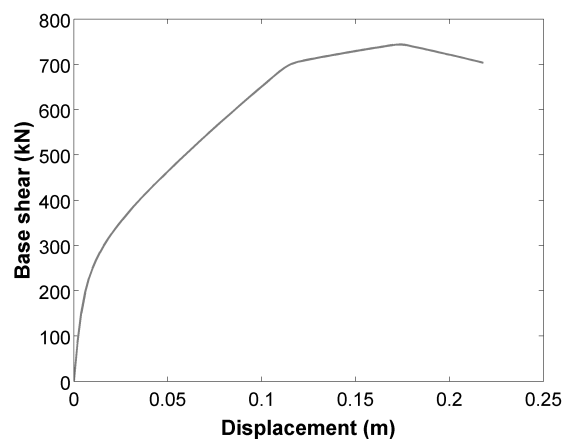


Figure 3.27. SDOF pushover curve for transverse and longitudinal directions of RC pre-cast beam-column frame buildings

For the pre-cast reinforced concrete wall buildings, a single unit terraced building model (described in Mosayk, 2015a) has been calibrated using the results of experimental tests carried (EUCENTRE, 2015c), and the SDOF pushover curves given in Figure 3.28 were obtained. Convergence issues were experienced in the

longitudinal direction, and given that failure is defined when the connections between panels can no longer provide resistance to stop the panels failing out of plane, the same ultimate displacement (from the transverse direction) has been assumed in both directions.

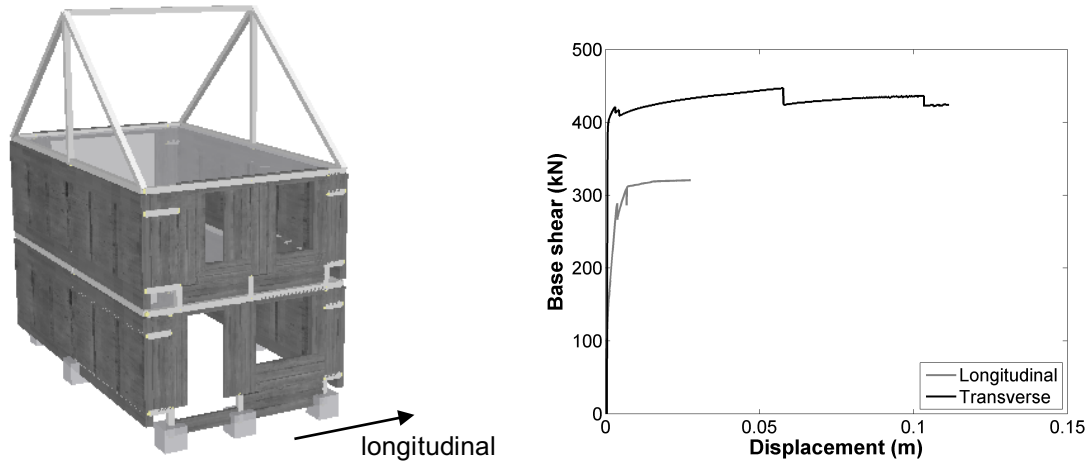


Figure 3.28. SeismoStruct model of RC pre-cast terraced house (REST-RC-B) and calibrated SDOF pushover curves for transverse and longitudinal direction

The same capacity curves have been considered for all precast buildings in the exposure model (about 0.1% of all buildings), until calibrated precast models for these other commercial and apartment buildings can be developed.

### 3.7 Summary of Backbone Curves

The SDOF pushover curves presented previously have been simplified with bi- and tri-linear curves, and are summarised in Table 3.1.

Table 3.1. Summary of SDOF pushover backbone curves for all building typologies

Building Typology	Dir.	Mass SDOF (t)	V <sub>1</sub> (kN)	D <sub>1</sub> (m)	V <sub>2</sub> (kN)	D <sub>2</sub> (m)	V <sub>3</sub> (kN)	Sd <sub>3</sub> (m)	T (s)	
RESD_W_A	Trans	17.7	60	0.003	87	0.02	95	0.12	0.19	
	Long	Same as Trans								
RESS_W_A	Trans	Same as RESD_W_A Trans								
	Long	Same as RESD_W_A Long								
A/I/C_W_B1	Trans	30.3	770	0.16	920	0.29	-	-	0.50	
	Long	30.6	200	0.03	350	0.4	350	0.64	0.43	
A/I/C_W_B2	Trans	Same as AGRI_INDU_COML_W_B1 Trans								
	Long	20	440	0.04	450	0.045			0.27	
A/I/C_W_A	Trans	Same as RESD_URM_A Trans								
	Long	Same as RESD_URM_A Long								
COMO_S_B_L4S	Trans	329	2250	0.03	2600	0.275	2000	0.35	0.42	
	Long	335	750	0.05	930	0.1	930	0.48	0.94	
COMO_S_B_G4S	Trans	987	1125	0.03	1300	0.275	1000	0.35	1.02	
	Long	1005	375	0.05	465	0.1	465	0.48	2.30	
A/I/C_S_A	Trans	15.7	150	0.07	230	0.42	-	-	0.54	
	Long	Same as Trans								
A/I/C_S_B	Trans	10.4	250	0.085	290	0.18	240	0.33	0.37	
	Long	Same as A/I/C_S_A Trans								
A/I/C_S_C	Trans	Same as COMO_S_A_L4S Trans								
	Long	Same as COMO_S_A_L4S Long								
COMO_S_A_L4S	Trans	329	2700	0.03	3120	0.275	2400	0.35	0.38	
	Long	335	900	0.05	1116	0.1	1116	0.48	0.86	
COMO_S_A_G4S	Trans	987	1350	0.03	1560	0.275	1200	0.35	0.93	

Building Typology	Dir.	Mass SDOF (t)	V <sub>1</sub> (kN)	D <sub>1</sub> (m)	V <sub>2</sub> (kN)	D <sub>2</sub> (m)	V <sub>3</sub> (kN)	Sd <sub>3</sub> (m)	T (s)	
	Long	1005	450	0.05	558	0.1	558	0.48	2.10	
REST_RC_A	Trans	228	4000	0.0008	8100	0.012	5000	0.08	0.04	
	Long	228	400	0.0275	620	0.2	500	0.4	0.79	
RESA_RC_A_L4S	Trans	1073	13000	0.006	15000	0.03	10000	0.06	0.14	
	Long	1073	4600	0.01	6800	0.04	6750	0.1	0.30	
RESA_RC_A_G4S	Trans	2146	9750	0.006	11250	0.03	7500	0.06	0.23	
	Long	2146	3450	0.02	5100	0.08	5062.5	0.2	0.70	
RECA_RC_A_L4S	Trans	Same as RESA_RC_A_L4S Trans								
	Long	1288	3450	0.009	4533	0.0267	4500	0.067	0.36	
RECA_RC_A_G4S	Trans	Same as RESA_RC_A_G4S Trans								
	Long	2575	2588	0.018	3400	0.0533	3375	0.133	0.84	
COMO_RC_A1_L4S	Trans	Same as RESA_RC_A_L4S Long								0.30
	Long	Same as RESA_RC_A_L4S Long								
COMO_RC_A1_G4S	Trans	Same as RESA_RC_A_G4S Long								0.70
	Long	Same as RESA_RC_A_G4S Long								
COMO_RC_A2_L4S	Trans	Same as RESA_RC_A_L4S Long								
	Long	Same as RESA_RC_A_L4S Long								
COMO_RC_A2_G4S	Trans	Same as RESA_RC_A_G4S Long								
	Long	Same as RESA_RC_A_G4S Long								
A/I/C_RC_A	Trans	719	475	0.006	1700	0.075	1650	0.218	0.60	
	Long	719	200	0.008	720	0.125	800	0.218	1.07	
A/I/C_RC_B1	Trans	719	200	0.006	700	0.12	700	0.218	0.92	
	Long	Same as Trans								
REST_RC_B	Trans	180	400	0.001	410	0.11			0.13	
	Long	180	300	0.006	320	0.11			0.38	
RESA_RC_B_L4S	Trans	Same as REST_RC_B Trans								0.13

Building Typology	Dir.	Mass SDOF (t)	V <sub>1</sub> (kN)	D <sub>1</sub> (m)	V <sub>2</sub> (kN)	D <sub>2</sub> (m)	V <sub>3</sub> (kN)	Sd <sub>3</sub> (m)	T (s)	
	Long	Same as REST_RC_B Long							0.38	
RESA_RC_B_G4S	Trans	Same as REST_RC_B Trans								
	Long	Same as REST_RC_B Long								
RECA_RC_B_L4S	Trans	Same as REST_RC_B Trans								
	Long	Same as REST_RC_B Long								
RECA_RC_B_G4S	Trans	Same as REST_RC_B Trans								
	Long	Same as REST_RC_B Long								
A/I/C_RC_B2	Trans	Same as REST_RC_B Trans							0.13	
	Long	Same as REST_RC_B Long							0.38	
COMO_RC_B_L4S	Trans	Same as REST_RC_B Trans								
	Long	Same as REST_RC_B Long								
COMO_RC_B_G4S	Trans	Same as REST_RC_B Trans								
	Long	Same as REST_RC_B Long								
A/I/C-URM-A	Trans	42	125	0.0002	180	0.025	160	0.045	0.05	
	Long	42	450	0.0002	460	0.01	310	0.032	0.03	
COMO-URM-A	Trans	Same as A/I/C-URM-A Trans								
	Long	Same as A/I/C-URM-A Long								
COMO-URM-B	Trans	Same as A/I/C-URM-A Trans								
	Long	Same as A/I/C-URM-A Long								
RECA-URM-A	Trans	Same as RESA-URM-A								
	Long	199	500	0.002	830	0.007	500	0.026	0.18	
RECA-URM-B	Trans	584	Same as RESA-URM-B							
	Long	584	591	0.002	1253	0.006	732	0.016	0.28	
RESA-URM-A	Trans	165	1400	0.0016	1200	0.01	1100	0.042	0.09	
	Long	165	1100	0.006	1325	0.02	820	0.031	0.19	
RESA-URM-B	Trans	485	1500	0.0015	2700	0.006	1620	0.044	0.14	

Building Typology	Dir.	Mass SDOF (t)	V <sub>1</sub> (kN)	D <sub>1</sub> (m)	V <sub>2</sub> (kN)	D <sub>2</sub> (m)	V <sub>3</sub> (kN)	Sd <sub>3</sub> (m)	T (s)	
	Long	485	1300	0.006	2000	0.016	1200	0.019	0.30	
RESD-URM-A	Trans	66	475	0.0003	360	0.011	338	0.021	0.04	
	Long	Same as Trans								
RESD-URM-B	Trans	52	240	0.0002	280	0.002	235	0.014	0.04	
	Long	Same as Trans								
RESD-URM-C	Trans	100	370	0.0005	550	0.002	460	0.011	0.07	
	Long	Same as Trans								
RESD-URM-D	Trans	Same as RESD-URM-A Trans								
	Long	Same as RESD-URM-A Long								
RESD-URM-E	Trans	Same as RESD-URM-A Trans							0.04	
	Long	Same as RESD-URM-A Long								
RESD-URM-F	Trans	132	475	0.0006	360	0.022	338	0.042	0.08	
	Long	Same as Trans								
RESS-URM-A	Trans	Same as RESD-URM-A Trans								
	Long	Same as RESD-URM-A Long								
RESS-URM-B	Trans	Same as REST-URM-B Trans							0.04	
	Long	Same as REST-URM-B Long								
RESS-URM-C	Trans	Same as REST-URM-C Trans								
	Long	Same as REST-URM-C Long								
REST-URM-A	Trans	32	160	0.0003	120	0.045			0.05	
	Long	32	64	0.002	85	0.008	51	0.068	0.20	
REST-URM-B	Trans	Same as REST-URM-A Trans							0.05	
	Long	Same as REST-URM-A Long							0.20	
REST-URM-C	Trans	47	260	0.0008	260	0.002	195	0.047	0.08	
	Long	47	62	0.002	130	0.007	78	0.053	0.24	
REST-URM-D	Trans	Same as REST-URM-C Trans								

Building Typology	Dir.	Mass SDOF (t)	V <sub>1</sub> (kN)	D <sub>1</sub> (m)	V <sub>2</sub> (kN)	D <sub>2</sub> (m)	V <sub>3</sub> (kN)	Sd <sub>3</sub> (m)	T (s)
	Long	Same as REST-URM-C Long							
REST-URM-E	Trans	37.5	205	0.0006	180	0.027			0.07
	Long	37.5	65	0.002	110	0.006	65	0.064	0.21
REST-URM-F	Trans	Same as REST-URM-E Trans							
	Long	Same as REST-URM-E Long							

### 3.8 Variability in Backbone Curves

The building models presented in the previous sections are index buildings that are assumed to represent the median capacity of a given building typology. The validity of this assumption for the URM buildings in particular should be studied during the development of the v3 fragility functions, and structural drawings for a number of index buildings of each typology are currently being collected for this purpose. The URM models presented previously do not account for the fact that some buildings could have, for example, weaker connections leading to failure of wall-to-floor connections, failure of the floor diaphragm, or premature failure of the vertical line joint present in the wall piers of a terraced house. This building-to-building variability is not currently treated as an aleatory variability and is instead considered to be part of the epistemic uncertainty, as discussed further in Section 7.2.

Instead, the uncertainty in the ultimate displacement capacity across a typology (which includes the influence of the variation in material and mechanical properties on the capacity for all typologies), is treated as an aleatory variability and has been assumed to follow a lognormal distribution with a coefficient of variation (CoV) of 30% (i.e. a dispersion of 0.294). This value has been obtained by taking upper and lower bound values of the ultimate drifts found in tests of rocking and non-rocking walls as the 5% and 95% percentile of a lognormal distribution (Guido Magenes and Andrea Penna, personal communication), and from the work of Silva et al. (2013), who produced capacity curves for one hundred reinforced concrete (RC) moment resisting frames using Monte Carlo simulation (to vary the geometrical and material properties). Similar coefficients of variation (CoV) for RC pre-cast industrial buildings were also found by Casotto et al. (2015), whilst Dymiotis et al. (1999) found a similar CoV in the ultimate inter-storey drifts capacities from experimental tests.

## 4 Development of In-plane Hysteresis Models

### 4.1 Introduction

As discussed in Section 3.1, the in-plane response of the building typologies from Table 1.2 is modelled using equivalent SDOF systems with appropriate backbone curves and hysteretic models. Backbone curves for each direction of the 56 typologies have been presented in the previous chapter. This chapter presents the hysteretic models, which have been developed for the following “hysteresis groups”:

1. URM walls
2. Timber frames
3. Steel moment frames
4. Steel braced frames
5. RC beam-column frames
6. RC dual wall-frames (i.e. tunnel construction)
7. Precast RC walls

The hysteretic behaviour of these groups has been based on the *Hysteretic*, *Self-centering* and *Pinching4* models implemented into the OpenSees finite element package (McKenna et al., 2000).

Hysteretic<sup>1</sup> is a general-purpose hysteretic material model that can model pinching, damage due to both ductility and energy, and unloading stiffness degradation (Figure 4.1).

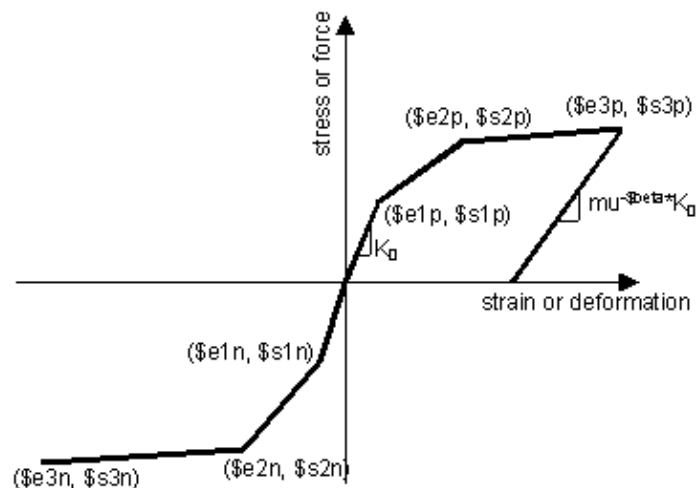


Figure 4.1. OpenSees Hysteretic material model

Self-centering<sup>2</sup> is a flag-shaped material object with optional non-recoverable slip behaviour and an optional stiffness increase at high strains (bearing behaviour)

<sup>1</sup> [http://opensees.berkeley.edu/wiki/index.php/Hysteretic\\_Material](http://opensees.berkeley.edu/wiki/index.php/Hysteretic_Material)

(Figure 4.2). The material was primarily developed to model a self-centering energy-dissipative brace, but it can be used for any comparable self-centering system that exhibits a flag-shaped hysteretic response (for example: rocking wall systems where the uniaxial material is used as a moment/rotation hysteresis).

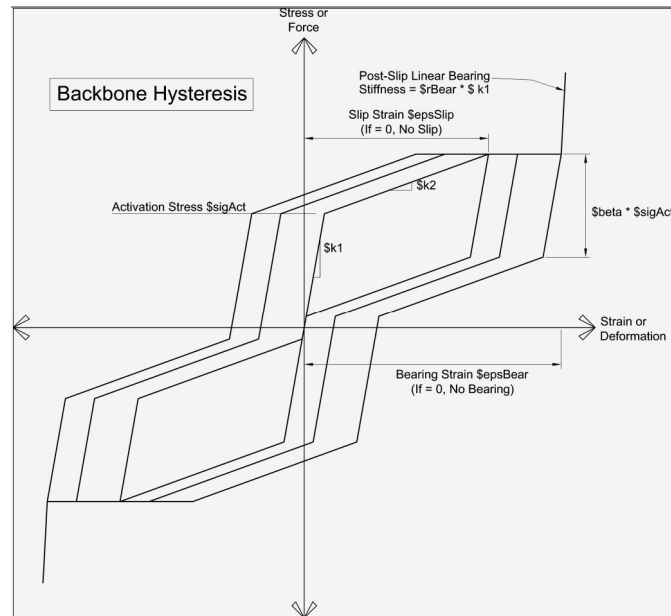


Figure 4.2. OpenSees Self-centering material model

Pinching4<sup>3</sup> is a uniaxial material that represents a 'pinched' load-deformation response and exhibits degradation under cyclic loading (Figure 4.3). Cyclic degradation of strength and stiffness occurs in three ways: unloading stiffness degradation, reloading stiffness degradation, strength degradation.

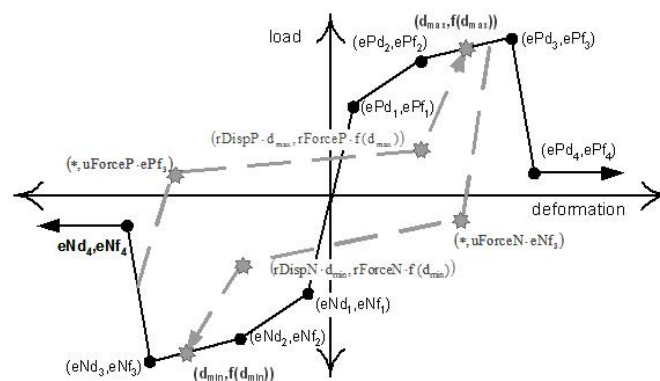


Figure 4.3. OpenSees Pinching4 material model

<sup>2</sup> [http://opensees.berkeley.edu/wiki/index.php/SelfCentering\\_Material](http://opensees.berkeley.edu/wiki/index.php/SelfCentering_Material)

<sup>3</sup> [http://opensees.berkeley.edu/wiki/index.php/Pinching4\\_Material](http://opensees.berkeley.edu/wiki/index.php/Pinching4_Material)

## 4.2 Calibration of Hysteresis Models

For the URM wall and precast RC wall groups, the hysteresis models have been calibrated using the available experimental test results.

For the non-URM groups, structural models for each hysteresis group have been selected (based on those presented in Chapter 2) and cyclic pushovers have been produced. The loading protocol for these cyclic pushovers has been taken from the suggestions of Mergos and Beyer (2014), considering 2 sets of cycles at each load level (the authors proposed this protocol specifically for European regions with low to moderate seismicity).

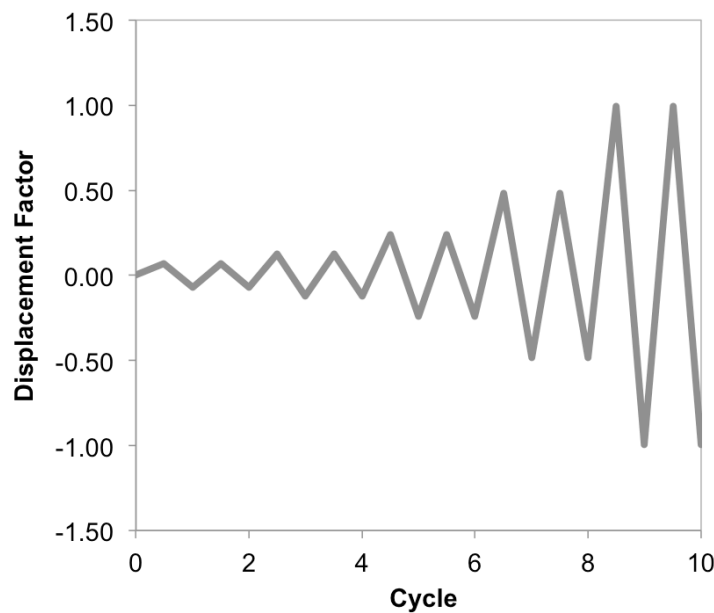


Figure 4.4. Loading protocol used for the cyclic pushover analyses of non-URM structures (based on proposals from Mergos and Beyer, 2014)

### 4.2.1 URM Walls

In order to calibrate the hysteretic model for masonry buildings, the dynamic response from the shaking table test of the full-scale terraced house has been used (EUCENTRE, 2015b). As mentioned previously, this was an incremental dynamic test and a number of records were applied in succession during the tests (EUCENTRE, 2015a), and thus the results of the later events in the sequence represent the response of a damaged structure. It was judged that the response under 160% of EQ2 was appropriate to represent an existing structure in the field, which may have pre-existing damage from small earthquakes, but has not been heavily damaged.

A pushover curve of the model presented in Section 3.2.2 (with the appropriate properties of masonry taken from the shaking table test building) was first undertaken to obtain a backbone curve, and then the additional parameters of the Hysteretic model were calibrated to obtain a similar response to the test (Figure 4.5).

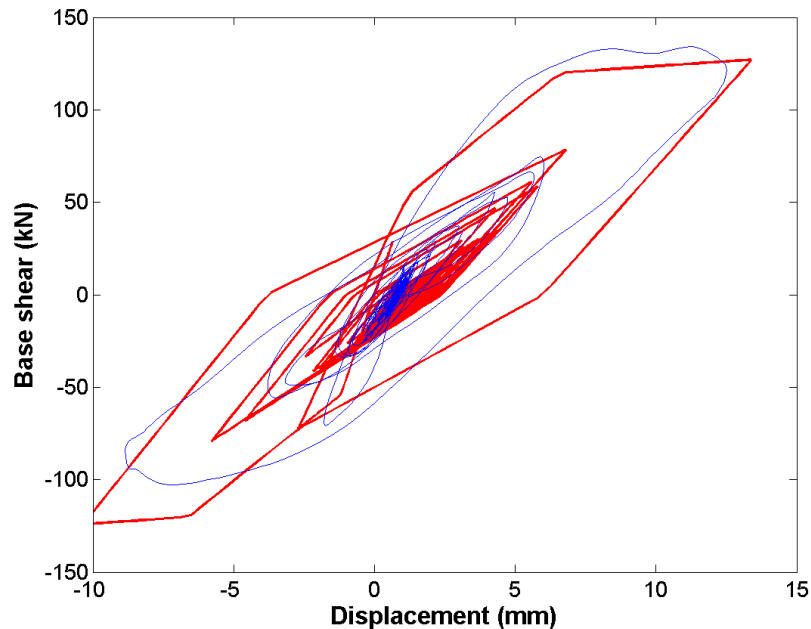


Figure 4.5. Shaking table test base shear versus displacement response and calibrated Hysteretic model

The calibration of a hysteretic model against one dynamic test is obviously not sufficient to ensure all the features of stiffness and strength degradation (between-cycle and in-cycle) of these URM buildings are being adequately represented. Other hysteretic models which allow between-cycle and in-cycle strength deterioration to be explicitly modelled (e.g. Ibarra et al., 2005) will also be considered in future updates. However, this is likely to be more important for estimating collapse due to global instability (see Section 1.4.3), whereas such variations in hysteretic models have been found to have a limited influence on the nonlinear displacement response before global collapse (e.g. Ibarra and Krawinkler, 2005) and so further developments to the hysteretic models for partial collapse may not be necessary.

#### 4.2.2 Timber Frames

The detached timber frame house model (without accounting for the timber panels) described in Section 3.3 has been used to calibrate the hysteresis model for timber buildings. The comparison of the cyclic pushover of the building and the calibrated hysteresis model is shown in Figure 4.6. As the Hysteretic model only allows a trilinear backbone curve, it has not been possible to capture well the change in initial stiffness in the response, but the calibrated model is deemed to be adequate for the purposes of developing fragility functions.

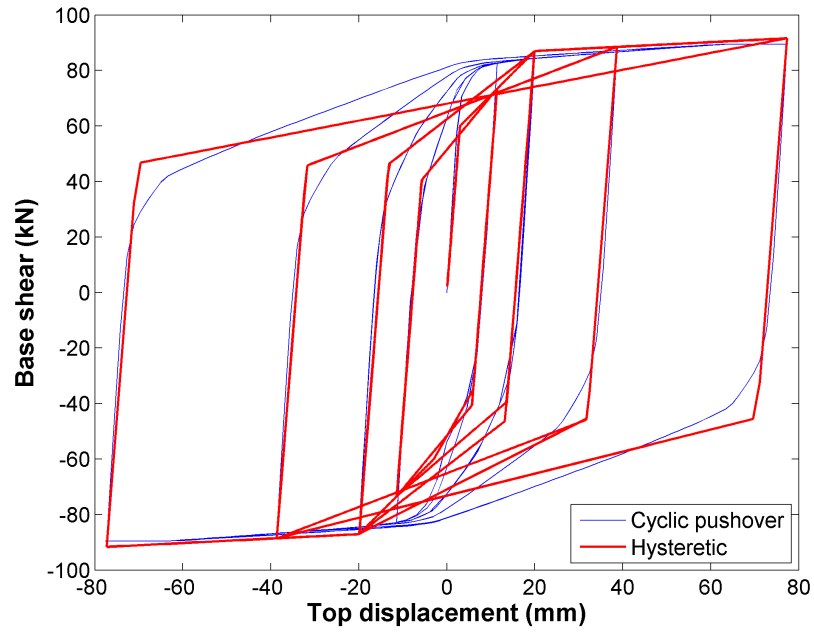


Figure 4.6. Cyclic pushover and calibrated Hysteretic model for timber frames

#### 4.2.3 Steel Moment Frames

The 2-storey commercial steel frame building model described in Section 3.4 has been used to calibrate a hysteresis model for steel moment frames. As shown in Figure 4.7, the model matches fairly well the cyclic response.

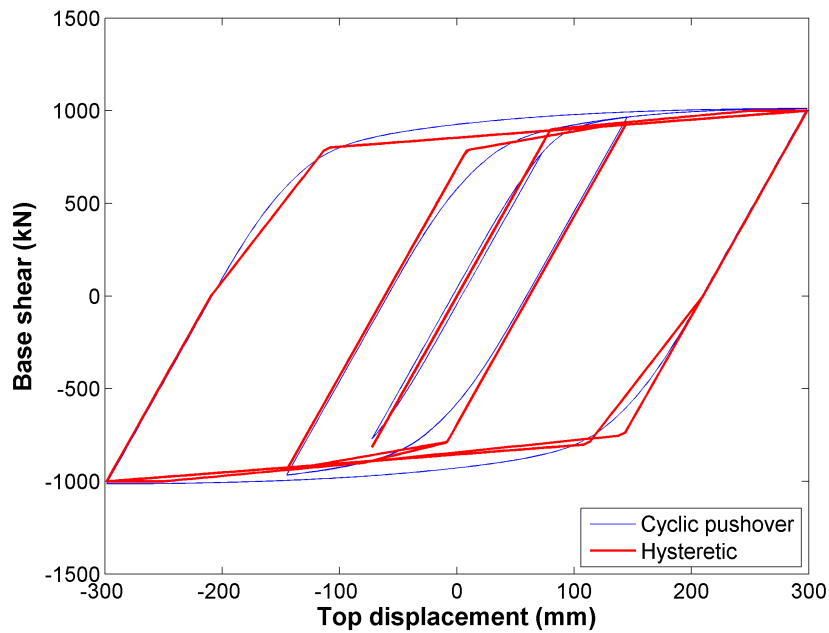


Figure 4.7. Cyclic pushover and calibrated Hysteretic model for steel moment frames

#### 4.2.4 Steel Braced Frames

The 1-storey industrial steel braced model described in Section 3.5 has been used to calibrate the hysteresis model for steel braced frames (where the frame action cannot be relied upon). Figure 4.8 shows the calibrated Hysteretic model.

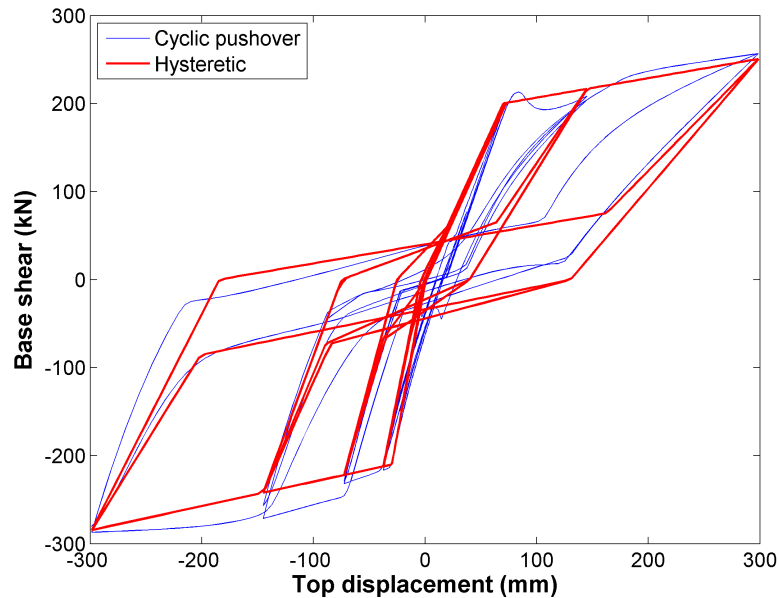


Figure 4.8. Cyclic pushover and calibrated Hysteretic model for steel braced frames

#### 4.2.5 Reinforced Concrete Beam-Column Frames

For RC beam-column frames, the structural model presented previously in Figure 3.26 has been used and the results are presented in Figure 4.9.

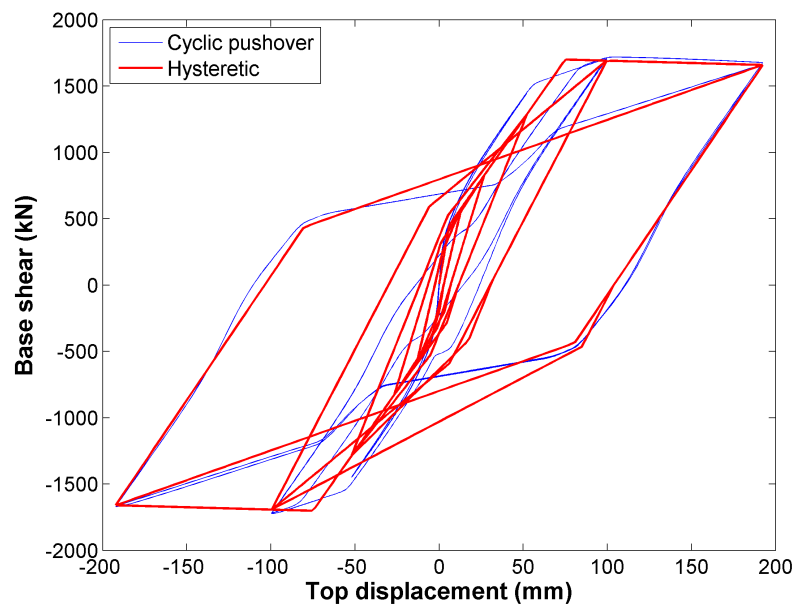


Figure 4.9. Cyclic pushover and calibrated Hysteretic model for RC beam-column frame buildings

#### 4.2.6 Reinforced Concrete dual wall-frames

The longitudinal direction of a tunnel frame building model without longitudinal walls has been used to calibrate a hysteretic model and as seen in Figure 4.10, there is very limited energy dissipation of these structures, which is due to the insufficient levels of reinforcement in the slab.

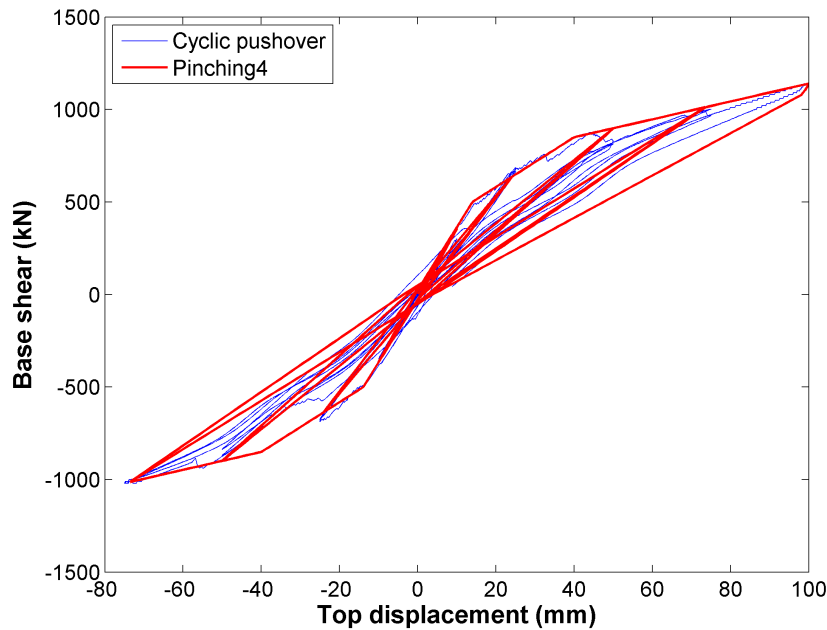


Figure 4.10. Cyclic pushover and calibrated Pinching4 model for RC tunnel buildings in the longitudinal direction (without longitudinal walls)

For buildings with walls in the longitudinal direction, a cyclic pushover of the longitudinal direction of the model in Figure 3.25 has been undertaken, and the calibrated hysteresis model was found to match well that presented previously in Figure 4.10. Hence, this model has also been used for RC buildings with walls.

#### 4.2.7 Precast Reinforced Concrete Walls

The tests carried out the EUCENTRE laboratory on connected precast panels (EUCENTRE, 2015c) have been used to calibrate a hysteresis model for structures with precast walls. The hysteresis of the connected walls with high overburden load (both with and without openings) was dominated by rocking behaviour. The calibration of one of the tested walls has been used for the SDOF system, and this required the use of both the Hysteretic and Self-Centering models in parallel (Figure 4.11).

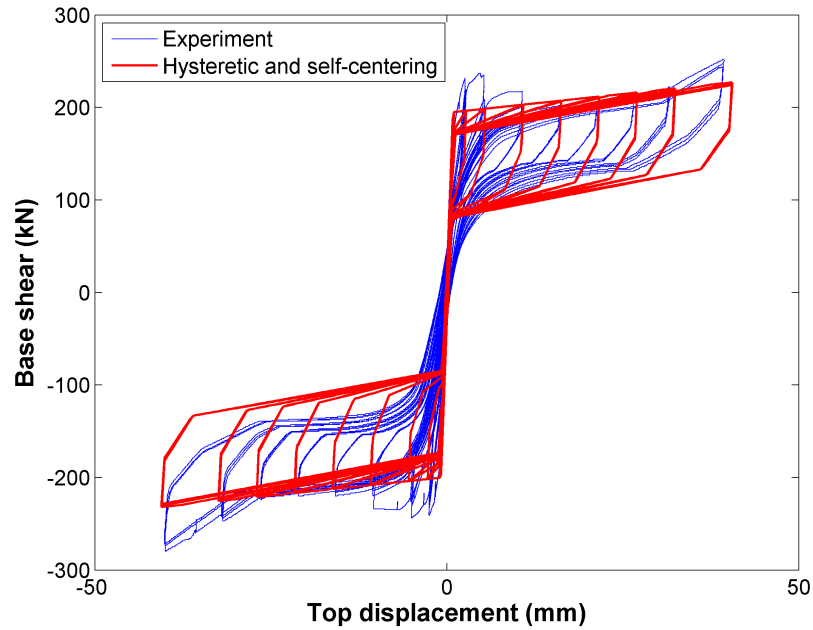


Figure 4.11. Cyclic test of precast wall panel and calibrated Hysteretic and self-centering models (placed in parallel)

The response shown in Figure 4.11 represents that of two connected panels, and not a full building. Hence, in the future, the test results will be used to calibrate a number of hysteretic models for the different walls of a pre-cast building (i.e. with different openings and levels of overburden load), and they will be combined to produce a plastic-hinge model of a full building, which could potentially be directly used for the development of the fragility functions, provided it is computationally efficient.

### 4.3 Summary of all hysteresis models

Table 4.1, Table 4.2 and Table 4.3 present a summary of the calibrated hysteresis parameters. These values are used for all building typologies of a given hysteresis group, whilst the parameters related to the backbone curve for each hysteresis model are not shown therein, as they are modified for each specific building typology (as presented previously in Table 3.1).

Table 4.1. Summary of calibrated OpenSees Hysteretic model parameters (all other parameters not provided are taken as zero)

Parameter	Description	URM wall	Timber frame	Steel Frame	Steel Braced	RC Precast Wall	RC Frame
pinchX	Pinching factor for strain (or deformation) during reloading	0	0.	0.2	0.95	0	0
pinchY	Pinching factor for stress (or force) during reloading	0	0.5	0.8	0.3	0	0.2
Damage 2	Damage due to energy	0	0	0	0	0.1	0
Beta	Power used to determine the degraded unloading stiffness based on ductility	0.4	0	0	0.45	0.4	0.4

Table 4.2. Summary of calibrated OpenSees Self-centering model parameters (all other parameters not provided are taken as zero)

Parameter	Description	RC Precast Wall
Beta	Ratio of Forward to Reverse Activation Stress/Force	0.2

Table 4.3. Summary of calibrated OpenSees Pinching4 model parameters (all other parameters not provided are taken as zero)

Parameter	Description	RC Frame-Wall
rDisp	Ratio of the deformation at which reloading occurs to the maximum historic deformation demand	-0.05
uForce	Ratio of strength developed upon unloading from negative load to the maximum strength developed under monotonic loading	-0.95

## 5 Development and Calibration of Out-of-Plane Models

### 5.1 Background to Out-of-Plane Model

The trilinear single degree of freedom (SDOF) out-of-plane (OOP) model presented in Doherty et al. (2002) has been used to model the rocking response of unreinforced masonry walls in the v2 fragility model; the incipient rocking force ( $F_0$ ), the static instability displacement ( $d_3$ ) and the other parameters of the model ( $F_1$ ,  $d_1$ ,  $F_2$ ,  $d_2$ ) are shown in Figure 5.1. For solid walls, the equations for a simply supported loadbearing wall can be considered (see Figure 5.2), whilst for cavity walls, the rocking force and effective mass for the simply supported loadbearing and non-loadbearing walls are added (considering that the two leaves are constrained to move together by the wall ties), and the static instability displacement is that which causes one of the walls to become unstable.

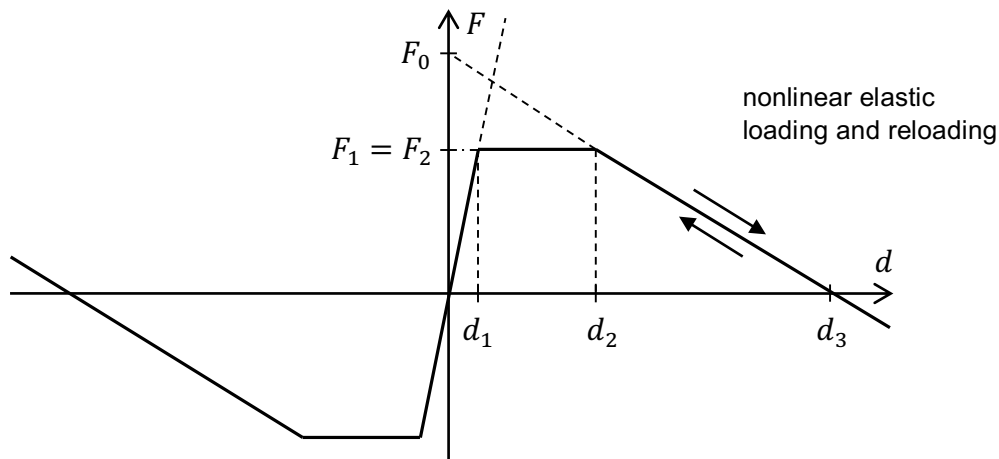


Figure 5.1. Trilinear model from Doherty et al. (2002)

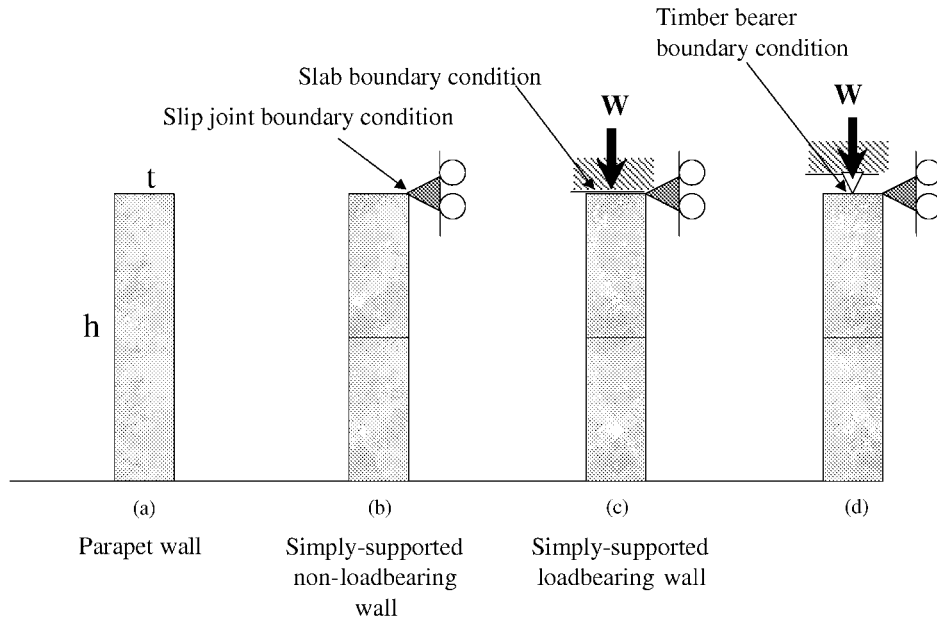


Figure 5.2. Support configurations for URM walls (Doherty et al., 2002)

The effective mass ( $M_e$ ) of the SDOF system has been calculated as follows:

$$M_e = \frac{3}{4}M \quad (5.1)$$

The incipient rocking force,  $F_0$ , can be calculated for parapets and simply supported walls, respectively, as follows:

$$F_0 = \frac{M_e g t}{h} \quad (5.2)$$

$$F_0 = \frac{4(1 + \Psi)M_e g t}{h} \quad (5.3)$$

Where  $t$  is the thickness of the wall,  $h$  is the height of the wall, and  $\Psi$  is the ratio of overburden force to the self-weight of the top half of the wall.

The static instability displacement is given by:

$$d_3 = \frac{2}{3}t \quad (5.4)$$

For new walls with little degradation, Doherty et al. (2002) suggest that  $d_1 = 0.06d_3$  and  $d_2 = 0.28d_3$ . Instead, for moderately degraded walls, they suggest  $d_1 = 0.13d_3$  and  $d_2 = 0.40d_3$ , and for severely degraded walls,  $d_1 = 0.20d_3$  and  $d_2 = 0.50d_3$ .

The values for  $F_1$  and  $F_2$  (which are taken to be equal) are given by the following formula:

$$F_1 = F_2 = \frac{d_2 - d_3}{K_0} \quad (5.5)$$

where  $K_0$  is the average secant stiffness, given by the ratio of  $F_0/d_3$ .

Nonlinear dynamic analyses of SDOF models with effective mass have been undertaken with OpenSees, using the ElasticMultiLinear model together with viscous damping. The frequency of vibration,  $f$ , used in the calculation of the viscous damping coefficient,  $C$ , has been based on the initial stiffness ( $K_1 = F_1/d_1$ ) and the critical damping ratio,  $\xi$ , has been taken as 3% (as suggested by Doherty et al., 2002):

$$C = 4\pi f \xi M_e = 2 \sqrt{\frac{K_1}{M_e}} \xi M_e \quad (5.6)$$

Ideally, an iterative approach would be used to account for the frequency-dependent damping, as discussed in Lam et al. (2003), but for the purposes of developing fragility functions, such additional refinement of the analyses was felt to be unnecessary.

The performance of this simple model for solid and cavity walls has been tested using experimental test data that has been developed specifically for the project, and appropriate calibrations to the model have been undertaken, as summarised in the next section.

## 5.2 Comparison with Experimental Test Data

Dynamic out-of-plane (OOP) tests of solid and cavity unreinforced masonry (URM) walls (EUCENTRE, 2015b) have been used to check/calibrate the OOP models presented in the previous section.

The following tests have been used for comparisons/calibrations, with the properties shown in the table and figure below:

- 1 x single leaf URM wall made of calcium silicate bricks with two different levels of overburden pressure ( $\sigma_v$ ) (EC\_COMP\_4)
- 2 x cavity walls with the inner calcium silicate wall and the outer veneer clay wall with 2 ties/m<sup>2</sup> with different levels of overburden pressure (EC\_COMP\_5/6)

- 1 x cavity walls with the inner calcium silicate wall and the outer veneer clay wall with 4 ties/m<sup>2</sup> (EC\_COMP\_7).

Table 5.1. Properties of the URM walls tested out-of-plane

Specimen	Wall	L [m]	t [m]	h [m]	$\sigma_v$ [MPa]	Boundary condition
EC_COMP_4	Single-leaf wall	1.438	0.102	2.754	0.3-0.1	Double-Fixed
EC_COMP_5	CS inner wall	1.438	0.102	2.754	0.1	Double-Fixed
	Clay outer wall	1.425	0.100	2.700	-	Cantilever
EC_COMP_6	CS inner wall	1.438	0.102	2.754	0.3	Double-Fixed
	Clay outer wall	1.425	0.100	2.700	-	Cantilever
EC_COMP_7	CS inner wall	1.438	0.102	2.754	0.1	Double-Fixed
	Clay outer wall	1.425	0.100	2.700	-	Cantilever

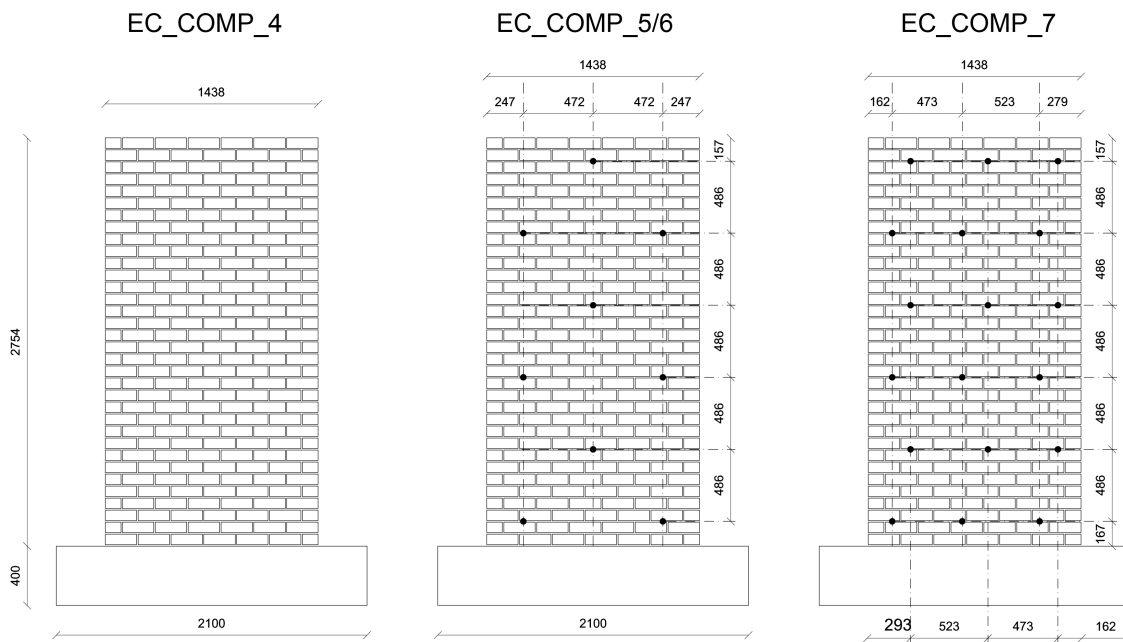


Figure 5.3. Details of the tested URM walls

Two different accelerograms were used in the tests, referred to herein as GR\_1 and GR\_2.

Using the results of the EC\_COMP\_4 analysis with overburden pressure of 0.1MPa and accelerogram GR\_1, the initial stiffness has been varied until a good match between the simple model and the experimental results was obtained.

A yield displacement ( $d_1$ ) of 3% (rather than the aforementioned 6%) of the static instability displacement led to the incremental dynamic analysis (IDA) results given in Figure 5.4. These parameters were then used in the OOP model for all other results presented herein (except Figure 5.12 and Figure 5.13, as discussed later) – it is

noted that the experimental results that were judged to be significantly affected by progressive damage have not been considered for the comparisons shown herein.

Figure 5.4 and Figure 5.5 show that the simple OOP model provides a good prediction of the response of solid URM walls with different overburden pressures.

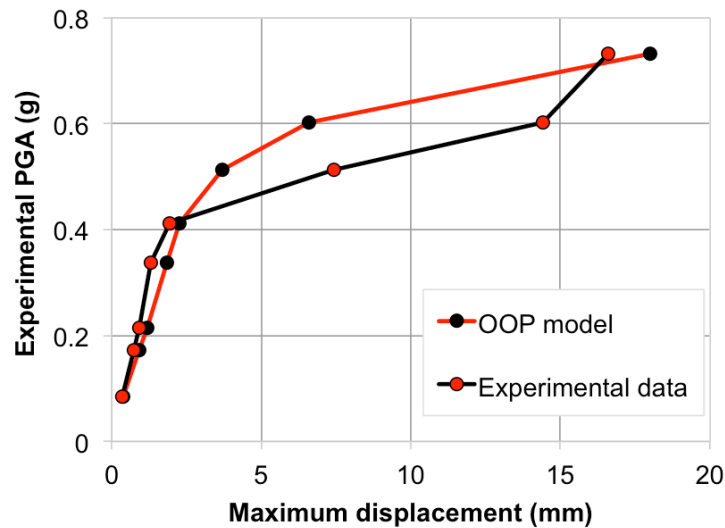


Figure 5.4. IDA results for EC\_COMP\_4 (0.1 MPa overburden pressure) with record GR\_1

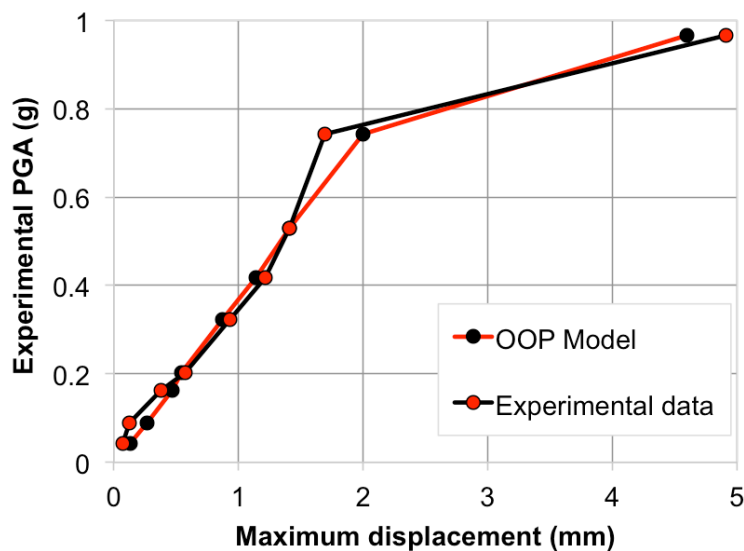


Figure 5.5. IDA results for EC\_COMP\_4 (0.3 MPa overburden pressure) with record GR\_1

Another good match between the analytical and experimental results is given in Figure 5.6 for the first cavity wall test (EC\_COMP\_5), which is further verified by the time history comparison of mid-height displacement under a PGA of 0.74g, as presented in Figure 5.7. A slight underestimation of the initial stiffness is present, but the response at large displacements is well matched. However, it should be noted that the highest PGA test shown in the figure corresponds to a later testing phase,

where accumulated damage was present. As this is not modelled in the SDOF system, it would appear that the latter is conservative.

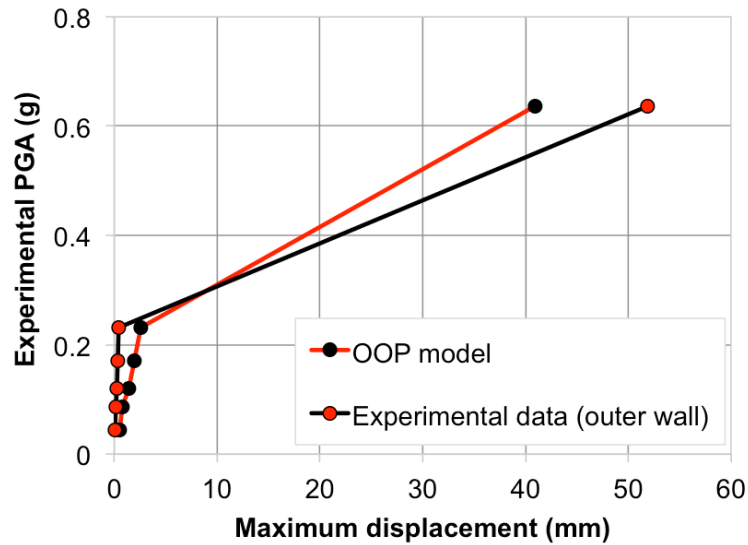


Figure 5.6. IDA results of outer clay wall for EC\_COMP\_5 with record GR\_1

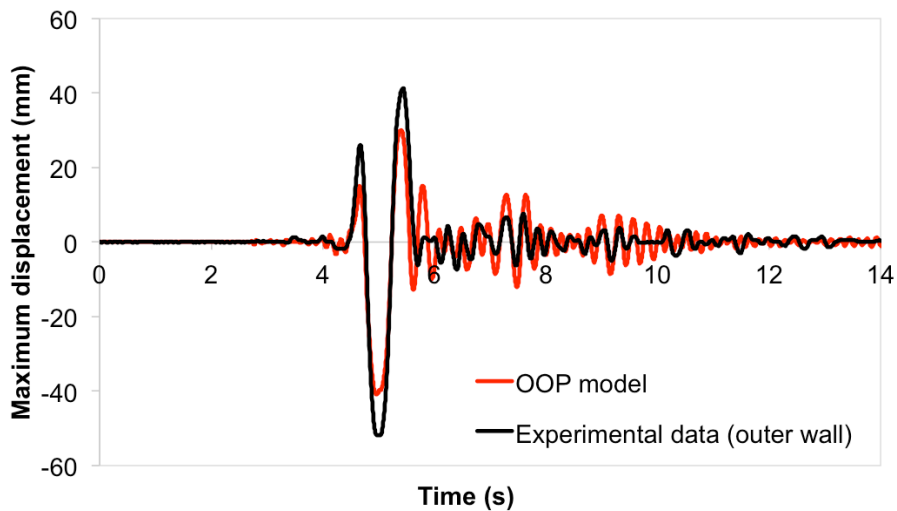


Figure 5.7. Time history of mid-height displacement of outer wall of EC\_COMP\_5 with record GR\_1 at PGA of 0.64g

Figure 5.8 shows a good estimation of the stiffness for EC\_COMP\_6 (which has a higher overburden pressure) under GR\_1, but under GR\_2 the initial stiffness appears to be underestimated and there is an underestimation of the incipient rocking force for these cavity walls with ties (see Figure 5.9). The test results shown in Figure 5.9 were also carried out following a number of initial tests, and so accumulated damage was present. It would thus appear that additional strength is needed in the OOP model. Results without accumulated damage are not available to calibrate the increase in strength, and so a 15% increase has been assumed for the

case with 2 ties per square metre (given also the results provided later for 4 ties per square metre).

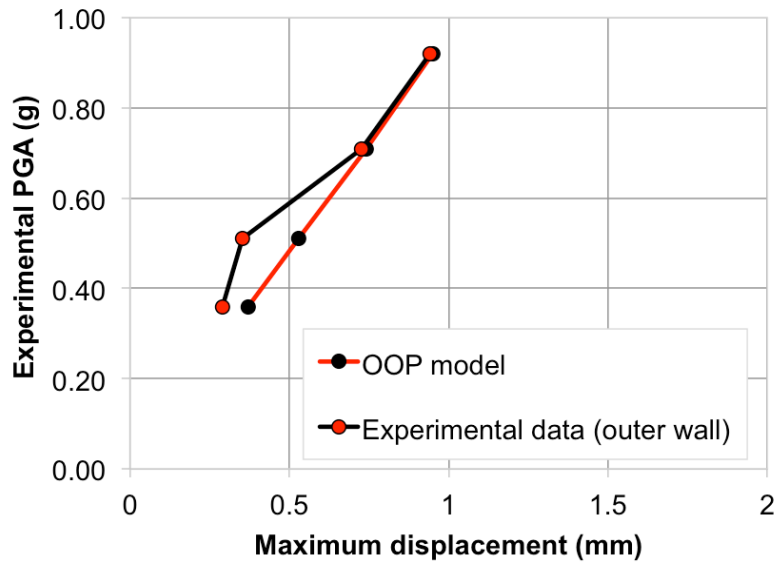


Figure 5.8. IDA results of outer clay wall for EC\_COMP\_6 with record GR\_1

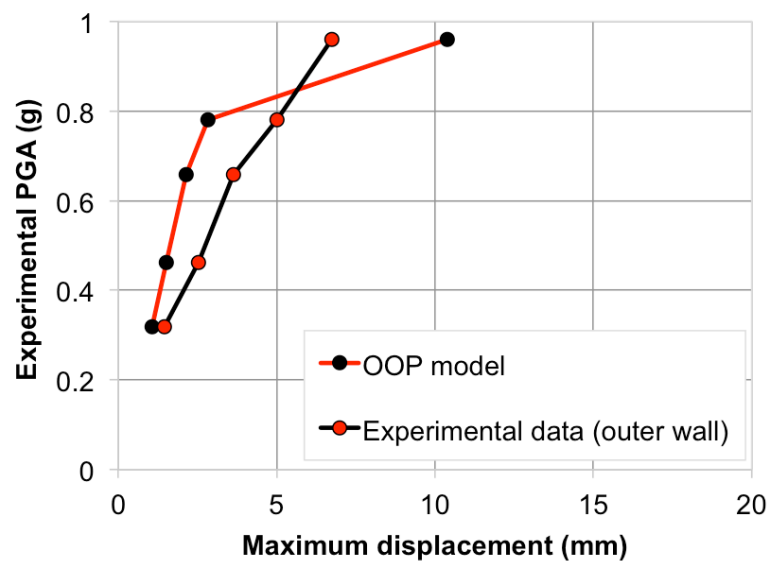


Figure 5.9. IDA results of outer clay wall for EC\_COMP\_6 with record GR\_2

Figure 5.10 shows that the initial stiffness of cavity wall EC\_COMP\_7 (with twice the number of ties as the previous specimens) is significantly underestimated with the analytical model, whilst Figure 5.11 shows that collapse is predicted to occur under 0.6g (given that the static instability displacement is predicted as 68mm), whilst the test manages to reach 0.89g. Hence, it appears that the influence of these more closely spaced ties on the incipient rocking force also needs to be accounted for. The yield displacement has thus been reduced to 0.75% of the static instability

displacement (to increase the initial stiffness), and the incipient rocking force has been increased by 30%, leading to the results shown in Figure 5.12 and Figure 5.13.

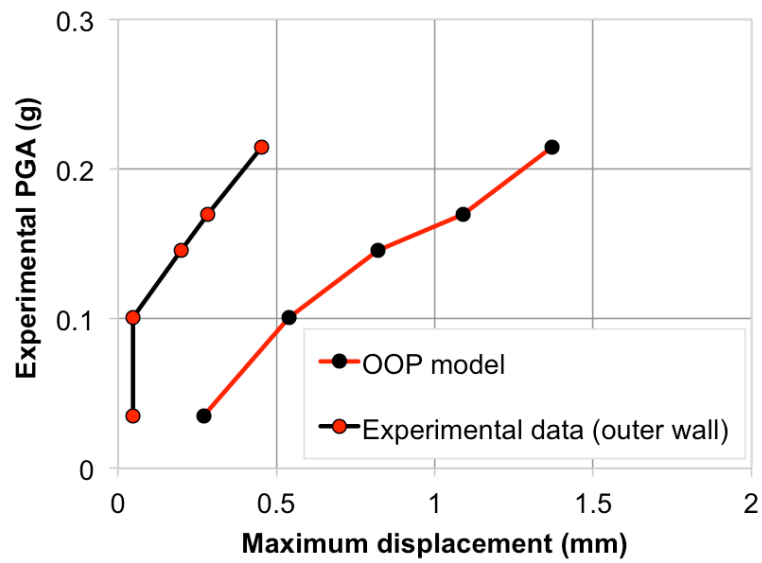


Figure 5.10. IDA results of outer clay wall for EC\_COMP\_7 with record GR\_1

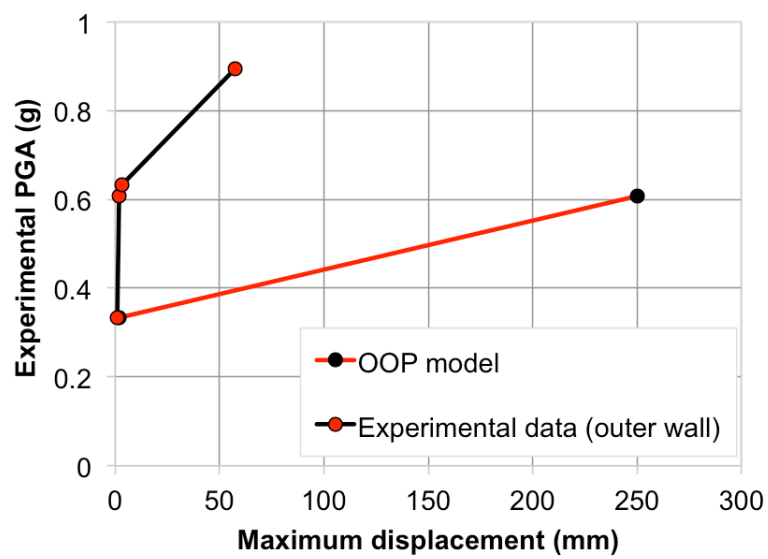


Figure 5.11. IDA results of outer clay wall for EC\_COMP\_7 with record GR\_2

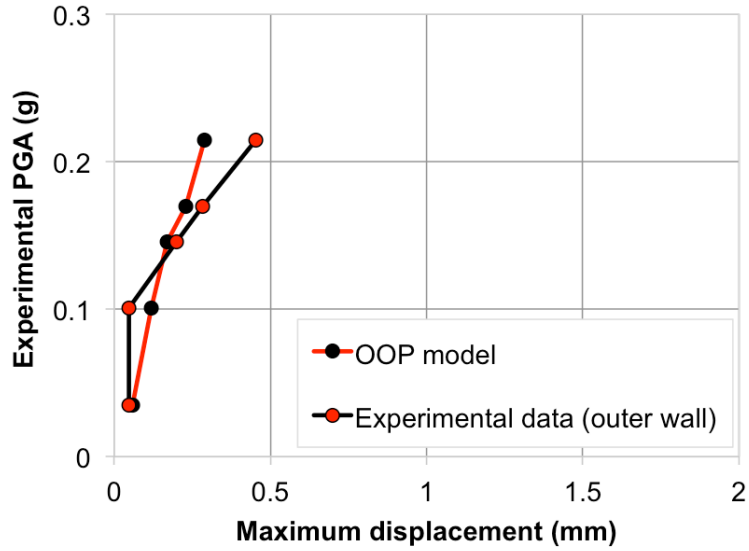


Figure 5.12. IDA results of outer clay wall for EC\_COMP\_7 with record GR\_1, and increased stiffness and strength to account for more closely spaced ties

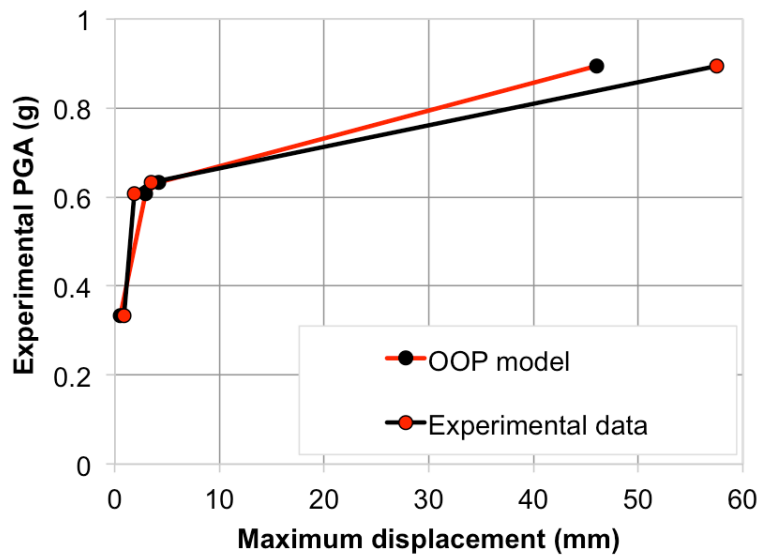


Figure 5.13. IDA results of outer clay wall for EC\_COMP\_7 with record GR\_2, and increased stiffness and strength to account for more closely spaced ties

The final calibrated OOP models for each test specimen are presented in Figure 5.14.

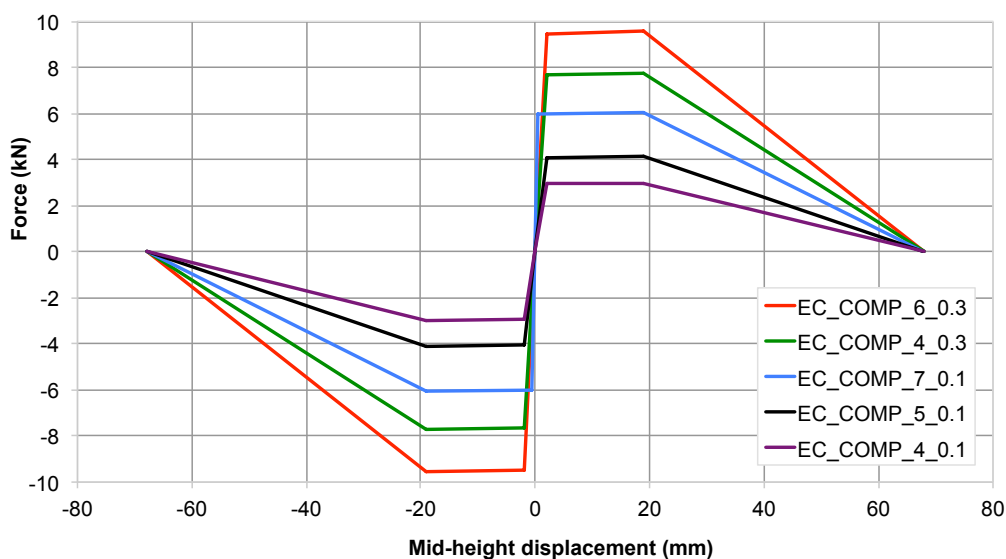


Figure 5.14. Final input models for each URM wall test specimen

The modifications to the Doherty et al. (2002) model presented herein will be maintained for predicting the response of URM simply supported walls for each typology, as presented in the next section.

### 5.3 Out-of-Plane Backbone Curves

All of the building typologies with load-bearing URM walls whose failure could cause debris inside of the structure (as they support the floor slabs) have been identified (see Chapter 2) and the input parameters for the OOP model presented in Section 5.1 have been defined.

The building typologies have been grouped as a function of floor/attic material (timber/concrete – as this influences the overburden pressure), type of wall (solid/cavity – as this influences the incipient rocking force), number of ties for cavity walls (as this influences the incipient rocking force and initial stiffness), height to base of the critical OOP walls (as this influences the level of floor amplification), age (as this is assumed to influence the level of degradation of the walls as well as the number of ties in cavity walls, and thus affects the initial stiffness and incipient rocking force assumed in the model, as described previously).

The critical walls have been identified as the highest structural load-bearing walls in the building, as they have the lowest overburden and the highest level of floor amplification. This has led to 11 groups, as presented in Table 5.2, and examples of each are shown in the photos in Figure 5.15.

Table 5.2. OOP model groups and associated assumptions

OOP Group	Typologies	Assumed overburden loads	Façade Wall type	Level of maintenance	Number of ties per m <sup>2</sup>	Height to base of wall (m)
1	RES-D-URM-A/D/E and RESS-URM-A	Timber attic + gable wall + roof	Solid	Low	N/A	0
2	RES-D-URM-B and RESS-URM-B	Timber attic + gable wall + roof	Cavity	Medium	2	0
3	RES-D-URM-C	Concrete attic + gable wall + roof	Cavity	High	4	0
4	RES-D-URM-F	Timber attic + gable wall + roof	Solid	Low	N/A	2.8
5	RES-T-URM-A	Timber attic + gable wall + roof	Solid	Low	N/A	2.8
6	RES-T-URM-B	Timber attic + gable wall + roof	Cavity	Medium	2	2.8
7	RESS and RES-T-URM-C/D	Concrete attic + gable wall + roof	Cavity	High	4	2.8
8	RES-T-URM-E/F	Timber attic + gable wall + roof	Cavity	High	4	2.8
9	RES-A/RECA-URM-A	Timber roof + installations	Solid	Medium	N/A	5.6
10	RES-A/RECA-URM-B	Concrete roof + installations	Cavity	High	4	8.4
11	AGRI/INDU/COM L-URM-A and COMO-URM-A/B	Light roof with installations	Solid	Medium	N/A	0

Typical wall dimensions have been considered to calculate the self-weight of each wall, and typical dead and live loads for floors, roofs, gable walls have been assumed for the estimation of the overburden load (as a percentage of the self-weight). Table 5.3 presents the assumed geometrical properties, and overburden loads for each OOP group, and Figure 5.16 shows the trilinear backbone curves that have been calculated for each OOP group. For some of the walls, a two-way bending mechanism is expected with a typical “envelope” crack pattern. In these cases the whole wall is not expected to rock out-of-plane, as assumed in the simplified model, and so only a central strip of wall has been considered in the calculations.

Table 5.3. Assumed geometric properties and overburden loads for each OOP model group

OOP Group	Thickness internal wall (m)	Thickness external wall (m)	Overburden load (% self-weight of wall)
1	0.21	-	120
2	0.1	0.1	120
3	0.1	0.1	180
4	0.21	-	120
5	0.21	-	110
6	0.1	0.1	110
7	0.1	0.1	150
8	0.1	0.1	110
9	0.21	-	60
10	0.15	0.1	120
11	0.15	-	40



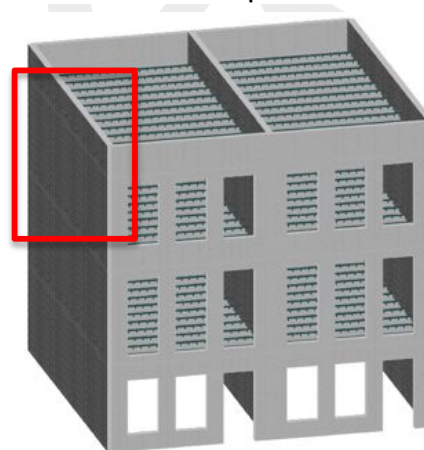
Group 1, 2 and 3



Group 4



Group 5, 6, 7 and 8



Group 9 and 10



Group 11

Figure 5.15. Photos of the load bearing walls considered in each OOP group

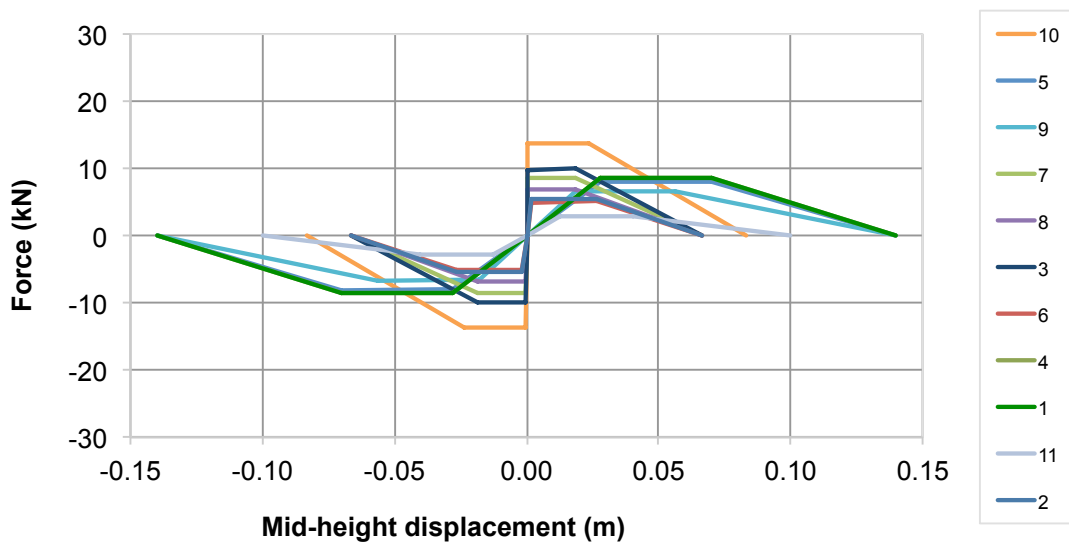


Figure 5.16. Trilinear backbone curves for each OOP group

For the nonlinear dynamic analyses, in order to estimate the ground shaking input to the OOP walls that are not placed on the ground (i.e. groups 4 to 10), an estimation of the amplification and filtering of the ground shaking caused by the in-plane response of the structure is required. The recommendations of NZS 1170.5 (2004) require an estimation of the floor amplification coefficient (see Figure 5.17a), which depends on the height to the base of the URM wall and the height to the uppermost seismic weight ( $h_n$ ), and the spectral shape coefficient, which depends on the period of vibration of the rocking URM wall. The two coefficients are multiplied together to produce a scaling factor to be applied to the seismic demand.

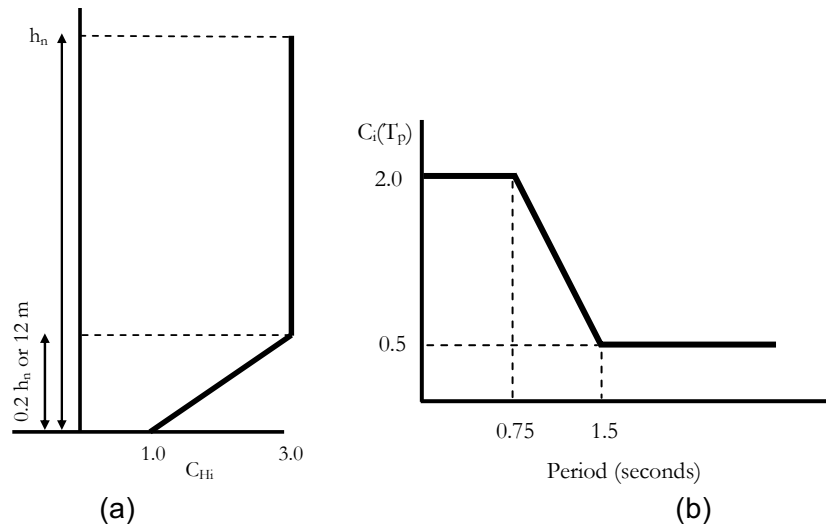


Figure 5.17. (a) Floor height coefficient  $C_{Hi}$  and (b) spectral shape coefficient from NZS 1170.5 (2004) (taken from Menon and Magenes, 2008)

When compared with the floor spectra from the shaking table test of the full scale terraced building at 160% of EQ2 (EUCENTRE, 2015b), it was found that the amplification given by NZS 1170.5 (2004) was highly conservative. Hence, the results of the shaking table test in terms of floor spectra (Figure 5.18) have been used to estimate amplification factors for each OOP group, by fitting a simple relationship to the spectral ratios provided in Figure 5.19, considering the amplification at the fundamental period of vibration of the building ( $T_1$ ) and the second mode of vibration, with a period of vibration that is assumed to be equal to  $0.2T_1$ .

To develop fragility functions, the accelerograms (see Section 6.2) are simply amplified by the values given in Figure 5.19 and applied to the OOP walls; this is, of course, a strong simplification since the walls at higher floors will be excited by a different motion from that at the base of the building. The building causes a ‘filtering’ of the signal, leading to amplification in certain spectral ranges and can create out-of-phase effects. In addition, there is interaction between the wall and building.

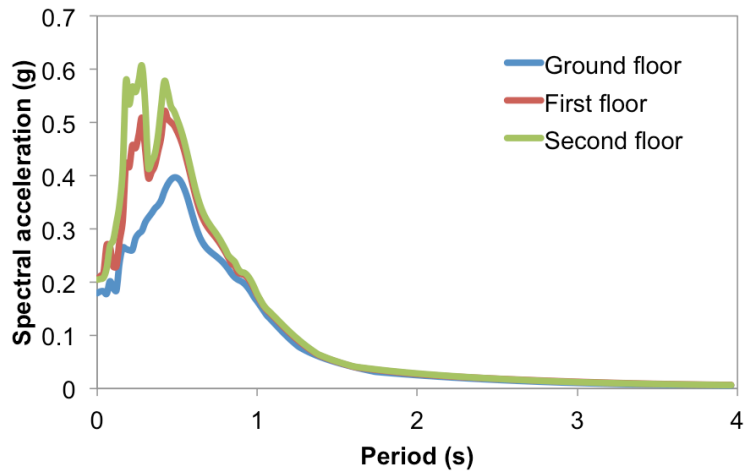


Figure 5.18. Floor spectra from the shaking table test at 160% EQ2

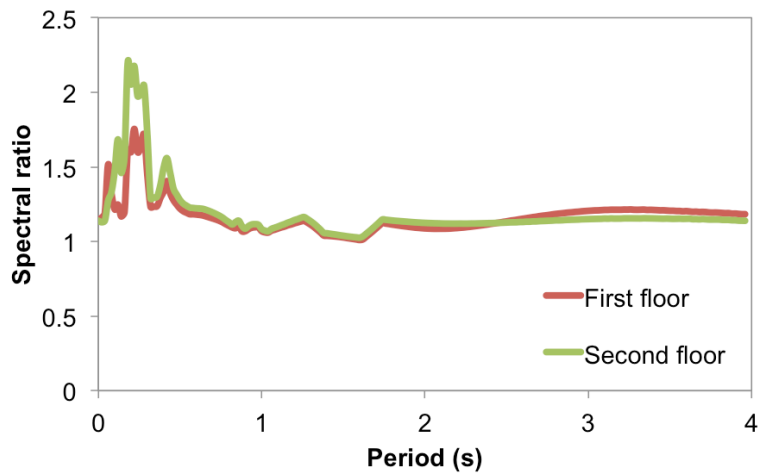


Figure 5.19. Spectral ratios from the shaking table test at 160% EQ2

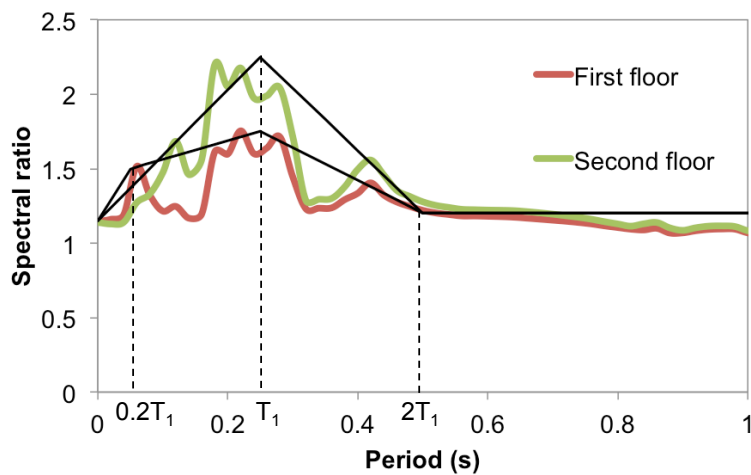


Figure 5.20. Simple linear equations for estimating amplification factors from the period of vibration of the structure

The final model input parameters for each OOP group are presented in Table 5.4.

Table 5.4. Input parameters for estimating OOP response of walls that could lead to volume loss inside the structure

<b>OOP Group</b>	<b>Effective mass (t)</b>	<b>Period of vibration (s)</b>	<b>Amplification factor</b>	<b>F1 (kN)</b>	<b>D1 (mm)</b>	<b>D2 (mm)</b>	<b>Df (mm)</b>
1	1.7	0.50	1.0	8.5	28	70	140
2	1.6	0.18	1.0	5.3	2.0	27	67
3	1.6	0.06	1.0	9.8	0.5	19	67
4	1.7	0.50	1.2	8.5	28	70	140
5	1.7	0.50	1.2	8.0	28	70	140
6	1.6	0.18	1.69	5.0	2.0	27	67
7	1.6	0.07	1.53	8.5	0.5	19	67
8	1.6	0.08	1.54	6.8	0.5	19	67
9	3.4	0.45	1.2	13.3	18	56	140
10	4.1	0.07	1.48	27.2	0.6	23	83
11	2.4	0.45	1.0	5.5	13	40	100

#### 5.4 Variability in Out-of-Plane Backbone Curves

The OOP models presented in the previous section are assumed to represent the median capacity of each group of walls responding out-of-plane. The variability of the geometrical properties and overburden loads on the trilinear models (and thus on the nonlinear response) will be studied during the development of the v3 fragility functions. This variation in models may include the possibility of insufficient anchorage at the floor-wall connection (which might lead to the walls responding as parapets with a much lower incipient rocking force) and the possibility of two-way bending of the walls (which was observed in the shaking table test, as shown in Figure 5.21). As discussed in Section 3.8, this building-to-building variability is not currently treated as an aleatory variability and is instead considered to be part of the epistemic uncertainty, as discussed further in Section 7.2.

Instead, in the v2 fragility functions, the aleatory variability in the ultimate displacement capacity has been modelled using a lognormal distribution with a coefficient of variation (CoV) of 30% (i.e. a dispersion of 0.294), based on the same reasoning provided previously in Section 3.8.

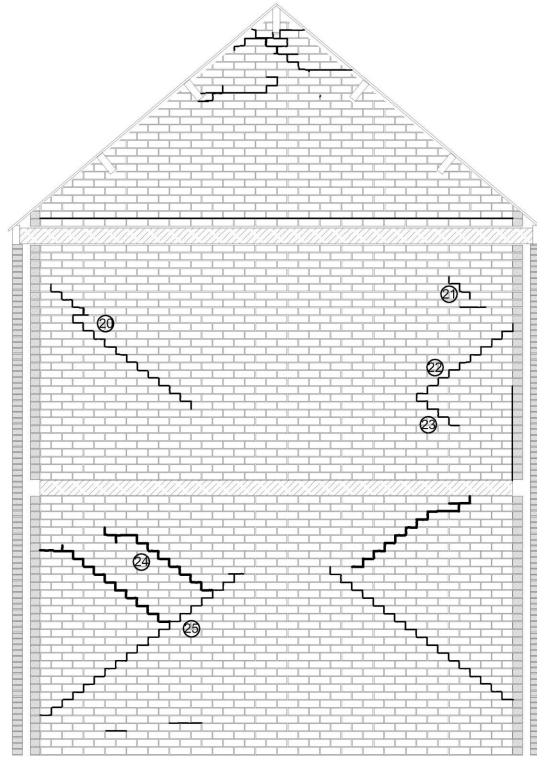


Figure 5.21. Final damage pattern of the end load-bearing wall of the terraced building tested on the shaking table

## 6 Nonlinear Response of SDOF systems

### 6.1 Introduction

Chapters 3, 4 and 5 of this report have described the calibration of SDOF systems for estimating the first mode nonlinear in-plane and out-of-plane response of a large number of building typologies. For the development of fragility functions, which describe the probability of partial collapse under increasing levels of ground shaking intensity, a model for the probabilistic relationship between ground motion intensity and the nonlinear structural response of the SDOF system is needed.

Baker (2007) discusses the various approaches that are commonly used for estimating this probabilistic relationship:

- Cloud method (Jalayer, 2003): regress on response data from (typically) unscaled ground motions to estimate the conditional mean and standard deviation of the response given the intensity level (Figure 6.1a).
- Multiple stripe method (Jalayer, 2003): scale sets of records to target intensity levels and fit a parametric distribution to response results (Figure 6.1b) or scale records to a target intensity level and fit an empirical distribution for response (Figure 6.1c).
- Incremental Dynamic Analysis (IDA) (Vamvatsikos and Cornell, 2002): scale many records to different intensity levels to estimate the probability distribution of the intensity measure (IM) that causes a given level of response (or engineering demand parameter, EDP) that is estimated (Figure 6.1d).

The cloud method is typically applied using an assumption of linear variation of response with IM and homoscedasticity of the residuals, which may not hold over the full range of intensity levels, but it typically requires much less computational effort than the multiple stripe and IDA methods. Although it does not account for the changing earthquake events that contribute to the hazard at different intensity levels (as can be employed with multiple stripe methods), it has been selected for the development of the v2 fragility functions, and dependence of the selected IM on various parameters of the recordings has been checked and these parameters have been included explicitly in the regression, where necessary.

A cloud method with a large suite of records has been selected to reduce the effort required to select/scale the records that would be appropriate to capture the nonlinear response of each typology. By applying the same large number of records to all structures, a wide range of nonlinear structural response (from pre-yield to collapse) can be captured for all typologies, together with an adequate modelling of the record-to-record variability.

Although it is common to check the dependence of the intensity measure (so-called *sufficiency*) with respect to magnitude and distance (see e.g. Luco and Cornell, 2007), the dependence on a measure of ground shaking duration has also been considered herein given the evidence from previous studies that the response of unreinforced masonry structures (and other strength and stiffness degrading structures) is dependent on the duration of strong ground shaking (e.g. Bommer et al., 2004). The interval related to 5-75% of the total Arias Intensity of the record (so-called 5-75% significant duration,  $D_{S5-75}$ ) was selected by Chandramohan et al. (2015) as the preferred duration parameter for the derivation of fragility functions, which may be because it has been found to isolate well the strongest portion of the record that generally corresponds to the arrival of shear waves. The  $D_{S5-75}$  duration definition has been used herein, but as discussed in Bommer et al. (2015), this definition was not always found to capture the strongest part of the shaking in the records from the Groningen field. For this reason, work is underway to explore other definitions of duration that could be used in future versions of the fragility functions.

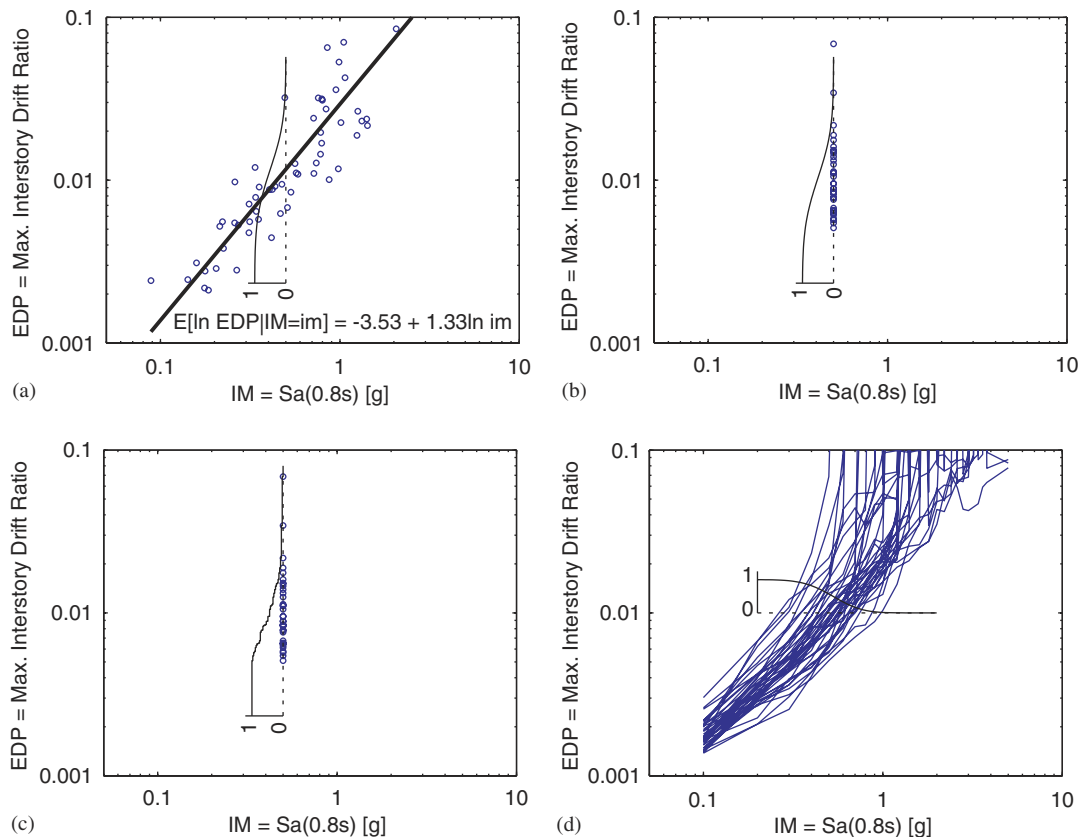


Figure 6.1. Methods for estimating the probabilistic relationship between ground motion intensity (IM) and nonlinear structural response (EDP) (Baker, 2007)

## 6.2 Selection of Records

A database of over 4000 accelerograms has been set up for the nonlinear dynamic analyses, by combining recordings from the NGA1 (Chiou et al., 2008), European

and Groningen databases (Bommer et al., 2015). The moment magnitude, epicentral distance and 5-75% significant duration for each accelerogram has been obtained/calculated, and it has been ensured that they cover the range of these parameters used in the probabilistic risk assessment for the Groningen field. In particular, the magnitude range has been taken to be between 3.5 and 6.5, and epicentral distances up to 60km have been used. However, now that the v2 probabilistic seismic hazard and risk assessment has been completed it will be possible to disaggregate the hazard (and risk) at a number of locations within the field to understand better the characteristics of the controlling events, and thus further refine this database.

The v2 ground-motion prediction equation (GMPE) for the risk assessment (Bommer et al., 2015) predicts the arbitrary component of spectral acceleration at 16 distinct periods of vibration. This choice of component, as opposed to the geometric mean, has allowed the spectral acceleration at a given period of vibration for a given horizontal component of ground shaking to be directly plotted against the predicted nonlinear dynamic response, thus requiring less dynamic analyses to predict the dispersion in response with a given level of confidence (see e.g. Baker and Cornell, 2006). For this reason, it has been possible to separately use both horizontal components of recordings in the aforementioned databases.

### **6.3 Linear Regression of Cloud Data**

Nonlinear dynamic analysis of each SDOF system has been undertaken in OpenSees using the full set of recordings. Given that the focus is currently on predicting the nonlinear behaviour close to collapse, all pre-yield response data has been removed. The aleatory variability in the pre-yield response is much lower than its post-yield counterpart (and is zero when the same damping is considered in the SDOF system and spectral ordinates), and so removing these points helps to create a set of data that is more likely to be homoscedastic. Furthermore, the aforementioned assumption of a linear relationship between the logarithm of response and IM is also more reasonable when the data is focused only on the nonlinear response. Although the data could have been further concentrated on the response closer to collapse, there are plans to produce fragility functions for other damage states in the future (in particular for history and consistency checks, as discussed in Section 7.2) and thus it was decided to use the whole range of nonlinear data.

Once the nonlinear dynamic displacement response of a given SDOF ( $D$ ) is obtained from all recordings, each response is plotted against its respective spectral acceleration at a given period of vibration (the IM) and regression is used to compute the conditional mean and standard deviation of  $D$  given IM. A linear relationship between the logarithms of these two variables is assumed:

$$\ln(D) = b_0 + b_1 \ln(IM) \quad (6.1)$$

where  $b_0$  and  $b_1$  are constant coefficients that are estimated from linear regression. To account for the fact that the initial period of vibration of the structure might not be the optimal period of vibration to describe the response (as the period of vibration increases as the structure is damaged), linear regression using the spectral acceleration at each of the 16 periods of vibration in the GMPE has been undertaken. In order to select the most *efficient* IM (i.e. that which leads to the lowest variability in the response given IM, and thus requires less nonlinear analyses to predict with a given level of confidence: Shome and Cornell, 1999) the conditional standard deviation of the regression (so-called dispersion,  $\beta_R$ ) is calculated, as given in Equation (6.2), and the period leading to the lowest value of  $\beta_R$  is selected as the IM:

$$\beta_R = \sqrt{\frac{\sum_i^n (\ln(d_i) - [b_0 + b_1 \ln(IM)])^2}{n - 2}} \quad (6.2)$$

where  $n$  is the number of records and  $i$  is a given realisation of nonlinear response.

To ensure that the regression is not biased by an abundance of data points over a specific range of intensity values, a uniform sampling of the data points between the highest and lowest intensity measure levels in the population has been undertaken. The range has been divided into 1000 bins, and so up to 1000 records can be included in Equation (6.2), though it tends to be lower as not all bins are filled with data.

It is furthermore noted that in order to correctly treat the results of the nonlinear dynamic analyses where the displacement response exceeds the ultimate displacement capacity (and thus these SDOF systems are deemed to have exceeded the partial collapse limit state), a censored regression has been undertaken when estimating the coefficients of Equation (6.1). In these cases, the value of displacement demand from the nonlinear dynamic analysis is not trusted, but it is known to exceed a given limiting value, and is thus referred to as a censored observation. If all censored observations were set to the limiting value, and a normal linear regression analyses were to be applied as above, the fitted model would be biased. To obtain an unbiased model, maximum likelihood techniques are used. The likelihood function for the model shown in Equation (6.1) with  $n$  observations is:

$$L = \prod_i^n \phi\left(\frac{\ln(D_i) - [b_0 + b_1 \ln(IM)]}{\beta_R}\right) \quad (6.3)$$

where  $\phi(z)$  is the probability density function for the standard normal distribution. However, rather than finding the values of  $b_0$ ,  $b_1$  and  $\beta$  that maximise  $L$ , it is necessary to minimise the negative of the log-likelihood function, given by:

$$\ln L = \sum_i^n \ln \phi \left( \frac{\ln(D_i) - [b_0 + b_1 \ln(IM)]}{\beta_R} \right) \quad (6.4)$$

With the presence of censored variables the likelihood function becomes:

$$L = \prod_j^{n_c} \left[ 1 - \Phi \left( \frac{\ln(D_i) - [b_0 + b_1 \ln(IM)]}{\beta_R} \right) \right] \prod_i^{n_o} \phi \left( \frac{\ln(D_i) - [b_0 + b_1 \ln(IM)]}{\beta_R} \right) \quad (6.5)$$

where there are  $n_c$  censored observations and  $n_o$  observed (uncensored) values and  $n_c + n_o = n$ . The  $\Phi(z)$  function is the cumulative standard normal distribution function.

Taking the logarithm of this expression, as before, gives:

$$\ln L = \sum_j^{n_c} \ln \left[ 1 - \Phi \left( \frac{\ln(D_i) - [b_0 + b_1 \ln(IM)]}{\beta_R} \right) \right] + \sum_i^{n_o} \ln \phi \left( \frac{\ln(D_i) - [b_0 + b_1 \ln(IM)]}{\beta_R} \right) \quad (6.6)$$

An example cloud data plot with censored regression is shown in Figure 6.2, where the censored observations have been plotted at the limiting displacement capacity value.

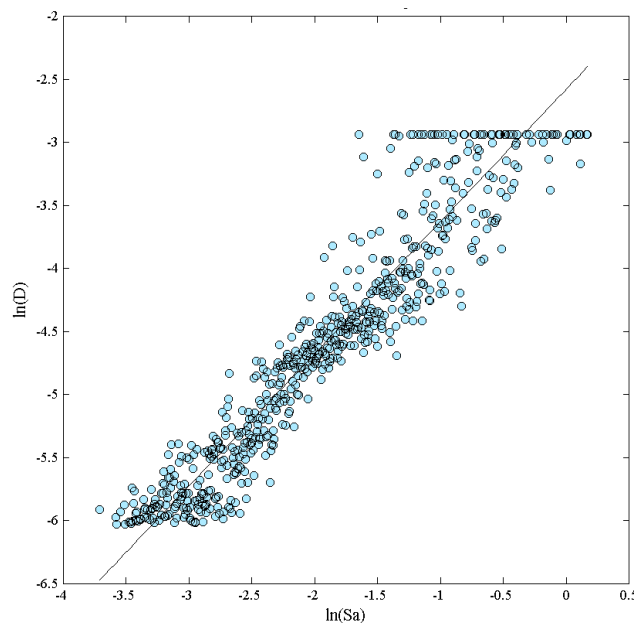


Figure 6.2. Example cloud data plot with censored regression

Once the censored linear regression has been undertaken for each response period spectral acceleration, and the most efficient IM selected, its dependence with respect to moment magnitude, epicentral distance and significant duration was then tested. The standard residuals from the linear regression were plotted against moment magnitude, logarithm of epicentral distance and logarithm of 5-75% significant duration, after which a standard linear regression was carried out (see Figure 6.3). It is noted that the censored observations were not used in this regression.

The statistical significance of the regression estimate was quantified using the p-value, and a value lower than 0.05 for any of the three parameters was considered as demonstrating a statistical significance between the residuals and that parameter (see e.g. Luco and Cornell, 2007). In such case, the use of spectral acceleration alone was deemed to be an insufficient intensity measure for the prediction of the nonlinear response.

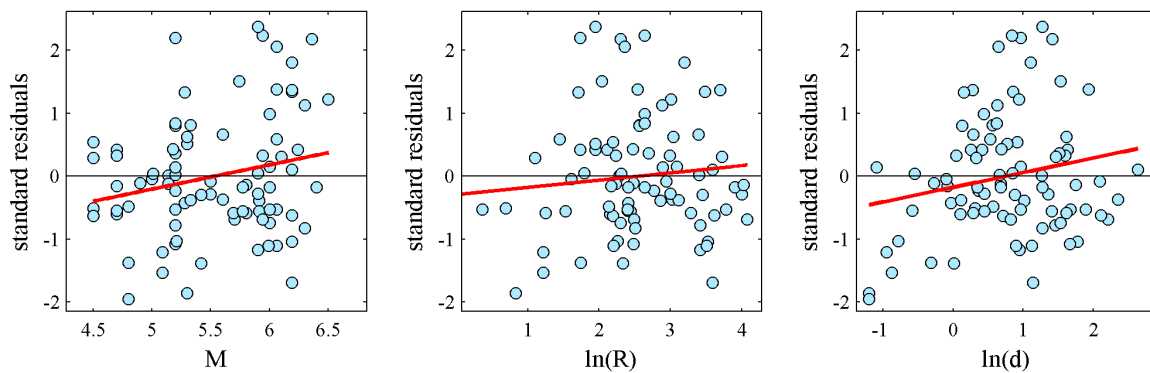


Figure 6.3. Illustrative plot of standard residuals of linear regression against moment magnitude (M), epicentral distance (R) and 5-75% significant duration (d)

For many of the SDOF systems, the use of spectral acceleration at a given period of vibration was found to be a sufficient intensity measure. In those cases where it was insufficient, it was found to be predominantly insufficient in terms of duration, frequently insufficient in terms of epicentral distance and rarely insufficient in terms of magnitude. To address the cases where the initial IM was insufficient, a multiple linear (censored) regression was undertaken, by including the insufficient parameter(s) as additional regression variables. It was found that in the majority of cases, including first the significant duration as an additional regression parameter led to a sufficient intensity measure in terms of magnitude and distance and thus it was not necessary to include these parameters as additional variables. For simplicity, it was thus decided to use a vector intensity measure of spectral acceleration,  $Sa(T)$ , and 5-75% significant duration,  $D_{S5-75}$ , in those cases where the former (scalar) IM was insufficient, thus leading to the following model:

$$\ln(D) = b_0 + b_1 \ln(Sa(T)) + b_2 \ln(D_{S5-75}) \quad (6.7)$$

The value of dispersion,  $\beta_R$ , for this formulation was recalculated, and was always found to be lower than that estimated using a scalar IM, as would be expected.

Although it would have been straightforward to include all necessary variables in the multiple linear regression and include these in the risk engine (as the latter is based on Monte Carlo simulation), it was decided to keep a simpler representation in terms of two variables in this first derivation of v2 fragility functions and to consider including other parameters (which might extend beyond the three used herein) in future updates. This assumption only led to a handful of cases where the selected IM was not sufficient.

When cloud analysis is used together with vector IM, it can be difficult to separate the effects of each IM when they are highly correlated, a condition referred to as *collinearity* (see e.g. Baker, 2007). In order to avoid the potential for collinearity, a few spot checks of the correlation coefficients between the logarithms of spectral acceleration and 5-75% significant duration used in the multiple linear regressions revealed that the correlation coefficients were relatively low (less than 0.2), but this should be systematically checked in the future. It is noted, however, that these two parameters are typically correlated in ground motions (e.g. Bradley, 2011) and this correlation is accounted for in the risk engine when the spectral acceleration and significant duration for a given event at a given site is estimated (see Bommer et al., 2015).

The influence of the 5-75% significant duration was not always found to be as expected, i.e. a longer duration should lead to a higher level of nonlinear response. Although this might be due to the fact that the selected response parameter was a peak deformation and this has been observed to be weakly influenced by duration (see e.g. Iervolino et al., 2006; Hancock and Bommer, 2007), many of the hysteretic models used herein do feature in-cycle deterioration and P- $\Delta$  effects, and Chandramohan et al. (2015) have shown that peak deformations can be affected by duration when these effects are modelled. Instead, the reason for longer significant durations leading to lower displacement demands in some cases could be due to the inclusion of soil-foundation-structure interaction (SSI). An increased number of cycles leads to increased foundation damping, which reduces the nonlinear response in the structure. In order to check this, all nonlinear dynamic analyses were repeated without SSI springs and dampers (i.e. fixed base) and it was found that for these models, when spectral acceleration alone was insufficient, the displacement response always increased with increased duration. However, the apparent influence of duration might instead be because duration is currently acting as a proxy for the spectral shape (and longer periods), and this will need to be further investigated.

A number of improvements in the application of the cloud method for the v3 fragility functions might include the following:

- Review and update the database of accelerograms in light of the latest hazard results.
- Check that the assumption of homoscedasticity holds, and where it does not, vary the dispersion as a function of IM.
- Check the sufficiency of the IM with respect to soil type (and/or restrict the database to recordings on similar soil types).
- Check whether the influence of significant duration varies with the level of non-linearity (and thus whether the current functional form is appropriate).
- Systematically ensure that the sampled cloud data does not feature high correlation between spectral acceleration and significant duration (for the cases where multiple linear regression is necessary).
- Check that the joint distribution of spectral acceleration and significant duration used in the multiple linear regression covers the full range of interest (and consider generating artificial records to fill any gaps).
- Together with the GMPE team, investigate other definitions of strong ground shaking duration, which both describe well the strongest portion of the recordings in Groningen and influence the nonlinear response.
- Investigate whether using spectral ordinates at other levels of damping (other than the 5% currently used) increases efficiency/sufficiency, given the increased level of damping provided by SSI.

#### **6.4 Influence of Building-to-Building Variability on Nonlinear Response**

The aleatory variability in the ultimate displacement capacity (see Section 3.8 and Section 5.4) is directly accounted for in the calculation of probability of collapse, as will be discussed in Section 7.1. There are other variations between buildings of a given typology that are expected to affect the nonlinear response rather than the capacity, such as structural dimensions. These variations are currently not being considered and only the median model is used in the cloud analyses presented in the previous section, and an implicit assumption is made that the variability in the most influential parameters of the SDOF systems (such as initial stiffness and ultimate base shear capacity) are lognormal.

Furthermore, the most important risk metric that is currently being estimated is the mean local personal risk (see Section 0), which does not require an understanding of the variability in the risk across a building typology. Instead, the variations in the response of buildings of a given typology is currently included in the epistemic uncertainty described in Section 7.2, but this has currently been defined in a qualitative manner.

In the future, an explicit definition of the influence of the building-to-building variability in the SDOF systems on the fragility functions and risk metrics could be made to better constrain the aforementioned epistemic uncertainty. For this purpose, the

Response Surface Method might provide a computationally efficient way of accounting for the variability in the nonlinear response (e.g. Franchin et al., 2003; Iervolino et al., 2004). In the latter study, the Design of Experiments (DoE) was used to produce a reasonable number of numerical models that captured the variation in two different parameters of interest and lognormal fragility functions were derived for each numerical model through nonlinear dynamic analysis. The median and dispersion of the fragility functions were each plotted against the pairs of parameters that were varied, and second order models were fit to the surfaces of data. These fitted models can then be used to estimate the median and dispersion for any two values of the selected parameters.

## 7 Fragility Functions

### 7.1 Introduction

Once the probabilistic model presented in Equation (6.6) is developed for each SDOF system, the probability of collapse for a given level of scalar or vector IM can be calculated as follows:

$$P_c = 1 - \Phi \left( \frac{\ln(D_u) - b_0 - b_1 \ln Sa(T) - b_2 \ln D_{S5-75}}{\beta_T} \right) \quad (7.1)$$

where  $\Phi$  is the cumulative distribution function of the standard normal distribution,  $D_u$  is ultimate displacement capacity (in metres),  $Sa(T)$  is spectral acceleration (in terms of g) for a given period of vibration  $T$ ,  $D_{S5.75}$  is 5-75% significant duration (in seconds) and  $\beta_T$  is the total dispersion. The total dispersion is given by combining the dispersion due to record-to-record variability,  $\beta_R$  as calculated in the previous chapter, and the dispersion due to building-building variability,  $\beta_{B-B}$  as discussed in Section 3.8 and 5.4, as follows:

$$\beta_T = \sqrt{\beta_R^2 + \beta_{B-B}^2} \quad (7.2)$$

The fragility functions for the in-plane and out-of-plane partial collapse mechanisms are provided in Table 7.1, Table 7.2 and Table 7.3. These collapse mechanisms are assumed to be perfectly correlated. For a given building, an estimate of the spectral acceleration at each period of vibration is made (using the v2 GMPE and cross correlation between spectral ordinates, see Bommer et al., 2015) together with an estimate of the 5-75% significant duration (which is correlated with the estimate of spectral acceleration) and the probability of partial collapse for each in-plane/out-of-plane mechanism is calculated, and the one with the highest probability of collapse is used in the fatality calculations.

Table 7.1. Parameters of the transverse direction fragility functions

Typology	Transverse direction					
	$b_1$	$b_2$	$b_0$	$\beta_T$	$D_u$	$T$ (s)
AGRI_INDU_COML_RC_A	0.998	-0.041	-2.001	0.384	0.218	0.85
AGRI_INDU_COML_RC_B1	0.829	-0.070	-1.224	0.424	0.218	1.5
AGRI_INDU_COML_RC_B2	3.483	0.000	-2.782	0.719	0.110	0.01
AGRI_INDU_COML_S_A	0.826	0.039	-2.315	0.349	0.420	0.6
AGRI_INDU_COML_S_B	0.621	0.000	-2.803	0.324	0.330	0.4
AGRI_INDU_COML_S_C	0.933	-0.119	-3.275	0.316	0.350	0.5

Typology	Transverse direction					
	$b_1$	$b_2$	$b_0$	$\beta_T$	$D_u$	T (s)
AGRI_INDU_COML_URM_A	4.900	0.000	-1.612	0.783	0.045	0.01
AGRI_INDU_COML_W_A	2.290	0.000	-7.792	0.758	0.021	0.2
AGRI_INDU_COML_W_B1	0.706	0.000	-2.360	0.306	0.290	0.5
AGRI_INDU_COML_W_B2	0.706	0.000	-2.360	0.306	0.290	0.5
CHURCH	2.290	0.000	-7.792	0.758	0.021	0.2
COMO_RC_A1_G4S	1.482	0.000	-1.238	0.391	0.200	1
COMO_RC_A1_L4S	1.516	-0.272	-3.391	0.445	0.100	0.6
COMO_RC_A2_G4S	1.482	0.000	-1.238	0.391	0.200	1
COMO_RC_A2_L4S	1.516	-0.272	-3.391	0.445	0.100	0.6
COMO_RC_B_G4S	3.483	0.000	-2.782	0.719	0.110	0.01
COMO_RC_B_L4S	3.483	0.000	-2.782	0.719	0.110	0.01
COMO_S_A_G4S	1.034	0.053	-1.460	0.359	0.350	1
COMO_S_A_L4S	0.933	-0.119	-3.275	0.316	0.350	0.5
COMO_S_B_G4S	0.559	-0.088	-1.636	0.376	0.350	1.5
COMO_S_B_L4S	0.982	-0.093	-3.188	0.325	0.350	0.5
COMO_URM_A	4.900	0.000	-1.612	0.783	0.045	0.01
COMO_URM_B	4.900	0.000	-1.612	0.783	0.045	0.01
HOSPITAL	1.516	-0.272	-3.391	0.445	0.100	0.6
RECA_RC_A_G4S	1.222	0.000	-3.777	0.517	0.060	0.4
RECA_RC_A_L4S	0.839	0.000	-4.830	0.498	0.060	0.3
RECA_RC_B_G4S	2.727	0.000	-2.963	0.626	0.110	0.01
RECA_RC_B_L4S	2.727	0.000	-2.963	0.626	0.110	0.01
RECA_URM_A	3.867	0.000	-4.772	0.614	0.042	0.01
RECA_URM_B	1.404	0.000	-3.789	0.450	0.044	0.01
RESA_RC_A_G4S	1.222	0.000	-3.777	0.517	0.060	0.4
RESA_RC_A_L4S	0.839	0.000	-4.830	0.498	0.060	0.3
RESA_RC_B_G4S	2.098	0.000	-3.528	0.639	0.110	0.01
RESA_RC_B_L4S	2.098	0.000	-3.528	0.639	0.110	0.01
RESA_URM_A	3.867	0.000	-4.772	0.614	0.042	0.01
RESA_URM_B	1.404	0.000	-3.789	0.450	0.044	0.01
RESD_URM_A	2.290	0.000	-7.792	0.758	0.021	0.2
RESD_URM_B	5.167	0.000	-3.832	0.757	0.014	0.01
RESD_URM_C	2.398	-0.078	-3.919	0.530	0.011	0.01
RESD_URM_D	2.290	0.000	-7.792	0.758	0.021	0.2
RESD_URM_E	4.717	0.000	-5.093	0.845	0.021	0.01
RESD_URM_F	3.049	0.000	-2.487	0.704	0.042	0.01
RESD_W_A	1.075	0.000	-4.586	0.393	0.120	0.2
RESS_URM_A	2.290	0.000	-7.792	0.758	0.021	0.2
RESS_URM_B	5.293	0.000	-3.713	0.771	0.045	0.01
RESS_URM_C	2.368	0.000	-4.593	0.601	0.047	0.01
RESS_W_A	1.075	0.000	-4.586	0.393	0.120	0.2
REST_RC_A	2.309	0.000	-7.402	0.543	0.080	0.01

Typology	Transverse direction					
	$b_1$	$b_2$	$b_0$	$\beta_T$	$D_u$	T (s)
REST_RC_B	2.727	0.000	-2.963	0.626	0.110	0.01
REST_URM_A	4.510	0.000	-4.195	0.674	0.045	0.01
REST_URM_B	4.055	0.000	-4.121	0.764	0.045	0.01
REST_URM_C	2.368	0.000	-4.593	0.601	0.047	0.01
REST_URM_D	2.368	0.000	-4.593	0.601	0.047	0.01
REST_URM_E	2.706	0.000	-4.619	0.656	0.027	0.01
REST_URM_F	2.706	0.000	-4.619	0.656	0.027	0.01
SCHOOL	4.900	0.000	-1.612	0.783	0.045	0.01

Table 7.2. Parameters of the longitudinal direction fragility functions

Typology	Longitudinal direction					
	$b_1$	$b_2$	$b_0$	$\beta_T$	$D_u$	T (s)
AGRI_INDU_COML_RC_A	0.824	-0.033	-1.198	0.398	0.218	1.5
AGRI_INDU_COML_RC_B1	0.829	-0.070	-1.224	0.424	0.218	1.5
AGRI_INDU_COML_RC_B2	0.875	-0.255	-3.432	0.521	0.110	0.5
AGRI_INDU_COML_S_A	0.826	0.039	-2.315	0.349	0.420	0.6
AGRI_INDU_COML_S_B	0.826	0.039	-2.315	0.349	0.420	0.6
AGRI_INDU_COML_S_C	0.678	0.000	-1.791	0.334	0.480	1
AGRI_INDU_COML_URM_A	7.614	0.000	-7.723	0.815	0.032	0.01
AGRI_INDU_COML_W_A	2.290	0.000	-7.792	0.758	0.021	0.2
AGRI_INDU_COML_W_B1	0.987	0.058	-2.745	0.432	0.640	0.5
AGRI_INDU_COML_W_B2	0.728	0.000	-3.429	0.527	0.045	0.3
CHURCH	2.290	0.000	-7.792	0.758	0.021	0.2
COMO_RC_A1_G4S	1.482	0.000	-1.238	0.391	0.200	1
COMO_RC_A1_L4S	1.516	-0.272	-3.391	0.445	0.100	0.6
COMO_RC_A2_G4S	1.482	0.000	-1.238	0.391	0.200	1
COMO_RC_A2_L4S	1.516	-0.272	-3.391	0.445	0.100	0.6
COMO_RC_B_G4S	0.875	-0.255	-3.432	0.521	0.110	0.5
COMO_RC_B_L4S	0.875	-0.255	-3.432	0.521	0.110	0.5
COMO_S_A_G4S	0.705	0.000	-0.371	0.342	0.480	2.5
COMO_S_A_L4S	0.678	0.000	-1.791	0.334	0.480	1
COMO_S_B_G4S	0.671	0.000	-0.534	0.327	0.480	2.5
COMO_S_B_L4S	0.726	0.000	-1.739	0.313	0.480	1
COMO_URM_A	7.614	0.000	-7.723	0.815	0.032	0.01
COMO_URM_B	7.614	0.000	-7.723	0.815	0.032	0.01
HOSPITAL	1.516	-0.272	-3.391	0.445	0.100	0.6
RECA_RC_A_G4S	1.090	0.052	-1.313	0.378	0.133	1
RECA_RC_A_L4S	1.325	0.000	-2.656	0.414	0.067	0.5
RECA_RC_B_G4S	0.772	-0.224	-3.446	0.532	0.110	0.5

Typology	Longitudinal direction					
	$b_1$	$b_2$	$b_0$	$\beta_T$	$D_u$	T (s)
RECA_RC_B_L4S	0.772	-0.224	-3.446	0.532	0.110	0.5
RECA_URM_A	1.625	0.000	-3.253	0.485	0.026	0.01
RECA_URM_B	1.365	0.000	-3.609	0.442	0.016	0.4
RESA_RC_A_G4S	1.214	0.057	-1.536	0.368	0.200	0.85
RESA_RC_A_L4S	1.369	0.000	-3.294	0.412	0.100	0.4
RESA_RC_B_G4S	1.100	0.000	-3.876	0.529	0.110	0.3
RESA_RC_B_L4S	1.100	0.000	-3.876	0.529	0.110	0.3
RESA_URM_A	1.625	0.000	-3.253	0.485	0.026	0.01
RESA_URM_B	0.992	0.000	-3.783	0.342	0.019	0.3
RESD_URM_A	2.290	0.000	-7.792	0.758	0.021	0.2
RESD_URM_B	5.167	0.000	-3.832	0.757	0.014	0.01
RESD_URM_C	2.398	-0.078	-3.919	0.530	0.011	0.01
RESD_URM_D	4.717	0.000	-7.792	0.758	0.021	0.2
RESD_URM_E	3.049	0.000	-5.093	0.845	0.021	0.01
RESD_URM_F	3.049	0.000	-2.487	0.704	0.042	0.01
RESD_W_A	1.075	0.000	-4.586	0.393	0.120	0.2
RESS_URM_A	2.290	0.000	-7.792	0.758	0.021	0.2
RESS_URM_B	5.293	0.000	-3.713	0.771	0.045	0.01
RESS_URM_C	1.091	0.000	-3.668	0.417	0.053	0.3
RESS_W_A	1.075	0.000	-4.586	0.393	0.120	0.2
REST_RC_A	1.056	0.049	-1.664	0.349	0.400	0.85
REST_RC_B	0.772	-0.224	-3.446	0.532	0.110	0.5
REST_URM_A	1.294	0.128	-3.055	0.512	0.068	0.01
REST_URM_B	1.282	0.111	-3.031	0.510	0.068	0.01
REST_URM_C	1.091	0.000	-3.668	0.417	0.053	0.3
REST_URM_D	1.091	0.000	-3.668	0.417	0.053	0.3
REST_URM_E	1.010	-0.065	-3.917	0.496	0.064	0.3
REST_URM_F	1.010	-0.065	-3.917	0.496	0.064	0.3
SCHOOL	7.614	0.000	-7.723	0.815	0.032	0.01

Table 7.3. Parameters of the out-of-plane (OOP) fragility functions

Typology	Out-of-plane					
	$b_1$	$b_2$	$b_0$	$\beta_T$	$D_u$	T (s)
AGRI_INDU_COML_RC_A	-	-	-	-	-	-
AGRI_INDU_COML_RC_B1	-	-	-	-	-	-
AGRI_INDU_COML_RC_B2	-	-	-	-	-	-
AGRI_INDU_COML_S_A	-	-	-	-	-	-
AGRI_INDU_COML_S_B	-	-	-	-	-	-
AGRI_INDU_COML_S_C	-	-	-	-	-	-
AGRI_INDU_COML_URM_A	1.075	0.000	-2.521	0.405	0.100	0.5

Typology	Out-of-plane					
	$b_1$	$b_2$	$b_0$	$\beta_T$	$D_u$	T (s)
AGRI_INDU_COML_W_A	1.149	0.000	-2.514	0.346	0.140	0.5
AGRI_INDU_COML_W_B1	-	-	-	-	-	-
AGRI_INDU_COML_W_B2	-	-	-	-	-	-
CHURCH	1.728	0.000	-5.271	0.721	0.083	0.1
COMO_RC_A1_G4S	-	-	-	-	-	-
COMO_RC_A1_L4S	-	-	-	-	-	-
COMO_RC_A2_G4S	-	-	-	-	-	-
COMO_RC_A2_L4S	-	-	-	-	-	-
COMO_RC_B_G4S	-	-	-	-	-	-
COMO_RC_B_L4S	-	-	-	-	-	-
COMO_S_A_G4S	-	-	-	-	-	-
COMO_S_A_L4S	-	-	-	-	-	-
COMO_S_B_G4S	-	-	-	-	-	-
COMO_S_B_L4S	-	-	-	-	-	-
COMO_URM_A	1.075	0.000	-2.521	0.405	0.100	0.5
COMO_URM_B	1.075	0.000	-2.521	0.405	0.100	0.5
HOSPITAL	-	-	-	-	-	-
RECA_RC_A_G4S	-	-	-	-	-	-
RECA_RC_A_L4S	-	-	-	-	-	-
RECA_RC_B_G4S	-	-	-	-	-	-
RECA_RC_B_L4S	-	-	-	-	-	-
RECA_URM_A	0.996	0.000	-2.432	0.409	0.140	0.5
RECA_URM_B	1.857	0.000	-5.240	0.741	0.083	0.1
RESA_RC_A_G4S	-	-	-	-	-	-
RESA_RC_A_L4S	-	-	-	-	-	-
RESA_RC_B_G4S	-	-	-	-	-	-
RESA_RC_B_L4S	-	-	-	-	-	-
RESA_URM_A	0.996	0.000	-2.432	0.409	0.140	0.5
RESA_URM_B	1.728	0.000	-5.271	0.721	0.083	0.1
RESD_URM_A	1.149	0.000	-2.514	0.346	0.140	0.5
RESD_URM_B	1.261	0.000	-4.290	0.595	0.067	0.2
RESD_URM_C	0.777	-0.109	-3.372	0.524	0.067	0.4
RESD_URM_D	1.149	0.000	-2.514	0.346	0.140	0.5
RESD_URM_E	1.148	0.000	-2.511	0.347	0.140	0.5
RESD_URM_F	1.191	0.041	-2.288	0.347	0.140	0.5
RESD_W_A	-	-	-	-	-	-
RESS_URM_A	1.149	0.000	-2.514	0.346	0.140	0.5
RESS_URM_B	1.261	0.000	-4.290	0.595	0.067	0.2
RESS_URM_C	2.262	0.000	-4.236	0.767	0.067	0.1
RESS_W_A	-	-	-	-	-	-
REST_RC_A	-	-	-	-	-	-
REST_RC_B	-	-	-	-	-	-

Typology	Out-of-plane					
	$b_1$	$b_2$	$b_0$	$\beta_T$	$D_u$	T (s)
REST_URM_A	1.290	0.041	-2.218	0.331	0.140	0.5
REST_URM_B	1.632	0.126	-1.818	0.645	0.067	0.01
REST_URM_C	2.262	0.000	-4.236	0.767	0.067	0.1
REST_URM_D	2.262	0.000	-4.236	0.767	0.067	0.1
REST_URM_E	1.945	0.000	-2.438	0.784	0.067	0.01
REST_URM_F	1.945	0.000	-2.438	0.784	0.067	0.01
SCHOOL	1.728	0.000	-5.271	0.721	0.083	0.1

## 7.2 Confidence Levels and Epistemic Uncertainties

As mentioned in Section 3.8, the building-to-building variability in the geometrical and material characteristics of a building typology is not currently treated as an aleatory variability and is instead modelled as an epistemic uncertainty. An effort to explicitly quantify the epistemic uncertainty due to building-to-building variability has not yet been carried out, and will be undertaken in future updates. Other sources of epistemic uncertainty include the model uncertainty and the representativeness of the current numerical models and assumptions for a given typology.

The epistemic uncertainty in the fragility functions is assumed to be a systematic uncertainty applied to all buildings within a given typology and is modelled through a logic tree. In order to assign a quantification of the epistemic uncertainty to each typology, confidence levels have been assigned and they are then used to adjust the fragility functions using the judgment-based multipliers presented in Table 7.4. As seen in Table 7.4, lower confidence levels result in higher levels of epistemic uncertainty.

Table 7.4. Judgment-based modifiers to model epistemic uncertainty in the fragility functions

Confidence Level	Lower bound Sa(T) multiplier	Best estimate Sa(T) multiplier	Upper bound Sa(T) multiplier
Low	0.6	1	1.8
Low-medium	0.7	1	1.6
Medium	0.8	1	1.4

Various considerations have been made when assigning the confidence levels (see Table 7.5, such as the available information on the typology, the confidence of the modelling teams in the current structural models, the model uncertainty associated with the SDOF systems and consideration or not of all failure criteria. As mentioned above, the epistemic uncertainty may be better quantified in the future by explicitly modelling the variation in fragility functions due to building-to-building variability (as also discussed in Section 6.4).

Table 7.5. Confidence levels (CL) for each transverse/longitudinal fragility function, and average number of buildings for each typology. It is noted that all OOP fragility functions are assigned LM confidence levels.

Typology ID	CL*	No.
AGRI_INDU_COML_RC_A	M	370
AGRI_INDU_COML_RC_B1	LM	148
AGRI_INDU_COML_RC_B2	LM	146
AGRI_INDU_COML_S_A	M	1079
AGRI_INDU_COML_S_B	M	1285
AGRI_INDU_COML_S_C	LM	401
AGRI_INDU_COML_URM_A	LM	260
AGRI_INDU_COML_W_A	LM	2097
AGRI_INDU_COML_W_B1	LM	333
AGRI_INDU_COML_W_B2	LM	289
CHURCH	L	167
COMO_RC_A1_G4S	LM	118
COMO_RC_A1_L4S	LM	350
COMO_RC_A2_G4S	LM	63
COMO_RC_A2_L4S	LM	131
COMO_RC_B_G4S	LM	79
COMO_RC_B_L4S	LM	253
COMO_S_A_G4S	LM	177
COMO_S_A_L4S	LM	581
COMO_S_B_G4S	LM	129
COMO_S_B_L4S	M	315
COMO_URM_A	LM	1568
COMO_URM_B	LM	674
HOSPITAL	LM	4
RECA_RC_A_G4S	LM	45
RECA_RC_A_L4S	LM	191
RECA_RC_B_G4S	LM	5
RECA_RC_B_L4S	LM	66
RECA_URM_A	M	989
RECA_URM_B	L	453
RESA_RC_A_G4S	LM	2232
RESA_RC_A_L4S	M	1138
RESA_RC_B_G4S	LM	294
RESA_RC_B_L4S	LM	166
RESA_URM_A	M	7777
RESA_URM_B	LM	2363
RESD_URM_A	LM	16512
RESD_URM_B	LM	7388
RESD_URM_C	M	14904
RESD_URM_D	LM	213
RESD_URM_E	LM	52
RESD_URM_F	LM	357
RESD_W_A	M	967
RESS_URM_A	LM	5385
RESS_URM_B	LM	4674
RESS_URM_C	LM	12480
RESS_W_A	M	615
REST_RC_A	M	4983
REST_RC_B	M	1005
REST_URM_A	LM	2432
REST_URM_B	LM	1651
REST_URM_C	M	6676

Typology ID	CL*	No.
REST_URM_D	M	2537
REST_URM_E	LM	2451
REST_URM_F	LM	4498
SCHOOL	L	1648

\* L = low, LM = low-medium, M = medium, MH = medium-high, H = high

## 7.3 History and Consistency Checks

### 7.3.1 History check

A history check of the fragility functions presented above has been undertaken by taking the actual seismic catalogue that was recorded in the field, estimating ground-motion fields for each event in the catalogue using the central v2 GMPE model (Bommer et al., 2015) and calculating the number of buildings that would fail based on the v2 exposure model and fragility functions.

As discussed in Bommer et al. (2015), the residuals of the ground motions for each spectral ordinate have been correlated using the model of Akkar et al. (2014), and the residuals of spectral acceleration and duration have been correlated using the Bradley (2011) model. Spatial correlation of the ground motion residuals has not been explicitly modelled, but has been approximated by grouping the buildings together into grid cells and assuming full correlation within a cell and zero correlation between cells.

As shown in Figure 7.1, there is a 9% probability that 1 building would have collapsed, according to the v2 (central) GMPE, fragility and exposure models. Given that no buildings have collapsed to date in the field, the history check gives consistent outcomes with those predicted using the fragility functions, at least over the range of magnitude events that have been observed so far in the field. Given that no building has even been moderately damaged so far in the field, fragility functions based on lower displacement capacities could also be produced for further history checks in the future.

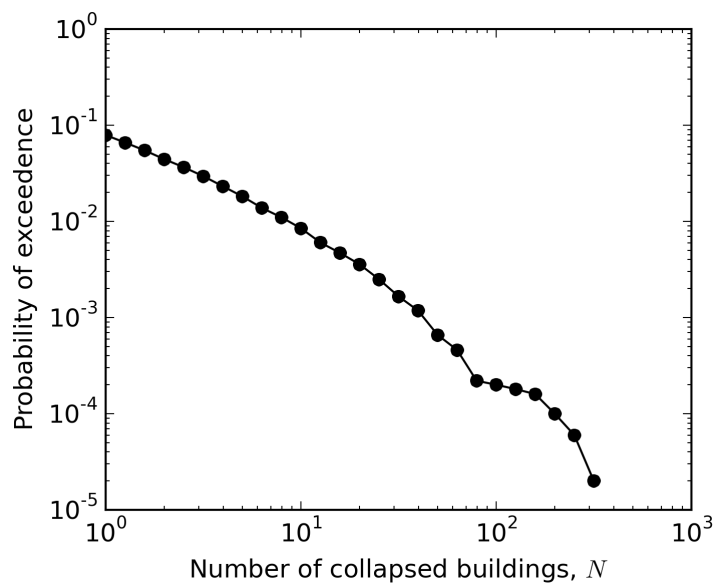


Figure 7.1. Expected distribution of collapsed buildings according to the observed seismicity in the Groningen field

### 7.3.2 Consistency checks

In order to set up a procedure for consistency checks of the fragility functions developed for the Groningen risk model, collapse/partial collapse damage data from a number of relevant earthquakes is being collected. Specific focus has been given to unreinforced brick masonry buildings, given their abundance in the Groningen field and their high levels of fragility. Data for the following events has currently been evaluated for testing purposes:

- $M_w$  3.6, 2012 Huizinge earthquake (Groningen field)
- $M_w$  5.4, 1992 Roermond earthquake (Netherlands and Germany)
- $M_w$  7.2, 2010 Darfield earthquake (New Zealand)
- $M_w$  6.3, 2011 Christchurch earthquake (New Zealand)

The 2012 Huizinge earthquake is of interest as it affected the Groningen field, and subjected a number of unreinforced masonry buildings in the area to levels of PGA (arbitrary component) up to a recorded value of 0.08g (though higher ground motions could have been experienced and not recorded). No buildings collapsed in this event.

On Monday 13th April 1992, at 03:20 local time, an earthquake of  $M_w$  5.4 and focal depth of 15 km struck the Roer River Valley on the southern border region between the Netherlands and Germany. The main shock's epicentre ( $51.15^\circ\text{N}$ ,  $5.93^\circ\text{E}$ ) was close to the town of Roermond in the Netherlands, inhabited by 43,000 people, and ground shaking was felt over an area larger than 600,000 km<sup>2</sup> between the Czech Republic, Switzerland, France and England. The UK-based Earthquake Engineering Field Investigation (EEFIT) mounted a three-day visit to the worst affected areas, about one week after the event. In order to cover the whole affected region, the three-member team travelled by car photographing buildings along the main streets in 37 locations (10 in the Netherlands and 27 in Germany). The survey included damage to Roermond town but not to the seriously affected Hersenbosch town. The survey concentrated on residential masonry buildings as this building type occurred in sufficient numbers. It is noted that although a proportion of the buildings that were surveyed were from the Netherlands, it was unlikely for there to have been a high proportion of modern terraced buildings that are common in the Groningen field. More investigation of the building types present in and around Roermond at the time of the earthquake is needed.

A total of 3,963 buildings were examined and the damage data was published in Pappin et al. (1994). None of these buildings were found to have exceeded a heavy state of damage in this earthquake. There were no recordings of the ground shaking for this event, though estimates of the peak ground acceleration (larger component) up to 0.22g have been made using ground-motion prediction equations (GMPEs)

developed for California<sup>4</sup>. This larger component PGA can be corrected to the arbitrary PGA by dividing by 1.1 (Beyer and Bommer, 2006), to give a value of 0.2g. The uncertainty in these GMPEs needs to be considered, as the ground motions could have been up to 3 standard deviations above or below this median value.

Christchurch, New Zealand, was subjected to a swarm of earthquakes in 2010 and 2011. The first major event occurred in the vicinity of Darfield (about 40 km from Christchurch) on 4th September 2010, and had a moment magnitude,  $M_w$ , of 7.1. A number of URM buildings in Christchurch were damaged by this event, as discussed in Ingham and Griffith (2011a). The second largest event of the swarm occurred on 22nd February 2011 and struck the centre of Christchurch with a moment magnitude,  $M_w$ , of 6.3. Ingham and Griffith (2011b) note that the characteristics of the Christchurch URM building stock depended on the location of the buildings, with a greater proportion with cavity wall construction found outside the Central Business District (CBD). Hence, it would appear to be justified to separate the damage data for buildings inside and outside the CBD, given the expected difference the seismic response of URM buildings with cavity walls. Furthermore, a number of URM buildings had been retrofitted, and so these buildings should not be considered further for comparison with the v2 fragility functions.

The URM damage data collected after the swarm of Canterbury earthquakes has been made available to the authors of this report, along with estimates of the ground shaking (in terms of PGA) to which each building was subjected, which was taken from the nearest recording (which, it is noted, might have been kilometres away from the buildings). As mentioned previously, given the large spatial variability that is observed in ground motions, the actual levels of PGA that the buildings were subjected to might have been much higher or much lower than the values provided in the database.

The Christchurch URM building damage data has been processed as follows:

- The data inside and outside of the CBD has been separated.
- Only URM buildings that were known to have not had any retrofitting work were considered.
- For the statistics of the 2011 event, only buildings that had no recorded damage in the 2010 event were considered.
- The statistics from two different damage scales were considered, ATC-38/13 (ATC, 1985) and Wailes and Horner (1933). Collapse was defined as major (60-100% replacement value) or destroyed (100% replacement value) using the ATC-38/13 scale, and as D (Major Damage to more than 50% of walls) and E (Unrepairable Damage, Demolition Probably Appropriate) using the

---

<sup>4</sup> <http://earthquake.usgs.gov/earthquakes/shakemap/atlas/shake/199204130120/>

Wailles and Horner (1993) scale. Both scales were found to give consistent damage statistics.

- Outside the CBD, the data were grouped into bins of ground motion, whereas inside the CBD they were all assigned the same level of PGA in the database.
- For each event, and both inside and outside the CBD, the number of buildings that collapsed (as defined above) was calculated for each ground motion bin, and divided by the total number of buildings in the database that were subjected to that level of ground motion.

The comparisons of the damage statistics for all of the above events with the  $v_2$  fragility functions for residential URM building typologies are given in Figure 7.2. The  $v_2$  fragility functions have been transformed to PGA by calculating first the median spectral acceleration of the lognormal distribution (ignoring, therefore, the influence of significant duration) and transforming this to PGA using the spectral shape from the  $v_2$  GMPE for moment magnitude 5 at zero epicentral distance, using the average amplification factors over a number of zones (309, 601, 820, 1009, 1705, 2011, 2204), as described in Bommer et al. (2015). For simplicity, the collapse mechanism with the lowest median spectral acceleration has been selected for each typology.

In order to account for the uncertainty in the actual level of PGA to which the buildings were subjected, dashed lines with  $\pm 1$  standard deviation (with an assumed total aleatory variability in the ground motion of 0.7) have also been plotted (noting that on average almost one-third of the actual ground-motion peaks would actually lie outside this range). Given more time to investigate the ground motions from these events, and in particular those from the Christchurch earthquakes, it could be possible to reduce the variability in the ground motion plotted herein by estimating the inter-event variability from the recordings (provided there is a sufficient number). Nevertheless, it is clear that the large variability in the ground motion reduces the usefulness of observed damage data for the 'validation' of analytical functions (as also discussed in Crowley et al., 2008).

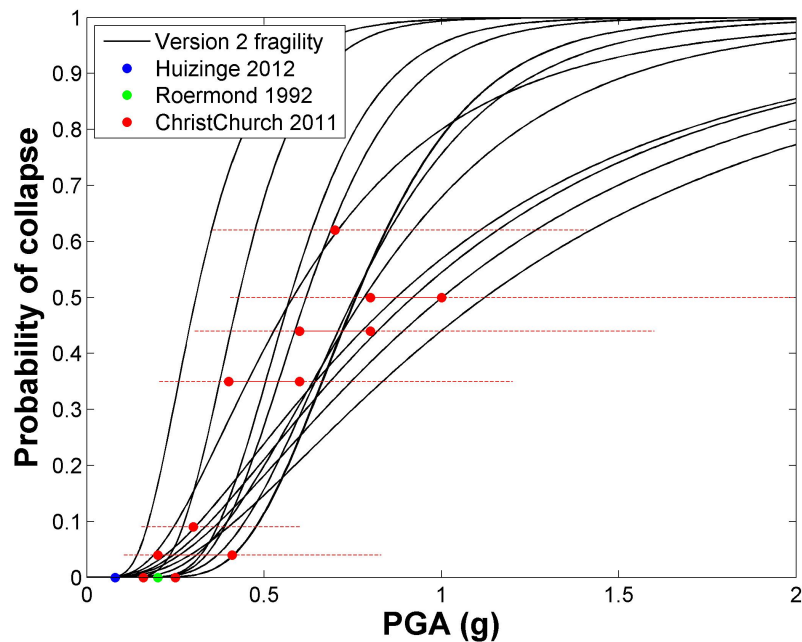


Figure 7.2. Comparison of v2 fragility functions (converted to PGA) for residential URM buildings with observed damage data. Dashed lines show +/1 standard deviation of the ground motion variability.

#### 7.4 Truncation of Lognormal Distribution

Although there are a number of drawbacks in attempting to check analytical fragility functions with observed damage data, as discussed in the previous section, one way in which this empirical data can be used is to provide a truncation to the lognormal distribution functions.

The probability of at least one building collapsing (and potentially causing fatalities) within a given time frame is driven by the lower tails of the lognormal distribution. As shown in Figure 7.3, with a lognormal distribution the probability of collapse does not reach zero until the PGA is equal to zero. If this function were to be applied to hundreds of thousands of buildings in a group risk calculation, a probability of collapse of  $10^{-4}$  at 0.05g would result in the prediction of tens of collapsed buildings. Given that experience shows that buildings do not collapse at such low levels of ground shaking, it would seem reasonable to truncate the fragility functions such that they reach zero at non-zero levels of ground shaking.

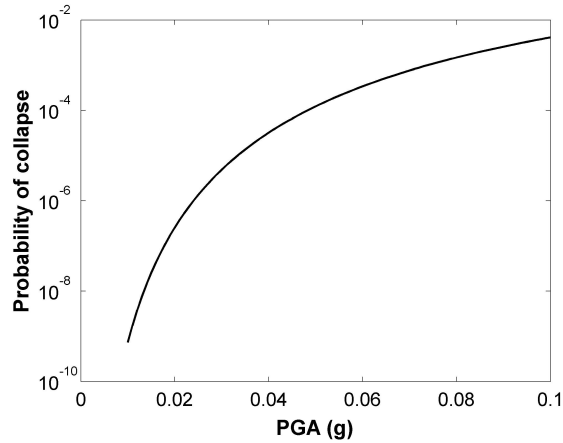


Figure 7.3. Lognormal fragility function (shown with a logarithmic y-axis)

One possibility for truncating the lognormal functions that has been investigated to date has been to use the highest value of PGA that has been recorded in the Groningen field to date (0.08g), and the probability of partial collapse has been set to zero at this level of ground shaking. This level of PGA has been related to the median spectral ordinates for the other periods of vibration (for an average soil type) using the v2 GMPE for magnitude 3.6 at zero epicentral distance. This truncation was not seen to have a significant influence on the risk results. Various other options for truncating the lognormal fragility functions may be investigated in the future.

## **8 Consequence and Fatality Modelling**

### **8.1 Introduction**

As discussed in Chapter 1, the estimation of fatality risk depends on the probability of collapse, associated to a given partial collapse mechanism, and its expected volume loss (for inside risk) or debris area (for outside risk). This Chapter summarises the assumptions that have been taken in the v2 model to estimate the consequences of collapse in terms of debris and fatalities inside buildings. It is noted that this area of the model is likely to receive the largest attention in future developments, together with a model for outside fatality risk.

### **8.2 Volume Loss**

A lower bound, best estimate and upper bound volume loss for each partial collapse mechanism has been defined by combining advanced numerical modelling of collapse, empirical evidence, and judgment.

The Applied Element Method (Meguro and Tagel-Din, 2000; Tagel-Din and Meguro, 2000a and 2000b) used in Extreme Loading for Structures (ASI, 2010) caters for the automatic tracking and propagation of cracks, separation of elements, element collision, and collapse of structures under extreme loads. This has been demonstrated for example by Salem et al. (2011) who modelled progressive collapse of a 5-storey reinforced concrete building, and Karbassi and Lestuzzi (2012) who used ELS to develop collapse fragility functions of URM structures (Figure 8.1).

This software has been used herein to model the URM and RC wall buildings (see Chapter 2), and the collapse mechanisms formed during the pushover analyses gave an insight into the volume losses that could be expected for these structures due to in-plane failure (see Figure 8.2 and Figure 8.3). A similar method has been applied by Furukawa and Ohta (2008) to estimate injury risk in masonry buildings. Many more analyses are needed in the future, in particular nonlinear dynamic analyses, to gain further insight into the collapse mechanisms of the structures studied herein.

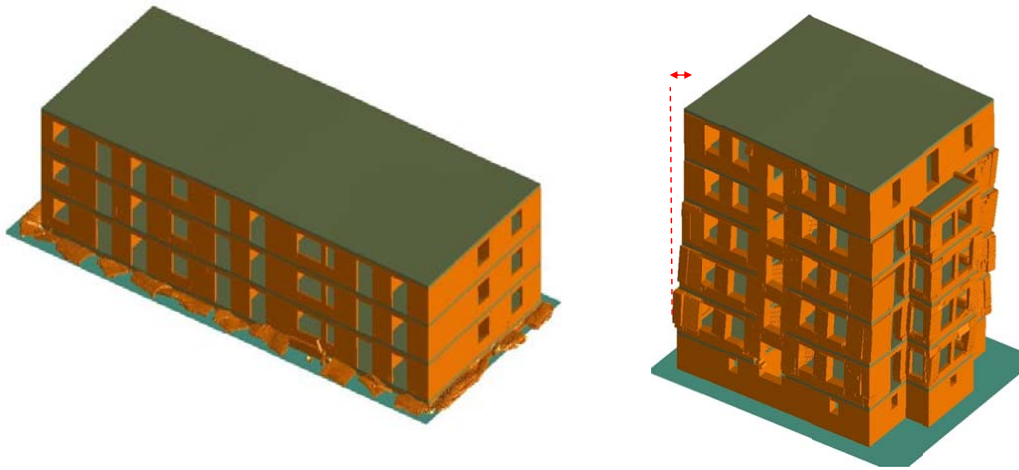


Figure 8.1. Collapse mechanisms of URM buildings obtained by Karbassi and Lestuzzi (2012) using ELS

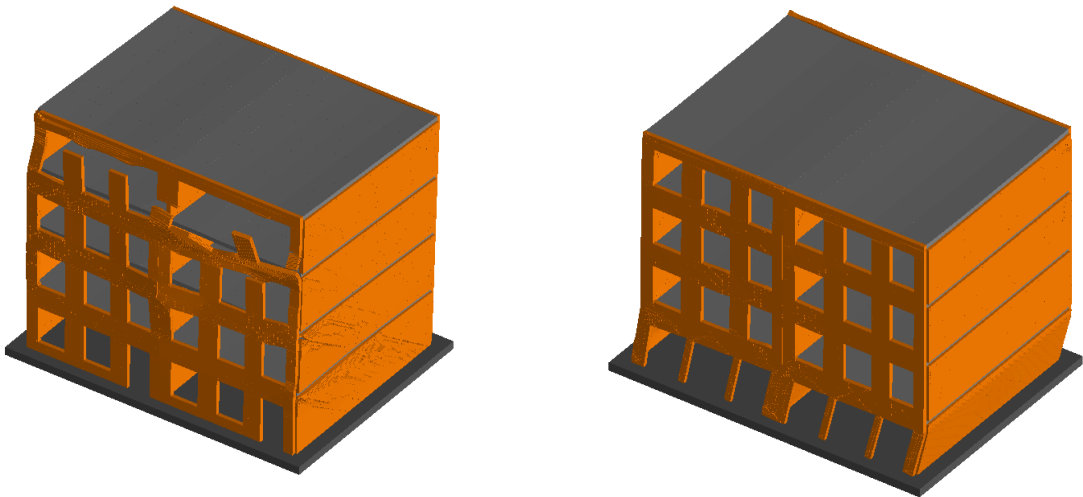


Figure 8.2. Collapse mechanisms of URM residential buildings with and without large openings at ground floor, obtained with ELS software

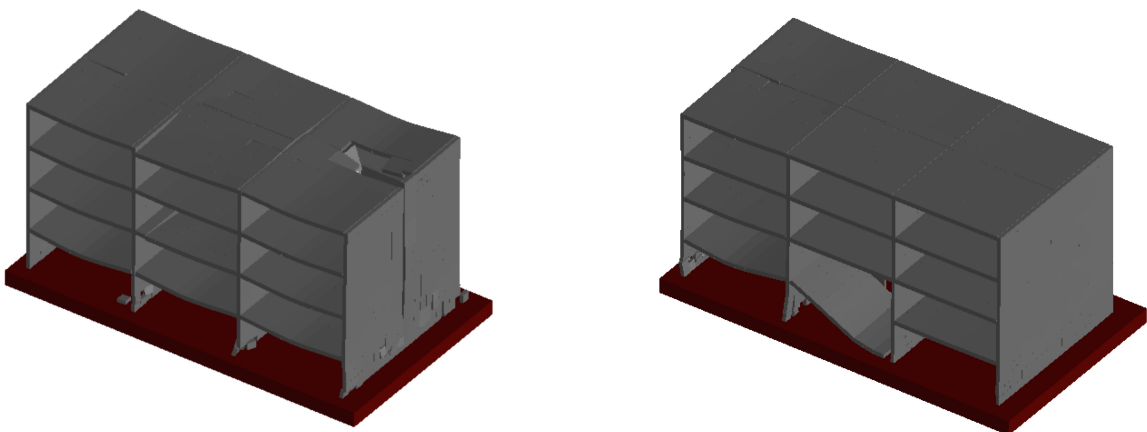
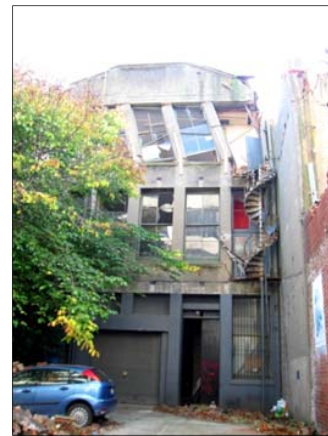


Figure 8.3. Collapse mechanisms for RC tunnel construction buildings from ELS software

Some examples of observed partial collapse mechanisms and volume losses from past earthquakes that have been used to inform the volume losses are given in Figure 8.6, Figure 8.4, and Figure 8.6.



(ChristChurch earthquake, 2011)



(ChristChurch earthquake, 2011)

Figure 8.4. Examples of photos used to inform volume losses due to in-plane failure of URM buildings (Ingham and Griffith, 2011b) (left: weak URM piers and pier rocking, right: collapse of top floor due to weak URM piers)



(ChristChurch earthquake, 2011)



(Emilia earthquakes, 2012)

Figure 8.5. Examples of photos used to inform volume losses due to failure of non-URM buildings (left: timber frame distortion, right: connection failure of precast RC frames)

The redundancy of the system is an important indicator of the volume loss that will develop following collapse, and this has been considered when assigning the volume losses. The detached URM buildings are typically redundant systems with many walls supporting the floors/roof, and slabs spanning in two directions. On the other hand, the terraced buildings have very little redundancy and typically have one-way spanning slabs. The weight of the floor/roof has also been taken into consideration when assigning volume losses, as it is assumed that the lighter timber floors can be more easily supported by the remaining walls that do not collapse. The size of the building is also of importance, especially for out-of-plane failure, as the volume of debris when one wall fails out of plane will be a small proportion of the total volume of the building.



(Newcastle earthquake, 1989)



(ChristChurch earthquake, 2011)



(Loma Prieta earthquake, 1989)



(Darfield earthquake, 2010)

Figure 8.6. Examples of photos used to inform volume losses due to out of plane failure of walls supporting roofs/slabs for different typologies of structures

Judgment has also been used to assign different volume losses between terraced buildings, as a function of whether they have cavity party walls (and thus each unit should be considered as a separate building) or solid party walls (and thus all units together can be considered as a single building). The volume loss of the latter due to out of plane failure is assumed to be much lower, given that the average number of units of a terraced house is 6. It is known that about 50% of the residential apartment and commercial buildings in the exposure database are part of aggregate, and thus out-of-plane failure is less likely to affect the internal buildings of the aggregate; assumptions have been made on the number of buildings per aggregate in order to adjust the volume losses. Future improvements to the exposure database could explicitly highlight the corner buildings of aggregates.

### 8.3 Inside Local Personal Risk Fatality Model

The plot shown in Figure 1.5 has been used to estimate fatality ratios for the volume losses assigned to each building typology. It is noted that the steel building data from this figure has not been used herein, as there was no clear relationship between volume loss and fatality ratio. Instead, given the recommended range of fatality ratios for steel structures provided in So (2015), the relationship for reinforced concrete frames has been used also for steel structures. Best-fit regression lines have been applied to the data, as shown in Figure 8.7.

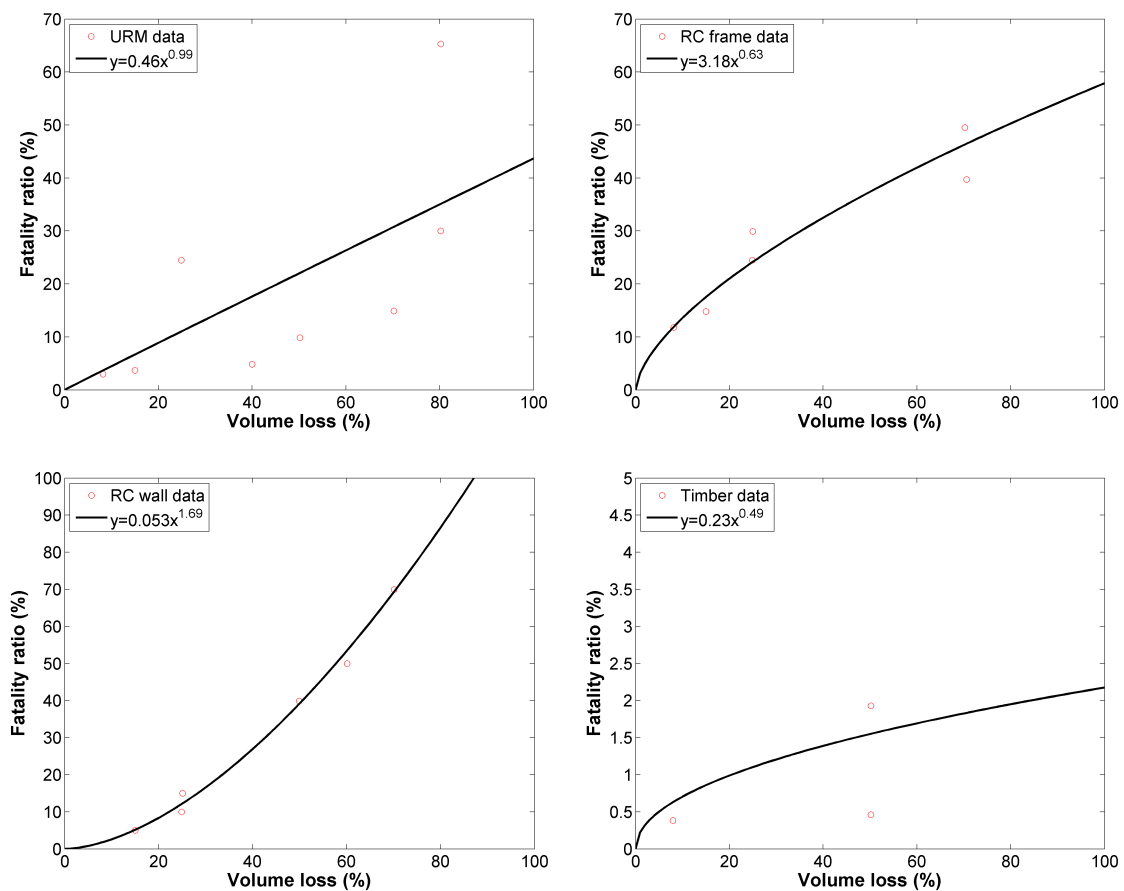


Figure 8.7. Best-fit relationships between volume loss (%) and indoor fatality ratios (%)

It is noted that zero volume loss does not correspond to zero fatalities, as a minimum fatality ratio of 0.1% for reinforced concrete, 0.15% for URM, 0.33% for timber and 0.5% for steel buildings has been assumed due to non-structural damage and other causes not directly related to collapse, based on the recommendations in HAZUS (FEMA, 2003). The HAZUS methodology provides fatality ratios to be applied to buildings with “complete” damage, and so these have been increased in order to be applicable with “collapse” fragility functions, based on the HAZUS ratios of collapsed to completely damaged buildings.

These models to relate volume losses to fatality ratios are based on observed volume losses for both partial collapse (D4) and global collapse (D5) mechanisms, and the inclusion of the latter might lead to a bias in the results for partial collapses. As the current focus is exclusively on partial collapse mechanisms, the models above are being extrapolated to low volume losses that might be outside the range of application. Volume loss may not be the best parameter to relate the analytical response with consequences, and this issue will be extensively reviewed in the developments for the v3 model. Ideally, a fatality model would be developed that relates collapse mechanisms to fatality ratios, but the available data on people that have died in earthquakes with different collapse mechanisms is scarce.

#### 8.4 Consistency Checks

A ‘sanity check’ has been carried out on the range of values of fatalities that are being estimated with the current fragility functions and volume loss - fatality ratio models for unreinforced masonry buildings (as they have been given the greatest focus in the development of the v2 fragility and consequence model, given the large number of buildings in URM in the Groningen field – see Section 1.2).

The semi-empirical collapse fragility and fatality ratios produced by the U.S. Geological Survey’s PAGER<sup>5</sup> (Prompt Assessment of Global Earthquakes for Response) program have been used for this consistency check. These functions have been developed through collaboration with experts from 26 countries, and led to building-specific fragility functions and fatality ratios that were checked by hindcasting losses using past fatal earthquakes. Jaiswal et al. (2011a) presents the parameters of the collapse fragility functions for brick masonry with lime/cement mortar. These functions are in terms of macroseismic intensity (MMI), and for the purposes of this consistency check they have been converted to PGA using the relationship proposed by Wald et al. (1999) (without considering the uncertainty in this relationship). The collapse probability for each value of PGA has then been multiplied by the fatality ratios proposed by Jaiswal et al. (2011b) that are conditional on collapse, to obtain vulnerability functions that describe the mean fatality ratio conditional on levels of ground shaking (see red curve in Figure 8.8). Vulnerability functions for the models presented herein have also been produced by combining the partial collapse fragility functions in terms of PGA (Figure 7.2) with the estimated volume losses and fatality model for URM buildings (Figure 8.7), and are presented by the black lines in Figure 8.8. The models presented herein consider the varying collapse capacity and mechanisms of different URM brick typologies and so the wide variation in vulnerability models is expected, whilst it is reassuring to note that the single model by Jaiswal et al. (2011a and b) falls inside the aforementioned range.

---

<sup>5</sup> <http://earthquake.usgs.gov/earthquakes/pager/>

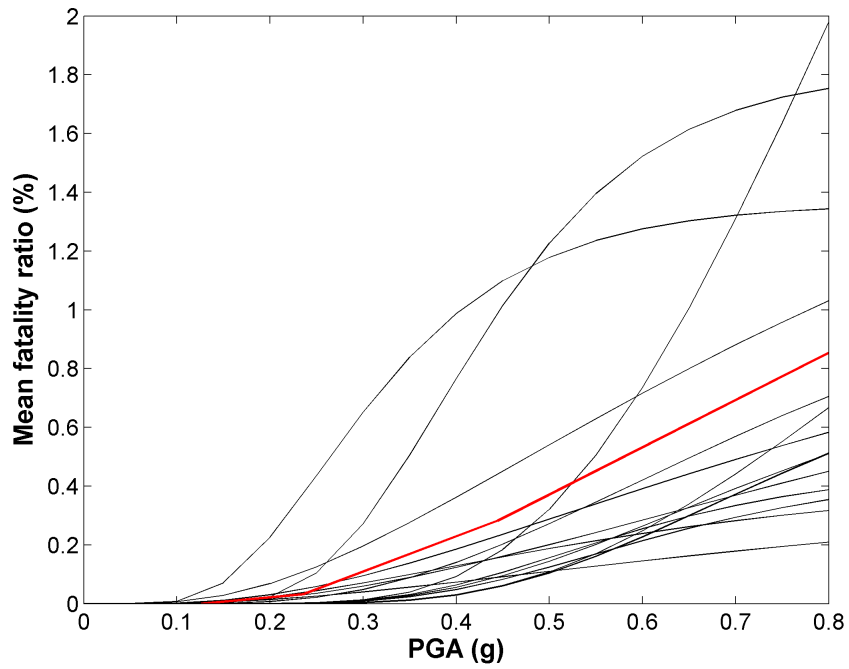


Figure 8.8. Mean vulnerability functions for the URM buildings considered herein (black) compared with the PAGER semi-empirical vulnerability function for brick masonry with lime/cement mortar (red).

## 9 Future Developments

A number of areas where further improvement is possible and/or desirable have been highlighted in the previous chapters. This Chapter summarises and prioritises the most important developments, and includes further suggestions for development stemming from the discussions that were held during the expert panel fragility review meeting that was held in London on 29<sup>th</sup> – 30<sup>th</sup> October.

### 9.1 Structural Modelling (in-plane and out-of-plane)

The focus on structural modelling for v3 will concentrate on the most fragile building typologies (i.e. URM and reinforced concrete buildings), and is likely to cover the following activities (in order of priority):

- The assumptions that were made for the development of some of the prototype models used herein (e.g. the URM apartment, industrial and commercial buildings and the tunnel-form reinforced concrete terraced buildings) will need to be checked against structural drawings of real buildings from the region.
- More information on the variations in geometry, material properties and detailing/connections within a typology will need to be collected, and the influence of these parameters on the capacity curves will be studied.
- More confidence on the displacements at which partial collapse mechanisms occur will be sought, also by comparing the values from the numerical models with available experimental test data in the literature (for example, Grammatikou et al. (2015) present a summary of the strength, deformation capacity and failure modes of reinforced concrete (RC) walls from a number of experimental tests that could be used to check the under-reinforced squat RC walls).
- Nonlinear dynamic analyses will be run for a number of models to gain more confidence on the predominant collapse mechanisms and consequences, and to produce the SDOF pushover curves of buildings with flexible diaphragms.
- The influence of vertical motion on buildings without adequate connections/anchorage will be studied by running nonlinear dynamic analysis of full scale building models with three components of ground motion, selected and scaled using the latest knowledge of ground shaking in the Groningen field (Bommer et al. 2015).

### 9.2 Fragility Modelling

The activities that will be undertaken during the development of the v3 fragility functions have been identified and prioritised as follows:

- The “falling objects” empirical fragility functions (NAM, 2015) will be reviewed and fully integrated into the v3 risk assessment. Non-structural elements such as chimneys, parapets and gable walls are connected to the structures that are considered in the partial collapse risk assessment, and consideration of their interaction will need to be made when integrating the outside risk due to falling objects and structural elements. Fragility functions for other non-structural elements, such as out-of-plane failure of façade and veneer walls, will also need to be developed for the outside risk assessment.
- Fragility functions for global instability collapse will be developed for some of the most fragile typologies to check the key assumption that partial collapse mechanisms contribute most to the inside local personal risk (see Section 1.4.3).
- The variation in capacity curves found from the additional structural modelling activities will be used to estimate the influence of building-to-building variability on the fragility functions, and thus better constrain the epistemic uncertainty.
- Further data and models for floor amplification will be sought to improve the modelling of out-of-plane rocking response, and the potential to use (less conservative) simplified two-way bending models for some typologies will be considered.
- Improvements to the cloud method will be investigated, as discussed extensively in Section 6.3. In particular, a better understanding of the influence of duration on the nonlinear response will need to be obtained by considering a variety of duration metrics.
- Schools and churches will receive a higher level of attention, with a dedicated effort to better understand the characteristics of these buildings so that they can be assigned more specific fragility functions in the risk assessment.
- A sensitivity study on the influence of cyclic degradation and pinching of the hysteretic models on the fragility functions will be undertaken to identify whether additional developments on this front (possibly by obtaining hysteretic models from other existing cyclic test results) is necessary.
- The Christchurch data that was used in Section 7.3.2 to consistency check the fragility functions has since been further elaborated and improved by Jason Ingham and colleagues and efforts will be made to collect and integrate such data, along with other relevant empirical damage data, in the v3 model.

### **9.3 Consequence Modelling**

The current approach to assign volume losses to partial collapse mechanisms, and relate the former to fatality ratios will be reviewed during the development of the v3 models. The feasibility of instead relating collapse mechanisms directly to fatality ratios will be investigated. Alternatively, data from buildings that have experienced partial collapse mechanisms and global (instability) collapse will be separated and

two separate fatality models will be developed. Focus will be given to obtaining damage and associated fatality data for reinforced concrete and brick masonry buildings with characteristics similar to those in Groningen.

The v3 risk assessment will include outside risk, and thus models for identifying the fatality risk to people outside of buildings due to both non-structural and structural elements will be developed, drawing upon the method that has already been applied in the falling objects risk model (NAM, 2015).

## 10 References

- Akkar S., Sandikkaya M.A. and Ay B.O. (2014) "Compatible ground-motion prediction equations for damping scaling factors and vertical-to-horizontal spectral amplitude ratios for the broader Europe region," *Bulletin of Earthquake Engineering*, 12, pp. 517-547.
- Alexander D. (1996) "The Health Effects of Earthquakes in the Mid-1990s," *Disasters* 20(3), pp. 231-247.
- Applied Science International (2010) Extreme Loading® for Structures (Version 3.1 B64).
- Arup (2015a) "Laboratory component testing: Modelling predictions and analysis cross validation," Internal Report submitted to NAM.
- Arup (2015b) "Blind prediction modelling and analysis – EUC BUILD," Internal Report submitted to NAM.
- Arup (2015c) "Modelling and Analysis Cross- Validation – Arup, EUCENTRE, TU Delft," Internal Report submitted to NAM
- ATC-13 (1985) "Earthquake damage evaluation data for California," Report ATC-13, Applied Technology Council, Redwood City, California.
- Baker J.W. (2007) "Probabilistic structural response assessment using vector-valued intensity measures," *Earthquake Engineering and Structural Dynamics*, 36, pp. 1861-1883.
- Baker J.W. and Cornell C.A. (2006) "Which spectral acceleration are you using?" *Earthquake Spectra*, 22(2), pp. 293-312.
- Baker H., So E., Spence R. and Pickup F. (2015) "Debris from collapsed and partially collapsed buildings in earthquakes: a study based on damage photographs," Cambridge Architectural Research Ltd and TTAC Ltd, Internal report submitted to NAM.
- Beyer K. and Bommer J.J. (2006) "Relationships between median values and between aleatory variabilities for different definitions of the horizontal component of motion," *Bulletin of Seismological Society of America*, 96(4A), pp. 1512-1522.
- Bommer J.J., Dost B., Edwards B., Rodriguez-Marek A., Kruiver P.P., Meijrs P., Ntinalexis M., Polidoro B. and Stafford P.J. (2015) "Development of Version 2 GMPEs for Response Spectral Accelerations and Significant Durations from Induced Earthquakes in the Groningen Field," Internal Report submitted to NAM.
- Bommer J.J., Magenes G., Hancock J. and Penazzo P. (2004) "The influence of strong-motion duration on the seismic response of masonry structures," *Bulletin of Earthquake Engineering* 2(1), pp. 1-26.
- Bradley B.A. (2011) "Correlation of significant duration with amplitude and cumulative intensity measures and its use in ground motion selection," *Journal of Earthquake Engineering*, 15(6), pp. 809-832.
- Brignola A., Podestà S. and Pampanin S. (2008) "In-plane stiffness of wooden floor," *Proceedings of the 2008 New Zealand Society of Earthquake Engineering*, Paper number 49.
- Calvi, G.M., R. Pinho, G. Magenes, J.J. Bommer, L.F. Restrepo-Velez & H. Crowley (2006), "Development of seismic vulnerability assessment methodologies over the past 30 years," *ISET Journal of Earthquake Technology*, Paper no. 472, 43 (3), pp. 75-104.
- Casotto, C., Silva, V., Crowley, H., Nascimbene, R. and Pinho, R. (2015) "Seismic Fragility of Italian RC Precast Industrial Structures", *Engineering Structures*, 94, pp. 122-136.

- Chandramohan R., Baker J.W. and Deierlein G.G. (2015) "Quantifying the influence of ground motion duration on structural collapse capacity using spectrally equivalent records," *Earthquake Spectra*, doi: <http://dx.doi.org/10.1193/122813EQS298MR2>
- Chiou B., Darragh R., Gregor N. and Silva W. (2008) NGA Project Strong-Motion Database, *Earthquake Spectra*, 24(1), pp. 23-44.
- CNR (2013) "Instructions for the seismic assessment of existing buildings" Consiglio Nazionale delle Ricerche, CNR-DT 212/2013. (*In Italian*)
- Coburn A. and Spence R. (2002) *Earthquake Protection*, 2<sup>nd</sup> Edition, John Wiley & Sons Ltd, Chichester.
- Coburn A.W., Spence R.J.S. and Pomonis, A. (1992) "Factors Determining Casualty Levels in Earthquakes: Mortality Prediction in Building Collapse," *Proceedings of the 10<sup>th</sup> World Conference on Earthquake Engineering*, Madrid, Spain.
- Comite Europeen de Normalisation (2003) *Eurocode 8, Design of structures for earthquake resistance—Part 1: general rules, seismic actions and rules for buildings*. Pr-EN 1998-1. Final Draft, December 2003.
- Crowley H., Stafford P.J. and Bommer J.J. (2008) "Can earthquake loss models be validated using field observations?" *Journal of Earthquake Engineering*, 12(7), pp. 1078-1104.
- Doherty K., Griffith M.C, Lam N. and Wilson J. (2002) "Displacement-based seismic analysis for out-of-plane bending of unreinforced masonry walls," *Earthquake Engineering and Structural Dynamics*, 31, pp. 833-850.
- Dymiotis C., Kappos A.J. and Chryssanthopoulos M.K. (1999) "Seismic reliability of RC frame with uncertain drift and member capacity," *Journal of Structural Engineering*, 125(9), pp. 1038–1047.
- EUCENTRE (2015a) "Protocol for shaking table test on full scale building v2", Internal report submitted to NAM.
- EUCENTRE (2015b) "Experimental campaign on cavity walls systems representative of the Groningen building stock", Internal report submitted to NAM.
- EUCENTRE (2015c) "Numerical and experimental evaluation of the seismic response of precast wall connections", Internal report submitted to NAM.
- EUCENTRE, P&P, TU-Delft, TU-Eindhoven (2015) "Material Characterisation," Version 1, Internal report submitted to NAM.
- FEMA (2003) "Direct Social Losses: Displaced Households Due to Loss of Housing Habitability and Short Term Shelter Needs," Chapter 14, HAZUS-MH MR4 Technical Manual, Washington DC.
- FEMA-440 (2005) "Improvement of nonlinear static seismic analysis procedures," Federal Emergency Management Agency, Washington, D.C., U.S.A.
- Franchin P., Lupoi A., Pinto P.E. and Schotanus M.I.J. (2003) "Seismic fragility of reinforced concrete structures using a response surface approach," *Journal of Earthquake Engineering*, 7 (Special Issue 1), pp. 45-77.
- Furukawa A. and Ohta Y. (2009) "Failure process of masonry buildings during earthquake and associated casualty risk evaluation," *Natural Hazards*, 49, pp. 25-51.
- Grammatikou S., Dionysis B. and Fardis M.N. (2015) "Strength, Deformation Capacity and Failure Modes of RC Walls under Cyclic Loading." *Bulletin of Earthquake Engineering*. doi:10.1007/s10518-015-9762-x.

- Grunthal, G. (ed.) (1998) "European Macroseismic Scale 1998 (EMS-98)," Cahiers du Centre Europeen de Geodynamique et de Seismologie 15, Centre Europeen de Geodynamique et de Seismologie, Luxembourg, 1998.
- Hancock J. and Bommer J.J. (2007) "Using spectral matched records to explore the influence of strong-motion duration on inelastic structural response," *Soil Dynamics and Earthquake Engineering*, 27, pp. 291-299.
- Ibarra L.F., Medina R.A. and Krawinkler H. (2005) "Hysteretic models that incorporate strength and stiffness deterioration," *Earthquake Engineering and Structural Dynamics*, 34(12), pp. 1489-1511.
- Ibarra L. F. and Krawinkler H. (2005) "Global collapse of frame structures under seismic excitations," John A. Blume Earthquake Engineering Center, Stanford, CA, 324.
- Iervolino I., Fabbrocino G. and Manfredi G. (2004) "Fragility of standard industrial structures by a response surface method," *Journal of Earthquake Engineering*, 8(6), pp. 927-945.
- Iervolino I., Manfredi G. and Cosenza E. (2006) "Ground motion duration effects on nonlinear seismic response," *Earthquake Engineering and Structural Dynamics*, 35, pp. 21-38.
- Ingham J.M. and Griffith M.C. (2011a) "The performance of URM masonry buildings in the 2010/2011 Canterbury earthquake swarm," Report to the Royal Commission of Inquiry, August 2011.
- Ingham J.M. and Griffith M.C. (2011b) "The performance of earthquake strengthened URM buildings in the Christchurch CBD in the 22 February 2011 earthquake," Addendum Report to the Royal Commission of Inquiry, October 2011.
- Jaiswal K., Wald D.J. and Hearne M. (2009) "Estimating Casualties for Large Worldwide Earthquakes using an Empirical Approach," US Geological Survey Open-File Report 1136.
- Jaiswal K., Wald D. and D'Ayala D. (2011a) "Developing empirical collapse fragility functions for global building types," *Earthquake Spectra*, 27(3), pp. 775-795.
- Jaiswal K., Wald D.J., Earle P.S., Porter K.A. and Hearne M. (2011b) "Earthquake Casualty Models Within the USGS Prompt Assessment of Global Earthquakes for Response (PAGER) System" in *Human Casualties in Earthquakes, Progress in Modelling and Mitigation*, Ed. Spence, So and Scawthorn, Springer.
- Jalayer F. (2003) "Direct probabilistic seismic analysis: Implementing non-linear dynamic assessments." Ph.D. Dissertation, Stanford University.
- Karbassi A. and Lestuzzi P. (2012) "Fragility analysis of existing unreinforced masonry buildings through a numerical based methodology," *The Open Civil Engineering Journal*, 6(Suppl 1-M2), pp. 121-130.
- Lam N.T.K., Griffith M., Wilson J. and Doherty K. (2003) "Time-history analysis of URM walls in out-of-plane flexure," *Engineering Structures*, 25, pp. 743-754.
- Luco N. and Cornell C.A. (2007) "Structure-Specific Scalar Intensity Measures for Near-Source and Ordinary Earthquake Ground Motions," *Earthquake Spectra*, 23(2), pp. 357-392.
- McKenna F., Fenves G.L., Scott M.H. and Jeremic, B. (2000) Open System for Earthquake Engineering Simulation (OpenSees), Pacific Earthquake Engineering Research Center, University of California, Berkeley, CA.
- Meguro K. and Tagel-Din H. [2000] "Applied element method for structural analysis: Theory and application for linear materials". *Structural engineering/earthquake engineering* (Japan: Japan Society of Civil Engineers (JSCE)) 17(1), pp. 21-35.

- Menon A. and Magenes G. (2008) "Out of plane seismic response of unreinforced masonry. Definition of Seismic Input," *Centre for Post-graduate Training and Research in Earthquake Engineering and Engineering Seismology*, Research Report No. ROSE-2008/04.
- Mergos P.E. and Beyer K. (2014) "Loading protocols for European regions of low to moderate seismicity," *Bulletin of Earthquake Engineering*, 12, pp. 2507-2530.
- Mosayk (2015a) "Report on structural modelling of non-URM buildings - v2 Risk Model Update" Deliverable D2 submitted to NAM.
- Mosayk (2015b) "Report on soil-structure interaction (SSI) impedance functions for SDOF systems" Deliverable D3 report submitted to NAM.
- NAM (2015) "Hazard and Risk for Induced Seismicity Groningen – Update 7<sup>th</sup> November 2015" Available from URL: [www.namplatform.nl](http://www.namplatform.nl)
- NZS 1170.5 (2004) "Structural Design Actions. Part 5: Earthquake action," Council of Standards New Zealand.
- Okada S. (1996) "Description for indoor space damage degree of building in earthquake," *Proceedings of 11<sup>th</sup> World Conference on Earthquake Engineering*, Paper no. 1760.
- Pappin J.W., Coburn A.R. and Pratt C.R. (1994) "Observations of damage ratios to buildings in the epicentral region of the 1992 Roermond earthquake, the Netherlands (extended abstract)," *Geologie en Mijnbouw*, 73, pp. 299-302.
- Salem H.M., El-Fouly A.K and Tagel-Din H.S. (2011) "Toward an economic design of reinforced concrete structures against progressive collapse," *Engineering Structures*, 33, pp. 3341-3350.
- Samardjieva E. and Badal J. (2002) "Estimation of the expected number of casualties caused by strong earthquakes," *Bulletin of Seismological Society of America*, 92, pp. 2310–2322.
- Seismosoft (2015) SeismoStruct — A computer program for static and dynamic nonlinear analysis of framed structures, (online). Available from URL: <http://www.seismosoft.com>.
- Seligson H.A. (2008) "Casualty Consequence Function and Building Population Model Development," Primary resource document for the "FEMA P-58 Seismic Performance Assessment of Buildings", FEMA, Washington.
- Shome N. and Cornell C.A. (1999) "Probabilistic seismic demand analysis of nonlinear structures," Reliability of Marine Structures Program Report No. RMS-35, Department of Civil and Environmental Engineering, Stanford University, California (also available at <http://pitch.stanford.edu/rmsweb/Thesis/NileshShome.pdf>).
- Silva V., Crowley H., Varum H., Pinho R. and Sousa R. (2013a) "Evaluation of analytical methodologies to derive vulnerability functions," *Earthquake Engineering and Structural Dynamics*, 43(2), pp. 181-204.
- So E. (2015) "Derivation of fatality rates for use in building collapse-based earthquake loss estimation models," USGS Internal File Report, *under review*.
- So E. and Pomonis, A. (2012) "Derivation of globally applicable casualty rates for use in earthquake loss estimation models," *Proceedings of the 15<sup>th</sup> World Conference on Earthquake Engineering*, Lisbon, Portugal, Paper no. 1164.
- So, E., Spence, R. and Baker H. (2015) "Volume loss in collapsed and partially collapsed buildings in earthquakes: a study based on damage photographs," Cambridge Architectural Research Ltd, Internal report submitted to NAM.

- Spence R. and So E. (2009) "Estimating Shaking-Induced Casualties and Building Damage for Global Earthquake Events," NEHRP Grant number 08HQGR0102, Final Technical Report.
- Tagel-Din H. and Meguro K. (2000a) "Nonlinear simulation of RC structures using Applied Element Method," *Structural engineering/earthquake engineering*, (Japan: Japan Society of Civil Engineers (JSCE)), 17(2), pp. 137-148.
- Tagel-Din H. and Meguro K. (2000b) "Applied Element Method for dynamic large deformation analysis of structures," *Structural engineering/earthquake engineering*, (Japan: Japan Society of Civil Engineers (JSCE)), 17 (2), pp. 215-224.
- Vamvatsikos D. and Cornell C.A. (2002) "Incremental dynamic analysis," *Earthquake Engineering and Structural Dynamics*, 31(3), pp. 491–514.
- Wailles C.D. and Horner A.C. (1933) 'Earthquake damage analysed by Long Beach Building Officials', *Engineering Xeu's Record*, May 25<sup>th</sup> 1933.
- Wald D.J., Quitoriano V., Heaton T.H. and Kanamori H. (1999) "Relationship between Peak Ground Acceleration, Peak Ground Velocity, and Modified Mercalli Intensity in California," *Earthquake Spectra*, 15(3), pp. 557-564.

## Appendix A Influence of SSI

In order to demonstrate the influence of including SSI effects on the fragility functions, a comparison of the nonlinear response of structures with and without SSI springs/dashpot dampers has been carried out using the typology REST-URM-D.

The characteristics of the springs/dashpot dampers have been calculated for piled, shallow concrete and shallow URM foundations (see Mosayk, 2015b). The nonlinear response to 100 records has been calculated both with and without SSI, and the results are compared in Figure A.1, Figure A.2 and Figure A.3.

The type of foundation does not have a significant influence on the response for this typology, but the inclusion of SSI is seen to reduce the nonlinear response by about 15%, on average. However, the influence of SSI on the responses decreases as the nonlinear response increases.

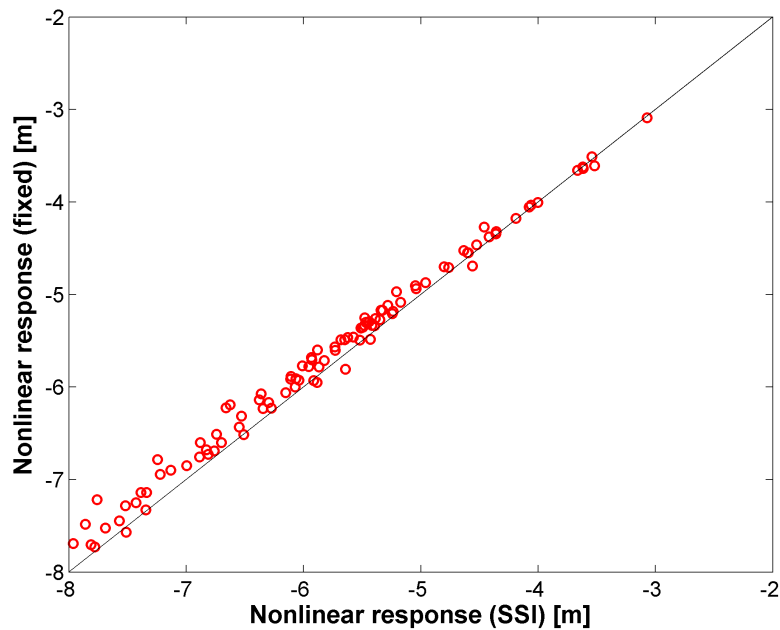


Figure A.1. Comparison of fixed base and piled foundation nonlinear response

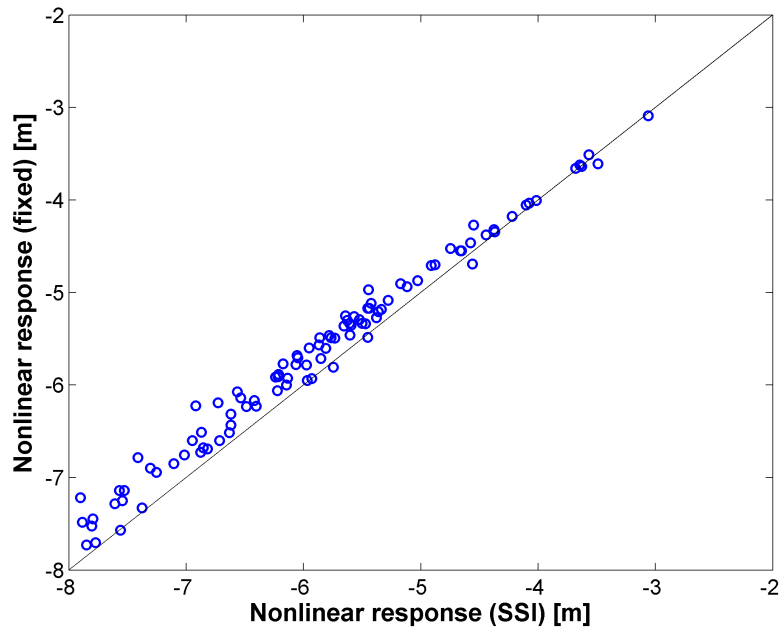


Figure A.2. Comparison of fixed base and shallow concrete foundation nonlinear response

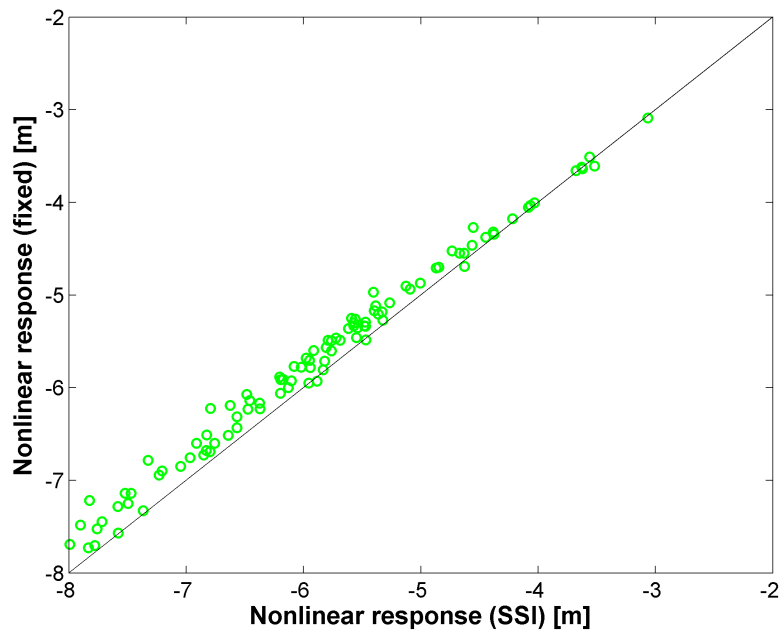
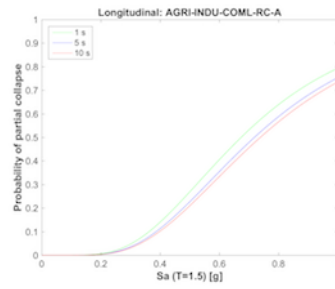
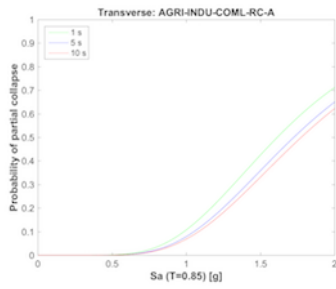
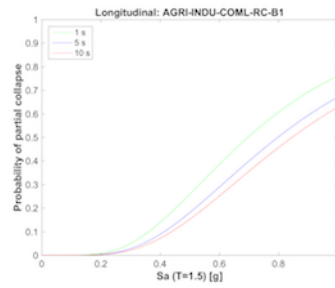
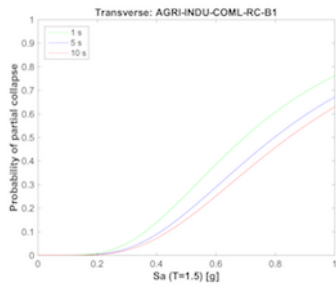


Figure A.3. Comparison of fixed base and shallow URM foundation nonlinear response

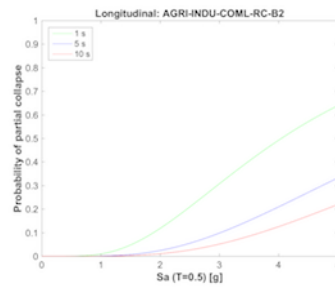
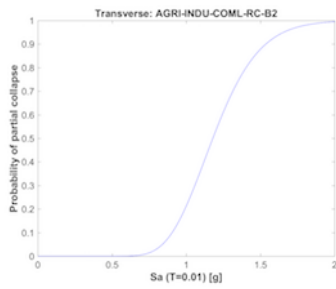
## Appendix B Plots of Fragility Functions



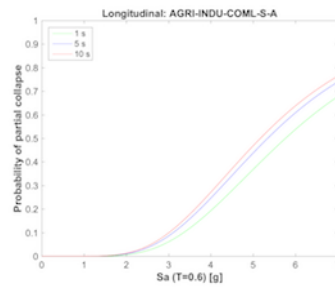
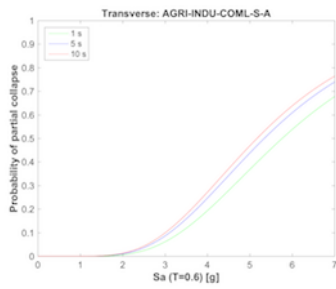
(Not applicable)



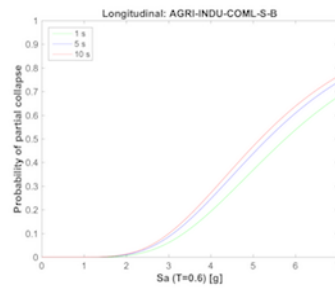
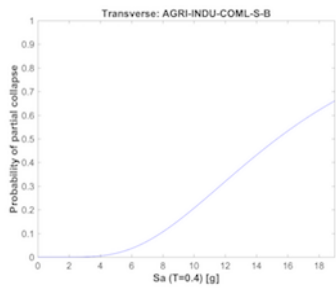
(Not applicable)



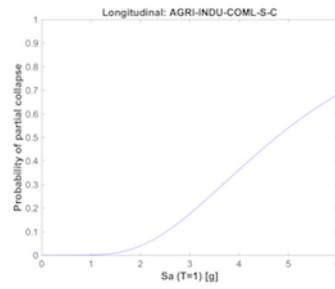
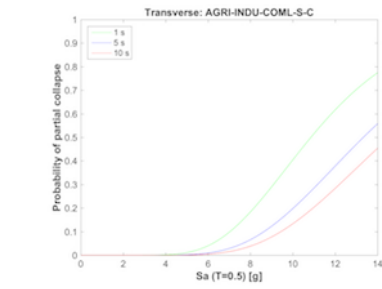
(Not applicable)



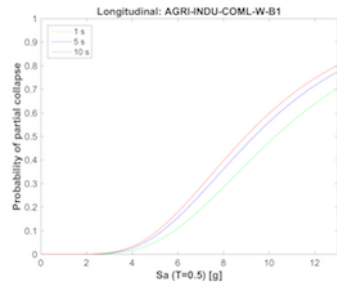
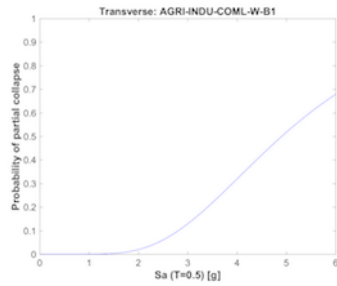
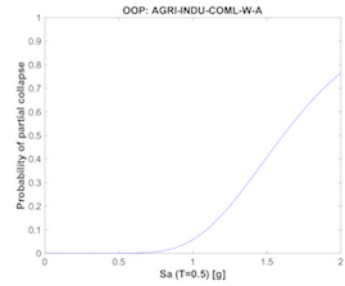
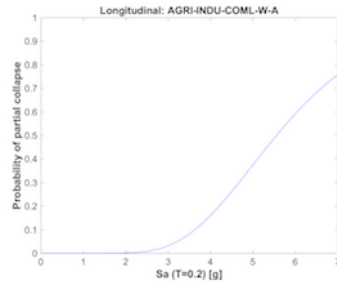
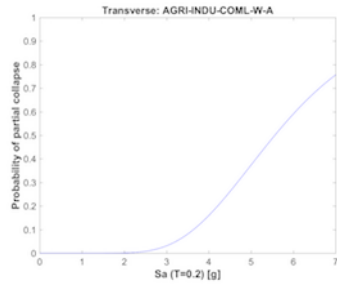
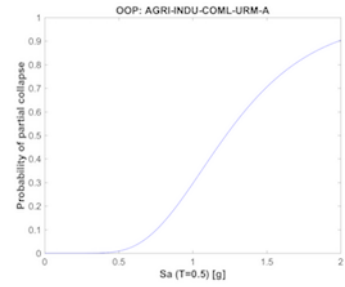
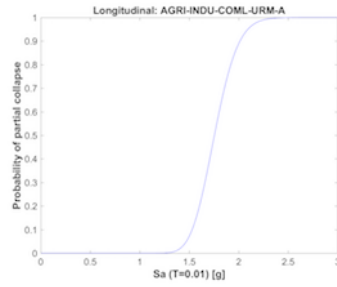
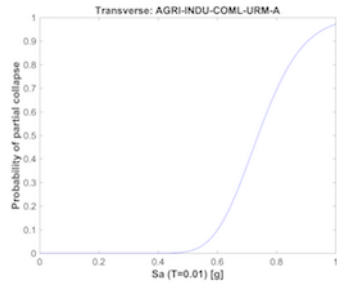
(Not applicable)



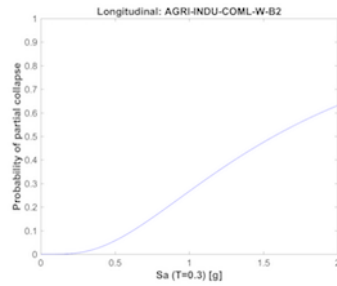
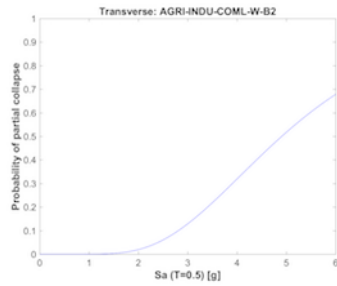
(Not applicable)



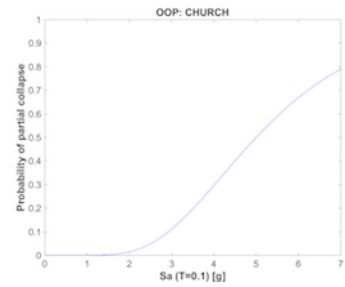
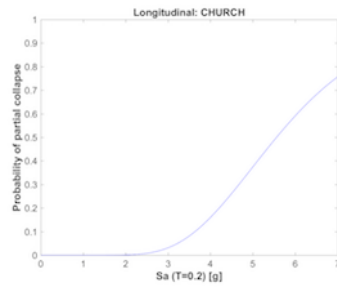
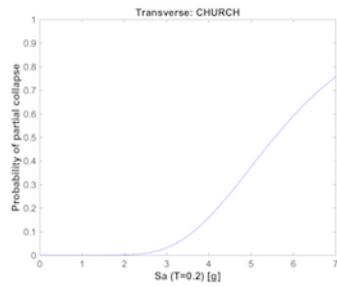
(Not applicable)

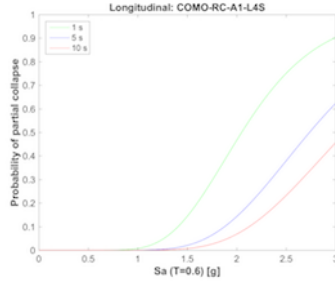
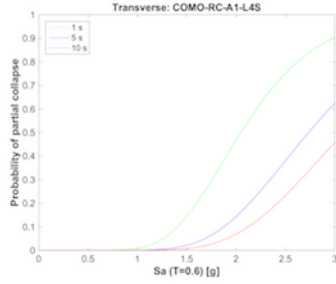
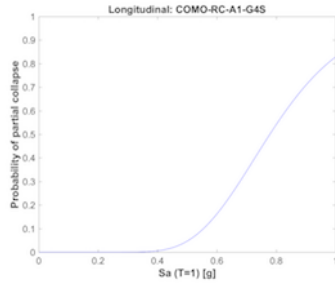
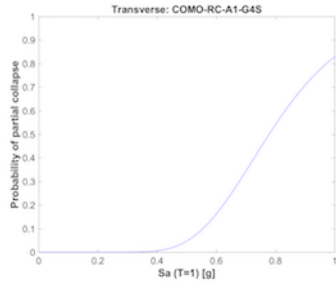


(Not applicable)

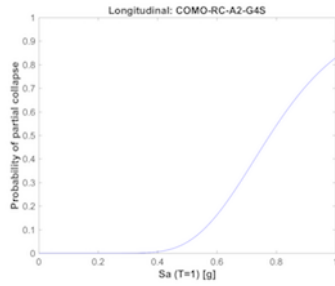
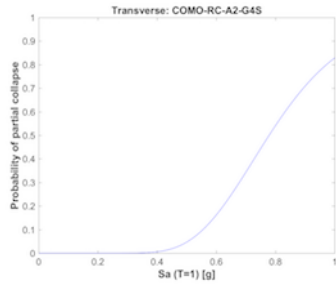


(Not applicable)

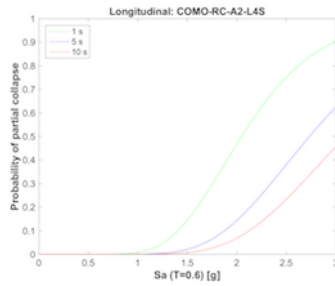
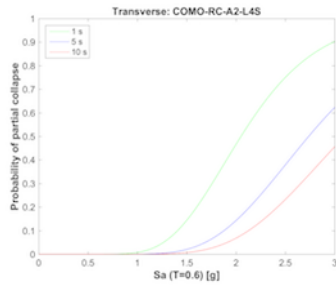




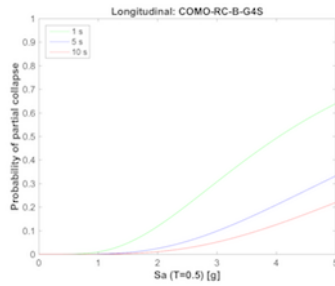
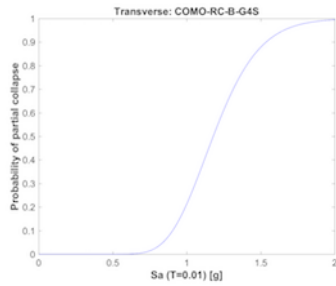
(Not applicable)



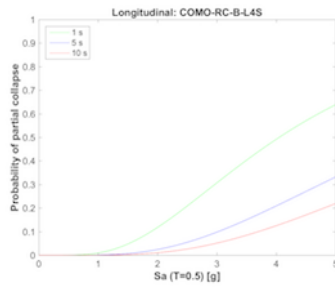
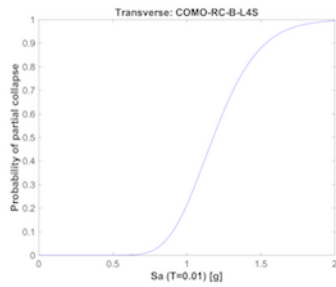
(Not applicable)



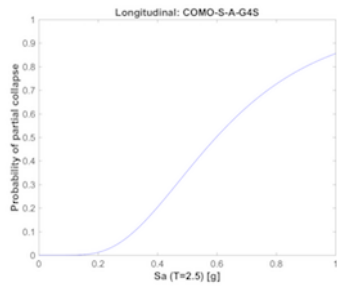
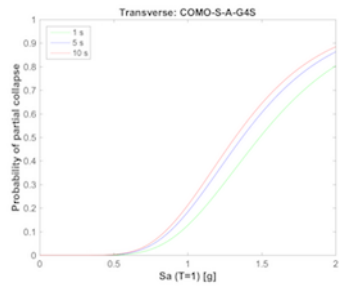
(Not applicable)



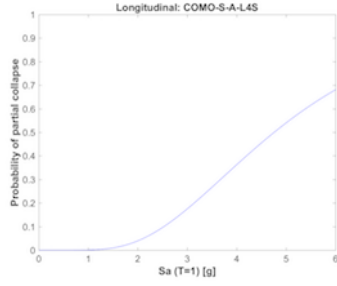
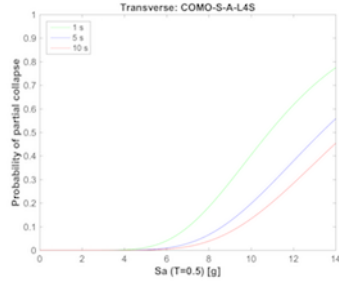
(Not applicable)



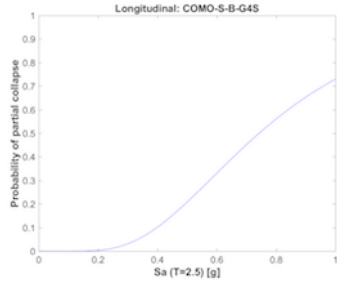
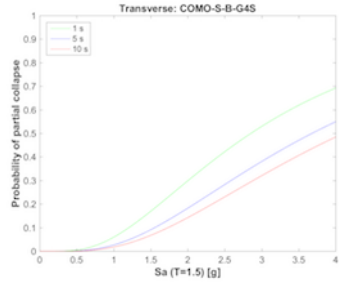
(Not applicable)



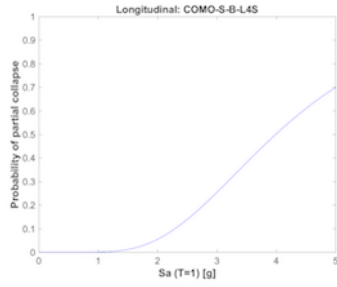
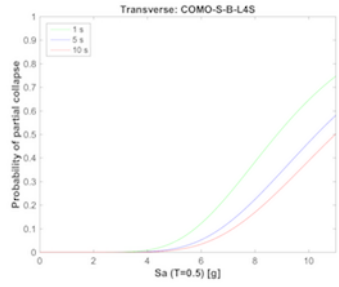
(Not applicable)



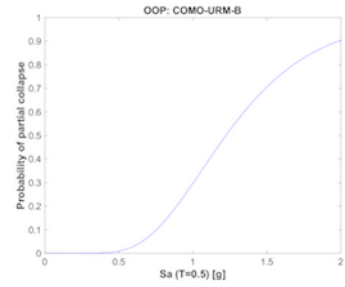
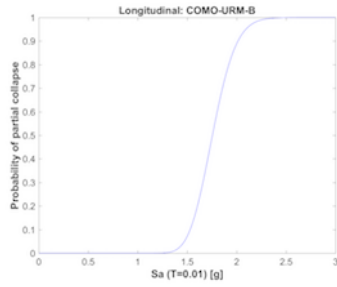
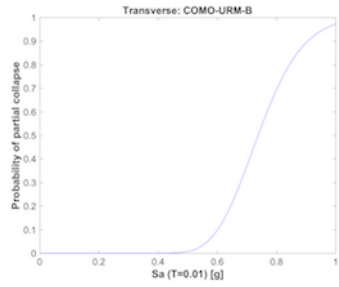
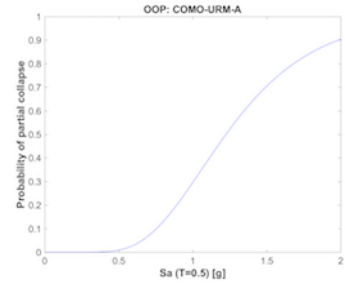
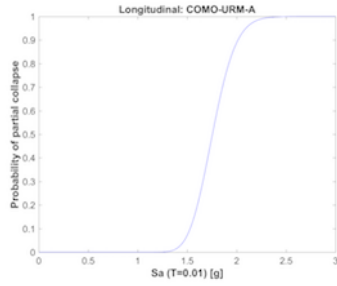
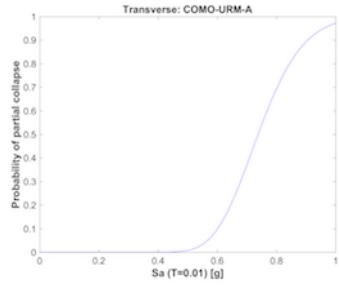
(Not applicable)

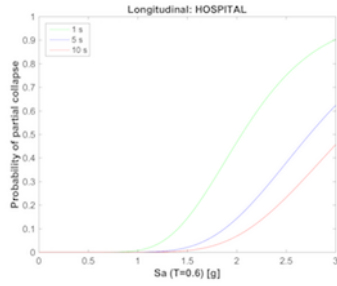
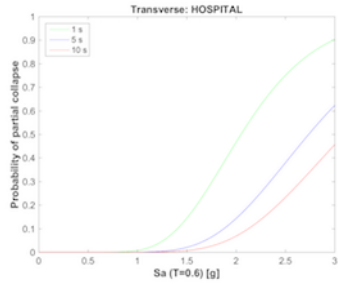


(Not applicable)

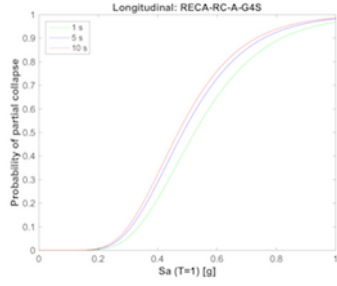
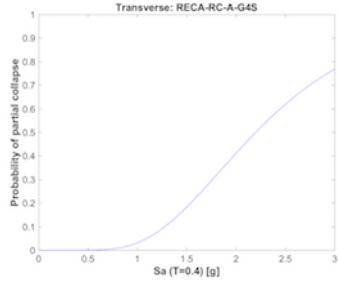


(Not applicable)

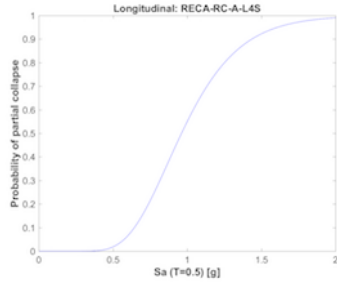
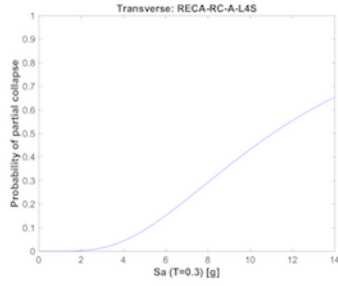




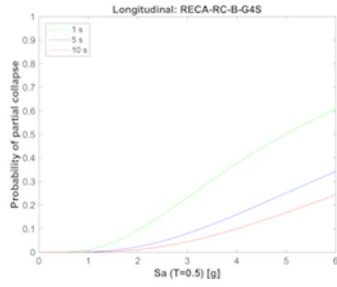
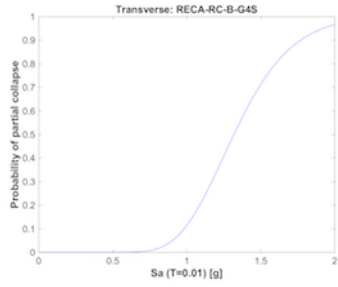
(Not applicable)



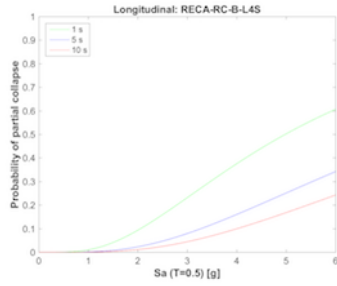
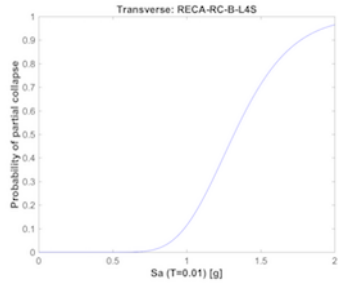
(Not applicable)



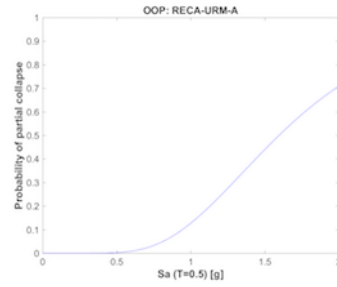
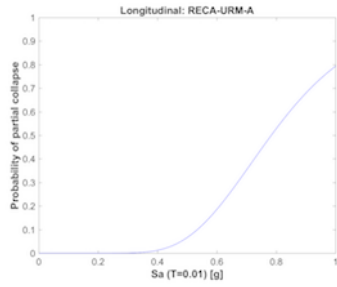
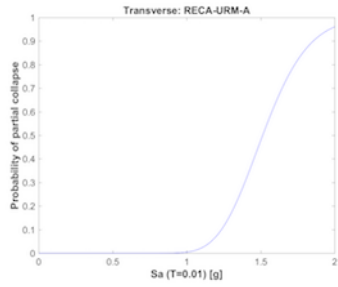
(Not applicable)

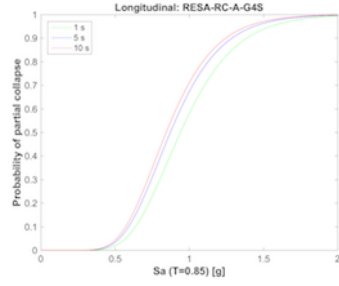
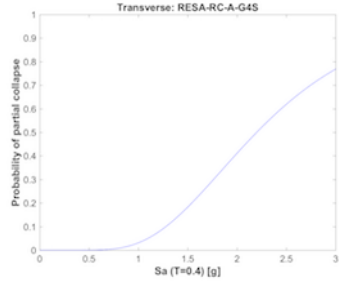
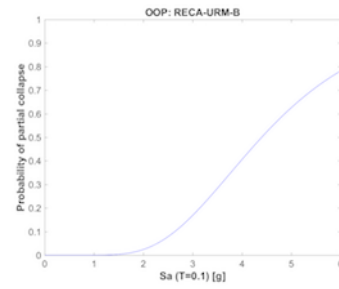
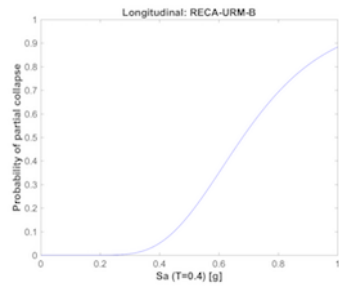
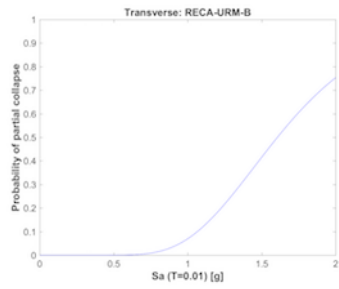


(Not applicable)

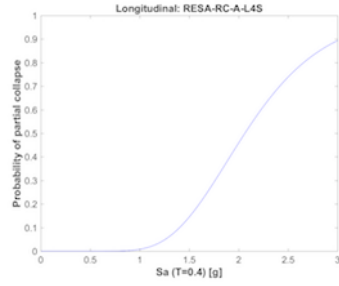
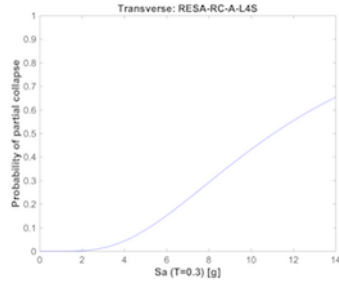


(Not applicable)

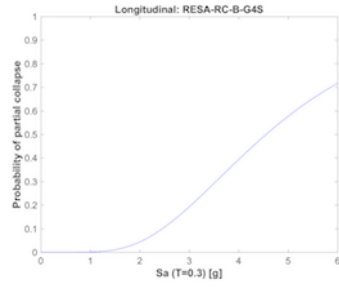
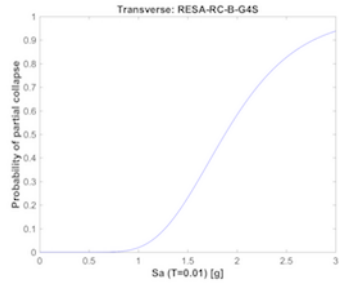




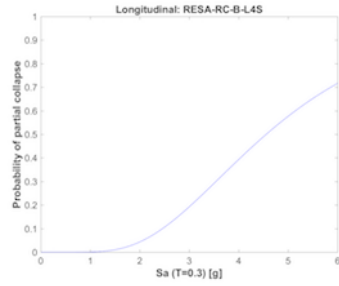
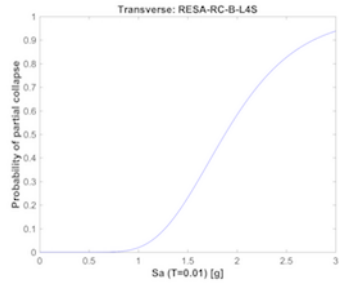
(Not applicable)



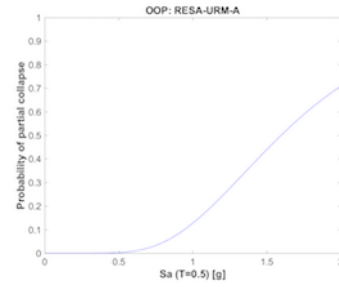
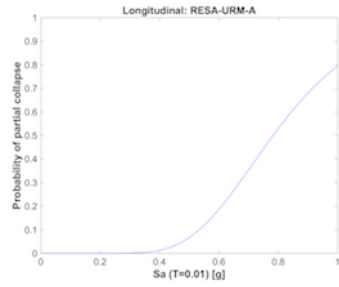
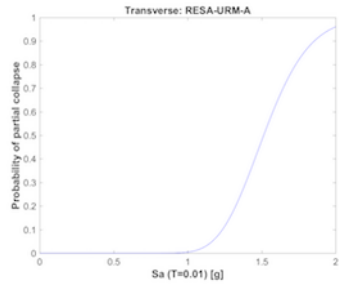
(Not applicable)

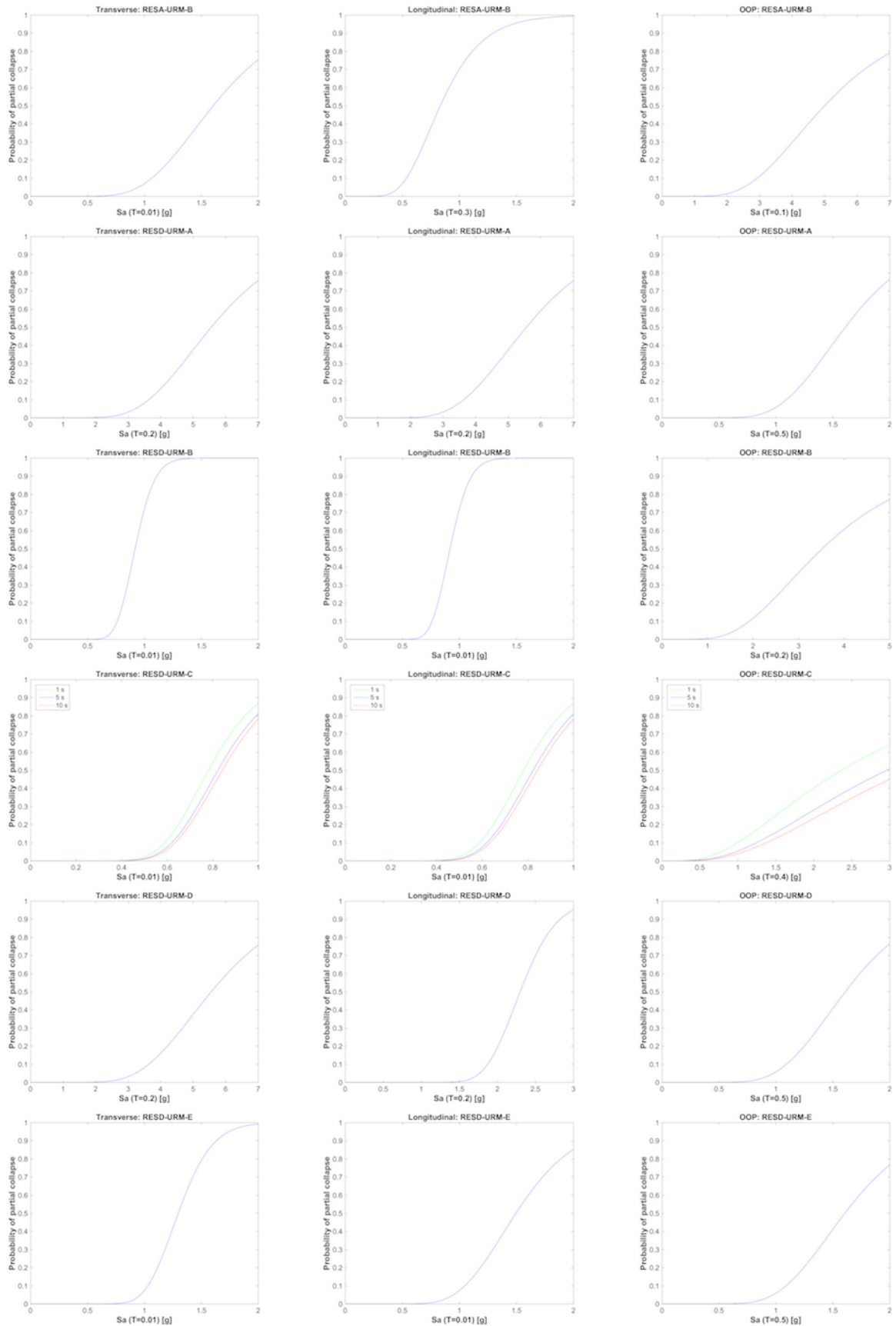


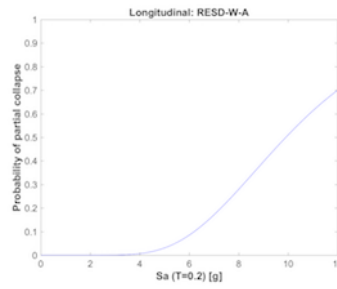
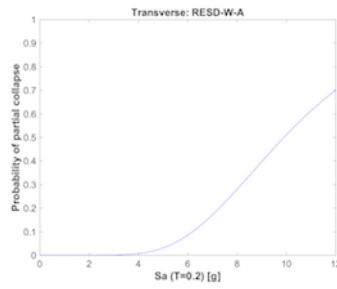
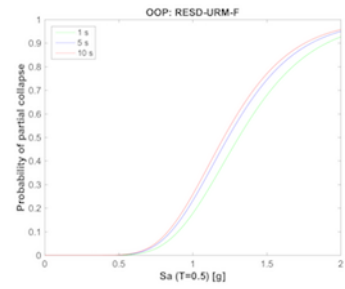
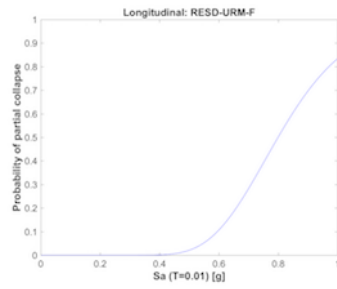
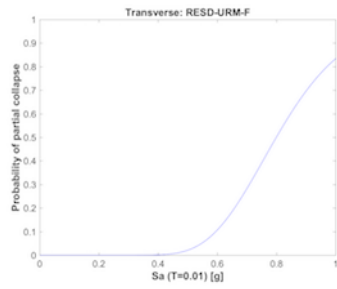
(Not applicable)



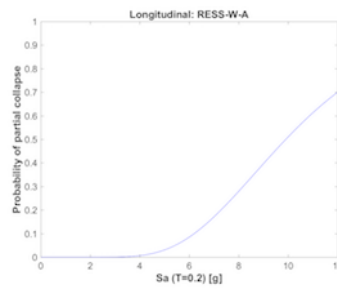
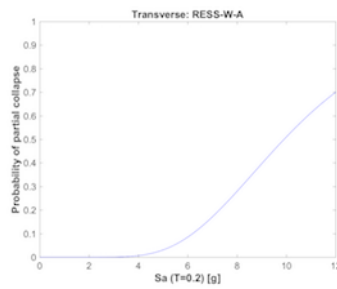
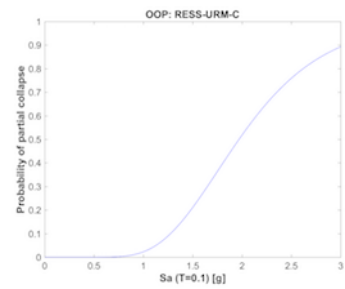
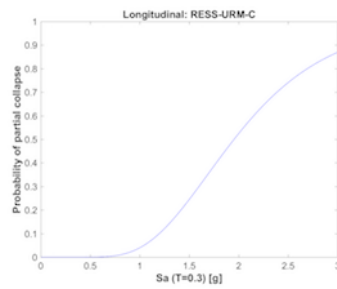
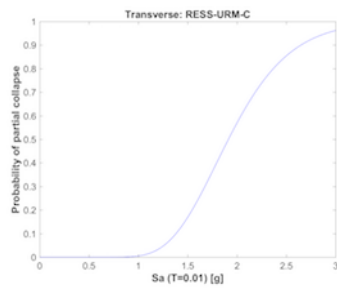
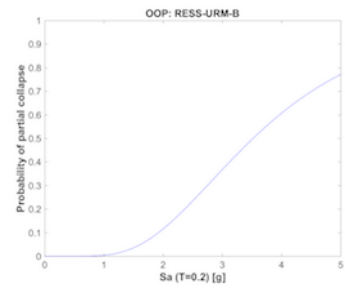
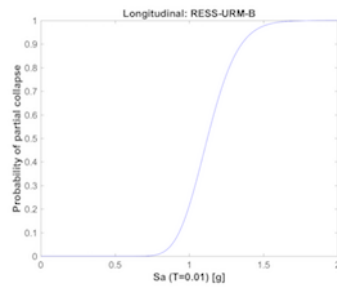
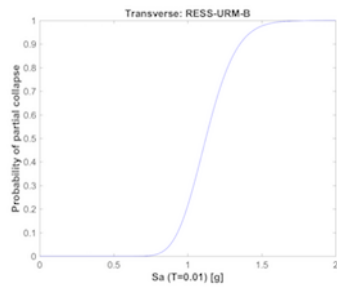
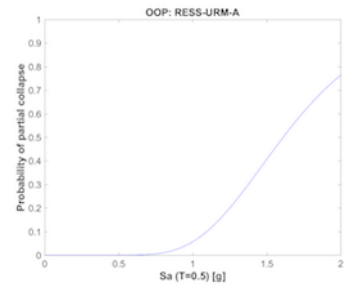
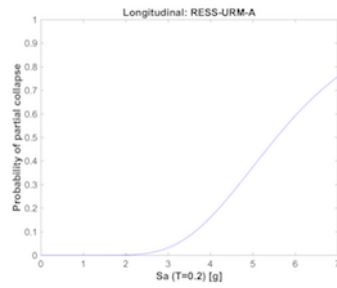
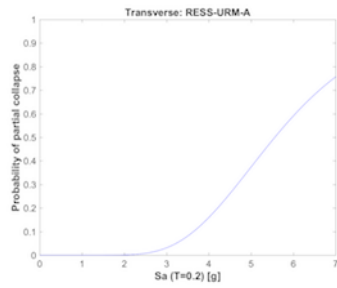
(Not applicable)



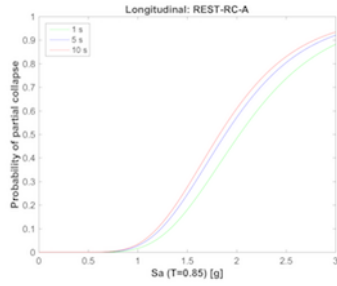
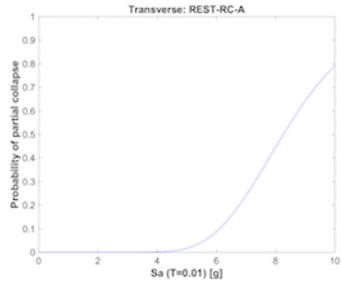




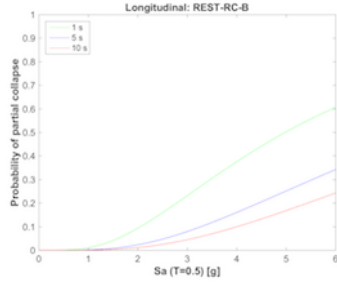
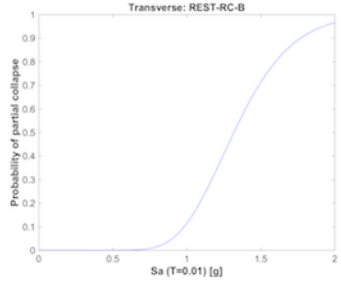
(Not applicable)



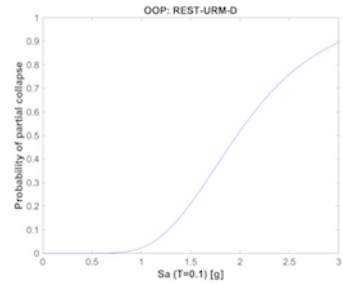
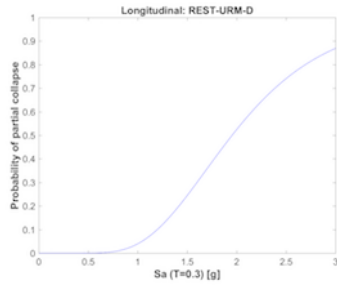
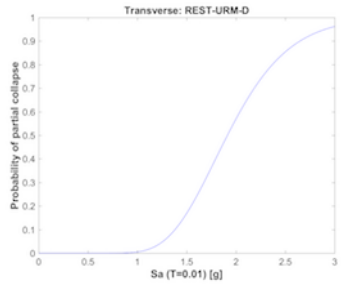
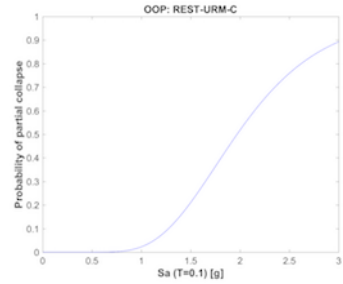
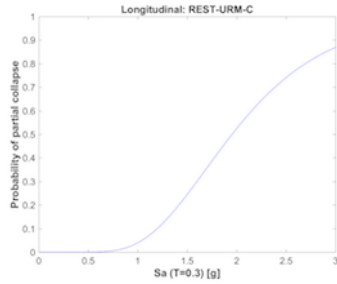
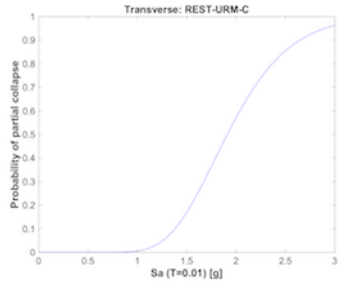
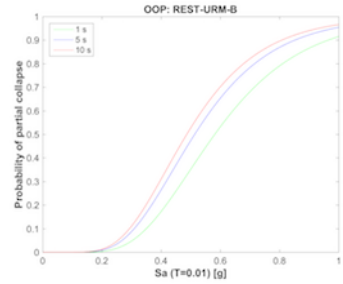
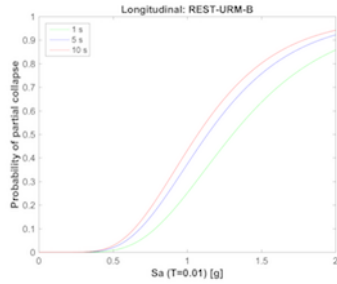
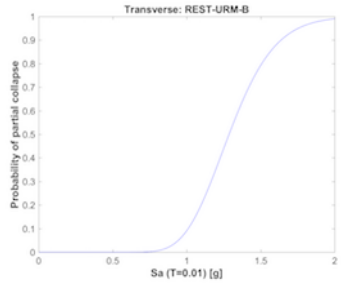
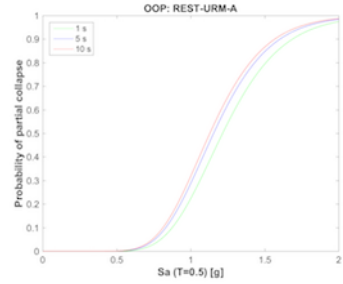
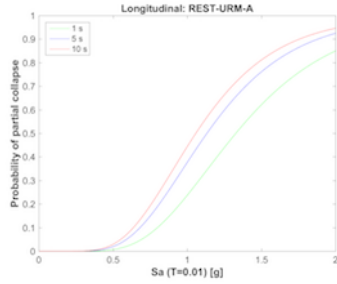
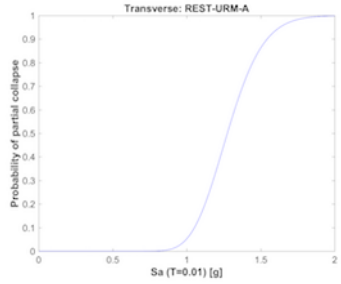
(Not applicable)



(Not applicable)



(Not applicable)



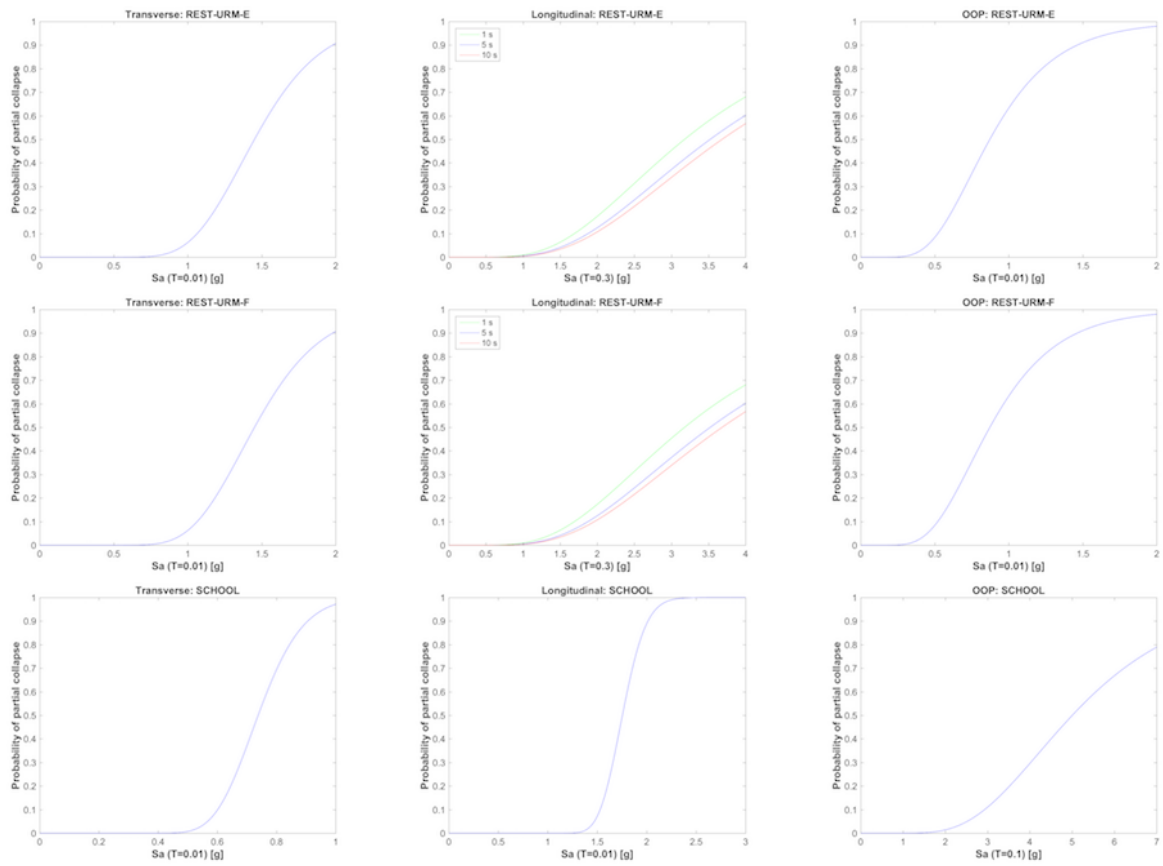


Figure B.1. Central branch (logic tree) fragility functions for all collapse mechanisms and building typologies